For Reference

NOT TO BE TAKEN FROM THIS ROOM

Ex libris
universitatis
albertensis

QUAECUMQUE VERA

THE UNIVERSITY OF ALBERTA

APPLICATION OF WALL JET THEORY TO SOME HYDRAULIC ENGINEERING PROBLEMS

by

© MURA HARI VALUPADAS

A THESIS
SUBMITTED TO THE FACULTY OF GRADUATE STUDIES
IN PARTIAL FULFILMENT OF THE REQUIREMENTS FOR THE DEGREE OF
DOCTOR OF PHILOSOPHY

DEPARTMENT OF CIVIL ENGINEERING

EDMONTON, ALBERTA
FALL, 1971

Digitized by the Internet Archive
in 2022 with funding from
University of Alberta Libraries

https://archive.org/details/Valupadas1971

1971 F
97D

UNIVERSITY OF ALBERTA

FACULTY OF GRADUATE STUDIES

The undersigned certify that they have read, and recommend to the Faculty of Graduate Studies for acceptance, a thesis entitled "APPLICATION OF WALL JET THEORY TO SOME HYDRAULIC ENGINEERING PROBLEMS" submitted by MURA HARI VALUPADAS, in partial fulfilment of the requirements for the degree of Doctor of Philosophy.

ABSTRACT

Three practical hydraulic engineering problems have been studied analytically and experimentally with the help of free jet and wall jet models as an initial step towards understanding the mechanics of these flows. These are, the plane turbulent wall jets with finite submergence, the mechanics of sloping channel jumps and the mechanics of forced hydraulic jumps.

In connection with the study of plane turbulent wall jets with finite submergence, a theoretical analysis of the flow is made considering zero pressure gradient when the submergence is appreciable and considering adverse pressure gradient when the submergence is small and the water surface profile is not level. Simple power law type expressions have been developed for the decay of velocity, growth of the jet and the bed shear stress distribution and correlated with the available experimental observations.

In connection with the mechanics of jumps on sloping channels, an analytical basis has been presented for the similarity of flow. The theoretical prediction for velocity scale, length scale and bed shear stress distribution have been correlated with the experimental observations.

In connection with the study of forced hydraulic jumps, presented herein is a detailed description of the various types of jumps and the mechanics of flow patterns of some jumps formed with the

assistance of baffle walls with and without tailwater. The form drag on the baffle walls under a forced hydraulic jump has also been measured and analysed. A preliminary design chart has been developed indicating the design procedure of stilling basins.

ACKNOWLEDGEMENTS

The author wishes to express his sincere thanks to Professor N. Rajaratnam for his guidance, advice and encouragement throughout the course of this work.

The assistance of the Hydraulics Laboratory staff in the construction of the apparatus is gratefully appreciated.

The author is grateful to the National Research Council of Canada for the financial support of this work.

TABLE OF CONTENTS

		Page
Title Page		i
Approval Sheet		ii
Abstract		iii
Acknowledgements		v
Table of Contents		vi
List of Tables		vii
List of Figures		viii
List of Symbols		xi
CHAPTER I	INTRODUCTION	1
CHAPTER II	EXPERIMENTAL FACILITIES	23
CHAPTER III	PLANE TURBULENT WALL JETS WITH FINITE SUBMERGENCE	31
CHAPTER IV	MECHANICS OF SLOPING CHANNEL JUMPS	58
CHAPTER V	MECHANICS OF FORCED HYDRAULIC JUMPS	95
CHAPTER VI	CONCLUSIONS AND RECOMMENDATIONS	128
LIST OF REFERENCES		130

LIST OF TABLES

TABLE		Page
I -1	Plane Turbulent Free Jet - Goertler Solution	18
I -2	Tollmiens Solution for the Plane Turbulent Free Jet	20
IV-1	Experimental Details for Sloping Channel Jumps	77
V -1	Details of Second Series of Experiments for Forced Hydraulic Jumps	107

LIST OF FIGURES

FIG.		PAGE
I -1	Schematic Representation of Jet Diffusion	17
I -2	Plane Turbulent Free Jet-Goertler Solution	19
I -3	Plane Turbulent Free Jet-Tollmien Solution	21
I -4	Definition Sketch of a Wall Jet	22
II -1	Experimental Set-up of Flume A	28
II -2	Flume B	29
II -3	Calibration Curves of Preston Tubes	30
III-1	Definition Sketch for Jets with Finite Submergence	50
III-2	Dimensionless Velocity Profiles	51
III-3	Deeply Submerged Flows	52
III-4	Velocity Distribution in the Jump	53
III-5	The Free Hydraulic Jump	54
III-6	Submerged Jumps	55
III-7	Variation of $\frac{b}{bo}$ with $\frac{\bar{x}}{bo}$	56
III-8	Deeply Submerged Flows with Reverse Flow	57
IV -1	Hydraulic Jump in Sloping Channels	78
IV -2	Flow Profiles	79
IV -3	Typical Velocity Distribution	80
IV -4	Similarity of Velocity Profiles-Free Jumps	81

FIG.		Page
IV -5	Similarity of Velocity Profiles-Submerged Jumps	82
IV -6	Definition Sketch for Sloping Channel Jumps	83
IV -7	Variation of u_m/U_1 with x/y_1 -Free Jumps	84
IV -8	Variation of u_m/U_1 with $1/\sqrt{x/y_1}$ -Free Jumps	85
IV -9	Study of Length Scale-Free Jumps	85
IV -10	Variation of τ_o with x	86
IV -11	Variation of c_f with x/y_1	87
IV -12	Effect of Slope on Bed Shear for Free Jumps	87
IV -13	Velocity Scale for Submerged Jumps	88
IV -14	Velocity Scales for Extreme Submergence Cases	89
IV -16	Study of c_f for Extreme Submergences	90
IV -17	Velocity Distribution in Boundary Layer - Free Jumps	91
IV -18	Velocity Distribution in Boundary Layer - Submerged Jumps	92
IV -19	Velocity Distribution in Boundary Layer	93
IV -20	Velocity Distribution in Inner Layer	94
V-1	Forced Hydraulic Jump - Definition Sketch	108
V-2	Baffle Wall Details	109

FIG.		Page
V-3	Typical Pressure Distribution on Baffle Wall	110
V-4	Plot of the Drag Coefficient	111
V-5	Variation of the parameter Λ	112
V-6	Design Curves for Λ	113
V-7	Plot of Equation 5.3	114
V-8	Variation of ξ_o with F_1	115
V-9	Plot of Equation 5.9	116
V-10	Flow Patterns for $K \simeq 1.0$	117
V-11	Flow Patterns for $K=0.4$	118
V-12	Flow Patterns for $K=0$ and Subcritical Tailwater	119
V-13	Flow Patterns for $K=0$ and Supercritical Tailwater	120
V-14	Velocity Distribution in Free Mixing Zone	121
V-15	Velocity Distribution in the Boundary Layer	122
V-16	Growth of the Boundary Layer Thickness	123
V-17	Growth of the Length Scale	124
V-18	Variation of the Velocity Scale	125
V-19	Velocity Distribution in the Curved Free Jet	126
V-20	Velocity Decay for Region-2	127

LIST OF SYMBOLS

a = opening of the sluice gate

$b, \bar{b}$ = length scales

b_o = nozzle height

b_o' = nozzle half height

c, c_1, c_2, c_3, c_4 = coefficients

c_f = skin friction coefficient

f = suffix for function; also function

F_1 = supercritical Froude number

G = function

G_1 = parameter

g = acceleration due to gravity

h = function, height of jump, height of baffle wall

j = suffix for jump

K = parameter

l = suffix to denote laminar flow; also mixing length

L_e = length of eddy

L_j = length of jump

L_1 = minimum length of forced jump

M_0, M_1 = momentum flux

M = momentum flux at any distance x

m = suffix to denote maximum

n = exponent

P = piezometric pressure ; also exponent

q = exponent

R = Reynold number

r = exponent

s = exponent

t = suffix to denote turbulent flow; also suffix for tailwater

u = turbulent mean velocity in x direction

u' = turbulent fluctuating velocity in the x direction

$\bar{u}_m$ = velocity scale for reverse flow

u_m = velocity scale

u_{mj} = maximum velocity in the plane of the nozzle

U = relative velocity for backward flow

U_o = initial velocity

U_1 = mean velocity of the supercritical stream

v = turbulent mean velocity in y direction

v' = turbulent fluctuating velocity in the y direction

x = distance from the virtual origin along channel bed; also distance from the toe of forced jump, distance from gate

x_o = distance of the baffle wall from the toe of the jump

$\bar{x}$ = distance from the nozzle

y = distance perpendicular to channel bed

y_1 = y_o,b_o, nozzle height, depth of supercritical stream

y_1 = supercritical vertical depth before jump

y_2 = subcritical vertical depth after jump

y_2^* = subcritical sequent depth of classical jump

y^* = upper limit of integration

y_t = tailwater depth

y^* = $y_t - \bar{y}$

$\bar{y}$ = depth of flow down stream of gate

$\propto$ = stands for proportional to ; also infinity

γ = specific weight of fluid

δ = boundary layer thickness

δ_1 = length scale

$\eta, \bar{\eta}$ = dimensionless distance from bed

μ = dynamic viscosity coefficient

ν = kinematic viscosity coefficient

ρ = mass density

τ_t, τ = shear stress

τ_o = bed shear stress

θ = angle of bed with the horizontal

λ = nondimensional y distance

ξ = parameter; also eddy viscosity

ξ_o = limiting value of ξ

Λ = parameter

1,2,3,4,.. = suffixes

primes denote differential operations

CHAPTER I

INTRODUCTION

1.1 General

Flow through submerged outlets is a common feature in many of the water-resources projects. At present, a large number of experimental observations are available describing the mean flow characteristics of flow below submerged outlets, but no rational analytical basis has yet been established. The submerged flow below an outlet, if the jet issues tangentially to the wall, can be analysed as a turbulent wall jet. In contrast to the classical wall jet flow, the jet under a sluice gate issues into a finite depth of fluid downstream. Consequently the flow picture consists of an expanding jet superimposed by a roller where in the flow recirculates. If the submergence is not appreciable the water surface profile downstream might not be horizontal, in which case adverse pressure gradients are set up. As a first step, a preliminary analytical basis has been worked out explaining the flow mechanism below submerged sluice gates considering the effects described above. It is believed that such a basis could be used for developing suitable design procedures for the submerged outlets.

Secondly, a large number of experimental investigations and model studies are available establishing the relationship between gross characteristics of jumps formed on sloping channels and forced hydraulic jumps. Information regarding the mean flow characteristics

and the analytical basis explaining the flow mechanism is not available. The hydraulic jump can be considered as a case of free turbulent shear flow. The flow pattern is determined by the turbulent diffusion process under adverse pressure gradient and the model of turbulent jet diffusion is a useful tool in explaining the flow mechanism. Extensive information is readily available about the mechanism and diffusion characteristics of free turbulent jet issuing into an infinite extent of ambient fluid (Abromovich, 1963). It is believed that sufficient knowledge about the flow mechanism and a rational analytical basis would help explain some of the misconceptions of the phenomenon and improving the design methods. Such a study is undertaken in the later part of this thesis.

Since the turbulent free jet and turbulent wall jet have been used as basic flow models in the analysis, it is considered necessary to give a review of the method of analysis of their diffusion process in the following sections.

1.2 Diffusion of Free Jets

Consider a plane turbulent jet issuing from a nozzle into an infinite expanse of the fluid of the same nature at rest as shown in Fig. I-1. The region of diffusion can be divided into two zones, namely the zone of flow establishment and the zone of established flow.

1.3 Zone of Flow Establishment

This zone starts from the efflux section, at which the velocity is uniform throughout the jet. When the jet enters into the

surrounding fluid, eddies are generated along the boundaries due to the large velocity discontinuity between the jet and the surrounding fluid. These eddies mix laterally into the potential core and out into the ambient fluid. Due to this mixing process the surrounding fluid is accelerated and the fluid within the jet is decelerated till the entire potential core is consumed. The end of the potential core is considered as the end of zone of flow establishment.

1.4 Zone of Established Flow

The beginning of this section is marked from the point where the lateral eddy mixing spreads up to the central part of the jet causing an end to the potential core. The flow from this point is turbulent and is considered as fully established because the diffusion process continues from this point without essential change in character. In this zone the inertial balance occurs between the surrounding fluid and reduction in velocity of entire central region.

1.5 Theoretical Analysis

The Reynolds equations of motion for a steady incompressible and two dimensional flow are :

$$u \frac{\partial u}{\partial x} + v \frac{\partial u}{\partial y} = - \frac{1}{\rho} \frac{\partial p}{\partial x} + \nu \nabla^2 u - \left(\frac{\partial \overline{u'^2}}{\partial x} + \frac{\partial \overline{u'v'}}{\partial y} \right) \tag{1.1}$$

$$u \frac{\partial v}{\partial x} + v \frac{\partial v}{\partial y} = - \frac{1}{\rho} \frac{\partial p}{\partial y} + \nu \nabla^2 v - \left(\frac{\partial \overline{u'v'}}{\partial x} + \frac{\partial \overline{v'^2}}{\partial y} \right) \tag{1.2}$$

$$\frac{\partial u}{\partial x} + \frac{\partial v}{\partial y} = 0 \tag{1.3}$$

where u and v are the turbulent mean velocities in the x (longitudinal) and y (normal) directions, u' and v' are the corresponding velocity fluctuations, p is the mean turbulent piezometric pressure, ρ is the mass density of the fluid and ν is the coefficient of kinematic viscosity.

With the assumptions that

$$u >> v, \frac{\partial}{\partial x} (\ldots) << \frac{\partial}{\partial y} (\ldots)$$

$$\frac{\partial \overline{u'v'}}{\partial x} \text{ is negligible}$$

$$\nu \nabla^2 v \text{ is negligible}$$

equation 1.2, reduces to

$$- \frac{1}{\rho} \frac{\partial P}{\partial y} - \frac{\partial \overline{v'^2}}{\partial y} = 0$$

or

$$\frac{P}{\rho} = - \overline{v'^2} + \text{constant } (c)$$

for

$$y \rightarrow \infty, \overline{v'^2} \rightarrow 0 \text{ and if } P = P_o\text{, then}$$

$$c = \frac{P_o}{\rho}$$

$$\frac{P}{\rho} = \frac{P_o}{\rho} - \overline{v'^2} \tag{1.4}$$

substituting equation (1.4) in equation (1.1)

$$u \frac{\partial u}{\partial x} + v \frac{\partial u}{\partial y} = - \frac{1}{\rho} \frac{\partial p_o}{\partial x} + \nu \nabla^2 u - \frac{\partial}{\partial x} \left[\overline{u'^2} - \overline{v'^2} \right] + \frac{1}{\rho} \frac{\partial \tau_t}{\partial y} \qquad (1.5)$$

where $\tau_t = -\rho \overline{u'v'}$

the quantity $\frac{\partial}{\partial x} (\overline{u'^2} - \overline{v'^2})$ is small and hence can be neglected. $\frac{\partial^2 u}{\partial x^2}$ is also negligible. Further in the developed flow region $\nu \frac{\partial^2 u}{\partial y^2}$ is negligible as the flow is turbulent and the pressure gradient along x direction is also negligible. With these assumptions, equations of motion for a plane turbulent free jet reduces to

$$u \frac{\partial u}{\partial x} + v \frac{\partial u}{\partial y} = \frac{1}{\rho} \frac{\partial \tau_t}{\partial y} \qquad (1.6)$$

$$\frac{\partial u}{\partial x} + \frac{\partial v}{\partial y} = 0 \qquad (1.7)$$

Now assuming similarity of flow, the flow field can be described by a single velocity scale and a single length scale. Choosing u_m the maximum velocity at any section as the velocity scale and 'b' the normal distance from the jet axis to a point where the velocity is $u_m/2$ as the length scale, the various quantities can be expressed as,

$$u = u_m f_1(y/b), \quad \frac{\tau_t}{\rho u_m^2} = g(y/b) \qquad (1.8)$$

In order to evaluate these functional forms let us assume

$$u_m \alpha x^p$$

$$b \alpha x^q$$

For further analysis and to evaluate the exponents p and q we use the equations of motion and the momentum integral relationship as

shown below,

Writing $y/b = \lambda$

$$\frac{\partial u}{\partial x} = f\, u'_m - u_m \frac{\lambda}{b} f'b'$$

where $f = f(\lambda)$, $u'_m = \frac{du_m}{dx}$, $f' = \frac{df}{d\lambda}$, $b' = \frac{db}{dx}$

$$u \frac{\partial u}{\partial x} = u_m\, f^2\, u'_m - u_m^2 \frac{\lambda}{b}\, f\, f'b' \qquad (1.9)$$

From the continuity equation

$$v = - \int_0^y \frac{\partial v}{\partial y}\, dy = - b \int_0^\lambda \frac{\partial u}{\partial x}\, d\lambda$$

$$= \int_0^\lambda (u_m \lambda\, f'b' - bf\, u'_m)\, d\,\lambda$$

$$\frac{\partial u}{\partial y} = \frac{u_m f'}{b}$$

$$v \frac{\partial u}{\partial y} = \frac{u_m f'}{b} \left\{ \int_0^\lambda u_m\, \lambda\, f'b'\, (d\lambda) - \int_0^\lambda b\, f\, u'_m\, (d\lambda) \right\} \qquad (1.10)$$

and $$\frac{\partial \tau_t}{\partial y} = \frac{u_m^2\, g'}{b} \qquad (1.11)$$

where $g' = \frac{\partial g}{\partial \lambda}$

substituting 1.9, 1.10 and 1.11 in equation (1.6)

$$u_m u_m' f^2 - u_m^2 \frac{\lambda}{b} f f' b' + u_m^2 \frac{b'}{b} f' \int_0^\lambda \lambda f'(d\lambda) - \frac{u_m u_m'}{b} f \int_0^\lambda f (d\lambda) = \frac{u_m^2 g'}{b}$$

or

$$g' = b \frac{u_m'}{u_m} f^2 - \lambda f f' b' + b' f' \int_0^\lambda \lambda f'(d\lambda) - \frac{b}{u_m} u_m' f' \int_0^\lambda f (d\lambda) \quad (1.12)$$

In equation 1.12 g' is the function of λ only. Therefore for similarity of flow, all the coefficients of functions of λ on right hand side of equation (1.12) should be either zero or constants. If we consider the condition that $b' = 0$, then b = constant, i.e. the width of mixing region along x direction is constant which is unrealistic.

Therefore $b' \alpha\ x^\circ$

or $\quad b = c\,x$

and $\quad q = 1$

To evaluate P we consider the integral momentum equation. Since $\frac{dp}{dx} = 0$ the momentum along the x direction is preserved.

i.e. $\frac{d}{dx} \int_0^\infty \rho\, u^2\, dy = 0$

or

$$\int_0^\infty \rho\, u^2\, dy = \text{constant} \quad (1.13)$$

substituting $u = u_m f$

$$\rho\, u_m^2\, b \int_0^\infty f^2 (d\lambda) = \text{constant}$$

which can also be written as

$$\rho u_m^2 b \int_0^\infty f^2 (d\lambda) = c_1 x^\circ \tag{1.14}$$

comparing the exponents of x on either side of equations (1.14)

$$x^{2p+q} = x^\circ$$

or

$$p = -\frac{1}{2}$$

Thus we could write $b = c_1 x$ (1.15)

and $$\frac{u_m}{U_o} = \frac{c_2}{\sqrt{x/b'_o}} \tag{1.16}$$

where U_o is the velocity at the efflux section b'_o is the nozzle half width. The well known experimental results for the decay of maximum velocity u_m, and the variation of b, taken from Abramovich (1963), Newman (1961), Zijnen (1957) and Albertson et al. (1950) indicate average values of $c_1 = 0.1$ and $c_2 = 3.5$ in the equations (1.15) and (1.16) respectively.

1.6 Velocity Distribution

Considering equation (1.6) it is obvious that to determine the expression for velocity distribution, we must know the expression for shear stress τ_t. If τ_t is expressed in terms of mixing length hypothesis then any choice of velocity distribution will result in a particular distribution of the mixing lengh l across the section. Conversely, a choice of the distribution of mixing length across the section, together with the assumption, that $l = c_3 \, x \, f(\lambda)$ will lead to a particular form of the velocity distribution.

1.7 Tollmien's [47] Solution for Velocity Distribution

Considering the mixing length hypothesis

$$\tau_t = \rho\, l^2 \frac{\partial u}{\partial y} \left(\frac{\partial u}{\partial y}\right) \qquad (1.17)$$

It is reasonable to assume that at any section

$l \propto b$ or l/b = constant.

Substituting the above expressions in equation (1.6) and simplifying, using equation of continuity, one could obtain

$$F''^2 + F\,F' = c \qquad (1.18)$$

where

$$F = \int_0^\phi f\,(d\phi),\ F' = f \text{ and } F'' = f',\ \phi = \frac{y}{ax}$$

a being constant.

Using the following boundary conditions, the value of c can be found as equal to zero.

(1) $y = 0,\ \phi = 0,\ F' = 1$

$y = 0,\ \phi = 0,\ v = 0,\ F(o) = 0$

$\lambda = 0,\ \tau_t = 0$ and therefore $F''(o) = 0$

(2) As $y \rightarrow \infty,\ \phi \rightarrow \infty$ where $u \rightarrow 0$ and therefore $F(\infty) = 0$

$y \rightarrow \infty,\ \lambda \rightarrow \infty,\ \tau_t \rightarrow 0$ and therefore $F''(\infty) = 0$

Thus equation (1.18)can be written as

$$F''^2 + F\,F' = 0 \tag{1.19}$$

The solution of equation (1.19) is shown on Table I-2 and Fig. I-3.

1.8 Göertler [15] Solution

According to Göertler solution, the assumption for shear stress expression is,

$$\tau_t = \rho \quad \xi \quad \frac{\partial u}{\partial y} \tag{1.20}$$

where ξ is the kinematic eddy viscosity and is assumed that $\xi \propto b\ u_m = K\sqrt{x}$ Using the above assumptions equation (1.6) can be reduced to

$$F'' + F\,F' = \text{constant } C \tag{1.21}$$

where

$$F = F(\eta) = \int_0^\eta f(d\eta)$$

and

$$F' = f,\ F'' = f',\ \eta = \sigma\, y/x,\ \sigma \text{ being constant}$$

Using the following boundary conditions the value of C=0 in the equation (1.21).

1) For $y = 0,\ \eta = 0,\ \frac{u}{u_m} = 1$ and $F'(0) = 1$

$y = 0,\ \eta = 0,\ v = 0$ and $F(0) = 0$

$y = 0,\ \eta = 0,\ \tau_t = 0$ and $F''(0) = 0$

2) For $y \to \infty$, $\eta \to \infty$, $u = 0$ and $F'(0) = 0$

i.e. $F'' + F'F = 0$ (1.22)

Evaluation of various parameters using the equation (1.22) is shown in Table I-1 and Fig. I-2.

1.9 The Wall Jet

The classical Wall Jet is described as a jet of fluid which issues on to a wall tangentially and grows along the wall in a surrounding stationary fluid of infinite extent as shown in Fig. I-4.

The phenomenon of the two dimensional wall jet was first investigated experimentally by Förthman [12] in 1936. A theoretical analysis of the problems was made by Glauert [14] in 1956 and later by Schwarz and Cosart [44]. It was found that similar to a free jet the wall jet flow can be divided into two regions, the flow development region and the developed flow region. The velocity profiles are similar in the wall jet if we exclude a small portion near the boundary where the effect of viscosity is dominant. The velocity scale at any section is the maximum velocity at that section and the length scale is the normal distance b from the boundary to the plane where the velocity u is equal to half the maximum velocity.

1.10 Theoretical Analysis

The Reynolds equations of motion for this problem could be written as

$$u \frac{\partial u}{\partial u} + v \frac{\partial u}{\partial y} = - \frac{1}{\rho} \frac{\partial p}{\partial x} + \nu \nabla^2 u - \left(\frac{\partial \overline{u'^2}}{\partial x} + \frac{\partial \overline{u'v'}}{\partial y} \right) \qquad (1.23)$$

$$u \frac{\partial v}{\partial x} + v \frac{\partial v}{\partial y} = - \frac{1}{\rho} \frac{\partial p}{\partial y} + \nu \nabla^2 v - \left(\frac{\partial \overline{u'v'}}{\partial x} + \frac{\partial \overline{v'^2}}{\partial y}\right) \qquad (1.24)$$

$$\frac{\partial u}{\partial x} + \frac{\partial v}{\partial y} = 0 \qquad (1.25)$$

With the boundary layer assumptions similar to that made in the case of free jet, equations of motion (1.23) and (1.25) can be reduced to

$$u \frac{\partial u}{\partial x} + v \frac{\partial u}{\partial y} = \frac{1}{\rho} \frac{\partial \tau_t}{\partial y} + \frac{\nu \partial^2 u}{\partial y^2} \qquad (1.26)$$

$$\frac{\partial u}{\partial x} + \frac{\partial v}{\partial y} = 0 \qquad (1.27)$$

Further, assuming similarity of flow, the flow field can be described by the length scale b and the velocity scale u_m. To evaluate the functional form of u_m and b we can assume

$$\begin{aligned} &u_m \infty x^p \\ &b \infty x^q \end{aligned} \qquad (1.28)$$

For further analysis, to evaluate the exponents p and q we can use the equations of motion and the momentum integral equation. Using equations of motion and adopting the simplification procedure as indicated in the case of free jet it could be shown that

$$g' = b \frac{u'_m}{u_m} f^2 - \lambda f f' b' + b' f' \int_0^\lambda \lambda f' \, d(\lambda) - \frac{b}{u_m} u'_m f' \int_0^\lambda f \, d(\lambda)$$

and $q = 1$ (1.29)

where the viscous term has been neglected.

Considering the integral momentum equation, since $\frac{dp}{dx} = 0$ the relationship between momentum and the bed shear stress along the x direction could be written as

$$\frac{d}{dx} \int_0^{\infty} \rho\, u^2\, dy = -\, \tau_o \tag{1.31}$$

or

$$M = M_o - \int \tau_o\, dx \tag{1.32}$$

where M is the momentum at any section distant x from the efflux section and M_o is the initial momentum. If the magnitude of bed shear stress is negligible compared to M_o then $M \simeq M_o$ which means that the momentum flux along the x direction is preserved.

i.e.
$$\frac{d}{dx} \int_0^{\infty} \rho\, u^2\, dy = 0 \tag{1.33}$$

from which using a procedure similar to the case of the free jet we can show that $p \simeq -\frac{1}{2}$

or

$$b = c_1\, x$$

$$u_m = c_2/\sqrt{x} \tag{1.34}$$

Experimental studies on plane turbulent Wall Jet under zero pressure gradient have been conducted by Sigalla [46], Bradshaw and Gee [4], Schwarz and Cosart [44], Myers et al [23] and others. It was found that the length of the flow development region was about 10 y_1 and the length and velocity scales were given by the equations

$$b/b_o = 0.50 + 0.065 \frac{x}{b_o} \qquad (1.35)$$

$$\frac{u_m}{U_o} = 3.45 \left(\frac{x}{b_o}\right)^{-0.5} \qquad (1.36)$$

The Reynolds number $R_1 = \frac{U_o b_o}{\nu}$, where ν is the kinematic viscosity has not been found to influence these relations to any appreciable extent when it is greater than about 10^4. The velocity distribution in the boundary layer was found to follow the one-seventh power low [12]. However, it was found by later investigations [44, 23, 10] that depending on the Reynolds number where R_1 lies between 10^4 abd 10^5, The value of the exponent is closer to 1/14 and that the logarithmic low can be a better fit [10] with the values of the coefficients being somewhat different from the well known equation for boundary layers. The flow structure of the boundary layer in a wall jet is different from that of a classical boundary layer because in a wall jet the boundary layer grows under a superimposed turbulent decelerating flow. The boundary shear stress in a fully developed wall jet flow has been found to be given by the equation

$$\tau_o = c_f \frac{\rho u_m^2}{2} \qquad (1.37)$$

where

$$c_f = 0.0565/\left(\frac{u_m \delta}{\nu}\right)^{1/4} \qquad (1.38$$

and c_f is the coefficient of shear stress

ρ is mass density of fluid and

δ is boundary layer thickness at that section

Equation (1.38) shows that c_f is a weak function of x. Myer et al [23] have expressed c_f as a function of $R_1 = \frac{U_o b_o}{\nu}$. Recently, experiments on free and submerged hydraulic jumps on horizontal floors were presented by Rajaratnam [30,31] as turbulent wall jets under adverse pressure gradient. The deeply submerged flow below sluice gate over smooth and rough boundaries was analysed by Rajaratnam [32, 42] as a wall jet. Lau [21] studied the wall jet growth on a porous boundary with and without suction.

1.11 The Present Investigation

The main aim of this investigation is :

1) to present an analytical basis describing the flow picture below sluice gates under finite submergence with and without reverse flow and with and without pressure gradient.

2) to explain the flow mechanism of free and submerged hydraulic jumps on sloping floors

and 3) to study the drag force experienced by baffle walls located inside forced hydraulic jumps and explain the flow processes of different types of forced hydraulic jumps.

The test facilities and limitations of measurement technics are described in Chapter II.

These studies are arranged in Chapters III, IV and V respectively.

In the first two problems, an analytical basis has been presented for the existence of flow similarity. The velocity profiles on center line were measured at various sections along the channel and were examined for similarity. The expressions for the variation of length and velocity scales and bed shear stress distribution along the flow have been correlated with the experimental observations. In the third problem an analysis of the experimental observations of form drag distribution on baffle walls and the velocity profiles on the centre line, (measured at various sections along the channel) are analysed for similarity and the variation of length and velocity scales along the flow have been studied and compared with the corresponding characteristics of classical hydraulic jump and the classical wall jet.

Chapter VI gives the general conclusions of the present investigation and recommendations for future studies.

The experimental investigation was carried out at the Hydraulics Laboratory of the University of Alberta, Canada, during the period 1969 - 1970.

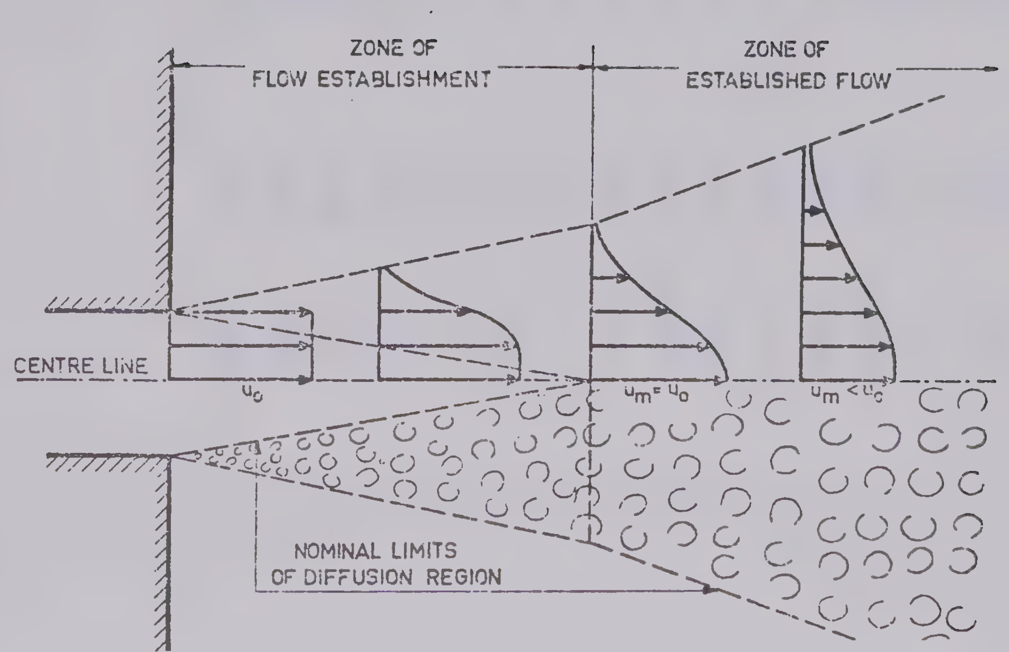

FIG.1–1. SCHEMATIC REPRESENTATION OF JET DIFFUSION

according to Albertson e.a. (1950).

TABLE I-1

PLANE TURBULENT FREE JET - GOERTLER SOLUTION

$\eta = \sigma \frac{y}{x}$	u/u_m	y/b
0	1.000	0
0.10	0.990	0.114
0.20	0.961	0.227
0.30	0.915	0.341
0.40	0.855	0.455
0.50	0.786	0.568
0.60	0.711	0.682
0.70	0.635	0.795
0.80	0.558	0.909
0.90	0.486	1.022
1.00	0.420	1.136
1.20	0.302	1.362
1.40	0.218	1.590
1.60	0.149	1.820
1.80	0.102	2.045
2.00	0.070	2.270
2.20	0.048	2.500
2.50	0.021	2.840

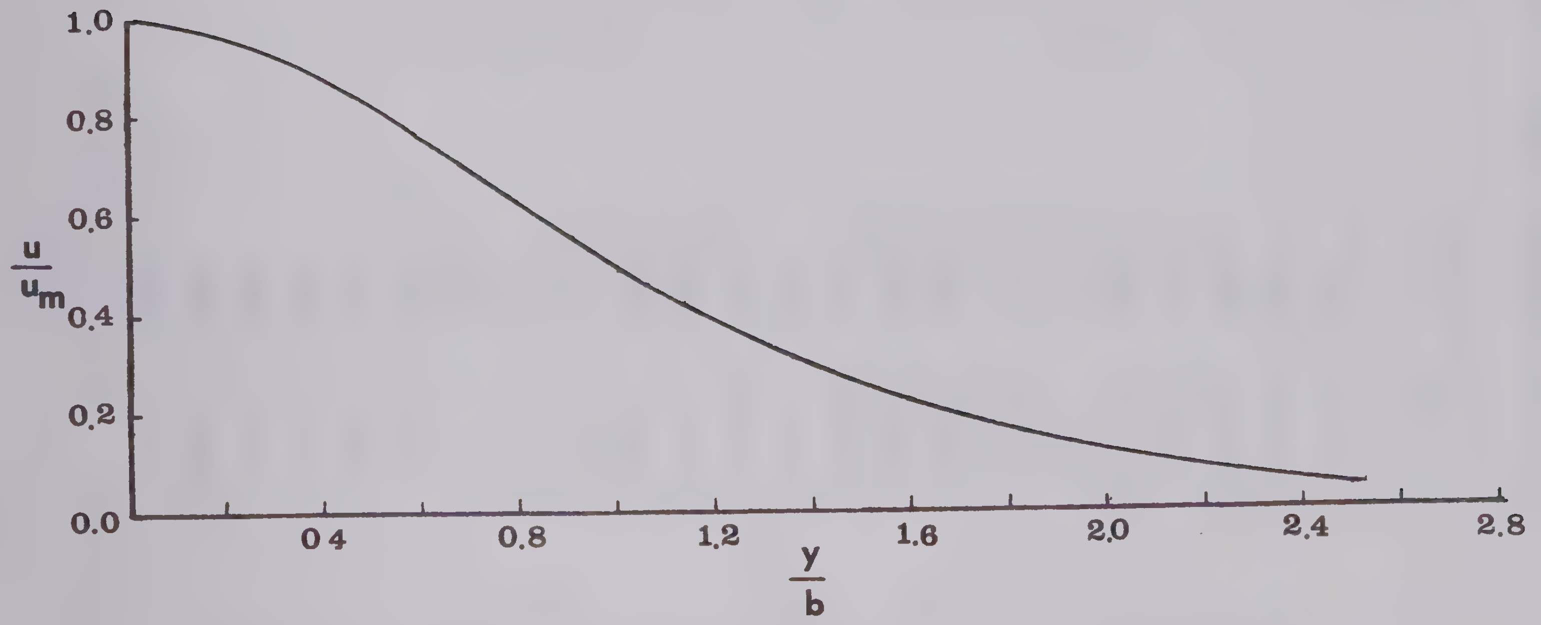

FIG. I-2. PLANE TURBULENT FREE JET – GOERTLER SOLUTION

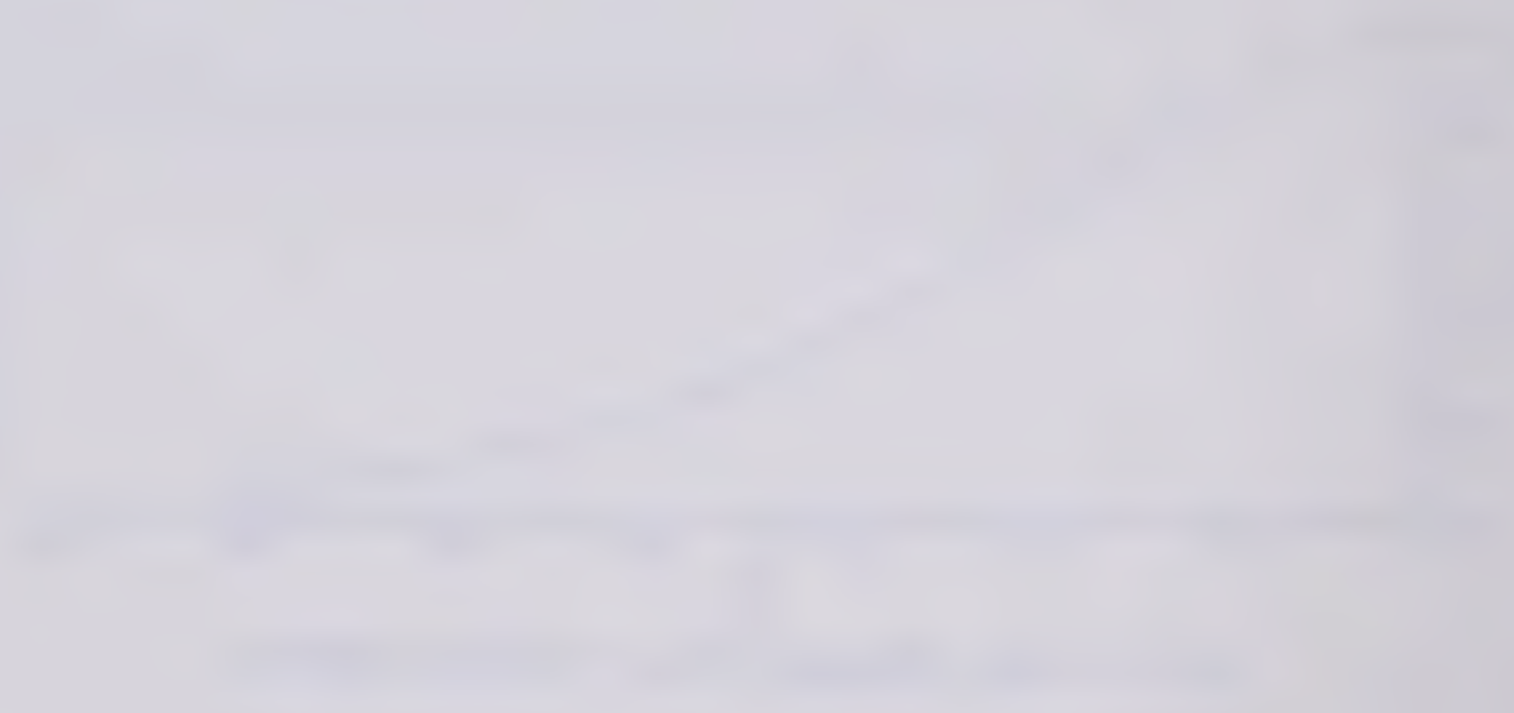

TABLE I-2

TOLLMIEN'S SOLUTION FOR THE PLANE TURBULENT FREE JET

$\phi = \frac{y}{ax}$	$F'(\phi) = \frac{u}{u_m}$	$\frac{y}{b}$	$\frac{u}{u_m}$
0	1.00	0	1.0
0.10	0.979	0.105	0.979
0.20	0.940	0.209	0.940
0.30	0.897	0.314	0.897
0.40	0.842	0.419	0.842
0.50	0.782	0.524	0.782
0.60	0.721	0.628	0.721
0.70	0.660	0.733	0.660
0.80	0.604	0.838	0.604
0.90	0.538	0.942	0.538
1.00	0.474	1.048	0.474
1.10	0.411	1.150	0.411
1.20	0.357	1.255	0.357
1.30	0.300	1.360	0.300
1.40	0.249	1.465	0.249
1.50	0.200	1.570	0.200
1.60	0.165	1.675	0.165
1.70	0.125	1.780	0.125
1.80	0.095	1.880	0.095
1.90	0.067	1.990	0.067
2.00	0.046	2.100	0.046
2.10	0.030	2.200	0.030
2.20	0.020	2.300	0.020
2.30	0.009	2.400	0.009
2.40	0	2.510	0

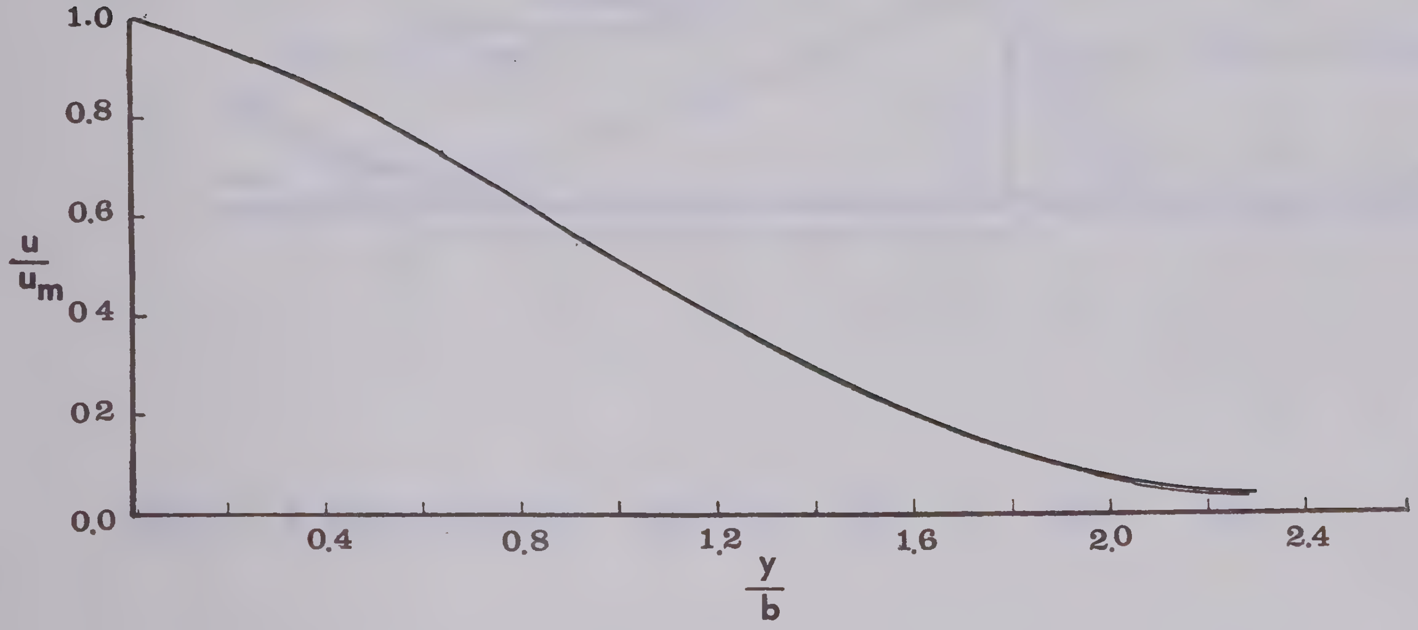

FIG. I-3. PLANE TURBULENT FREE JET-TOLLMIEN SOLUTION

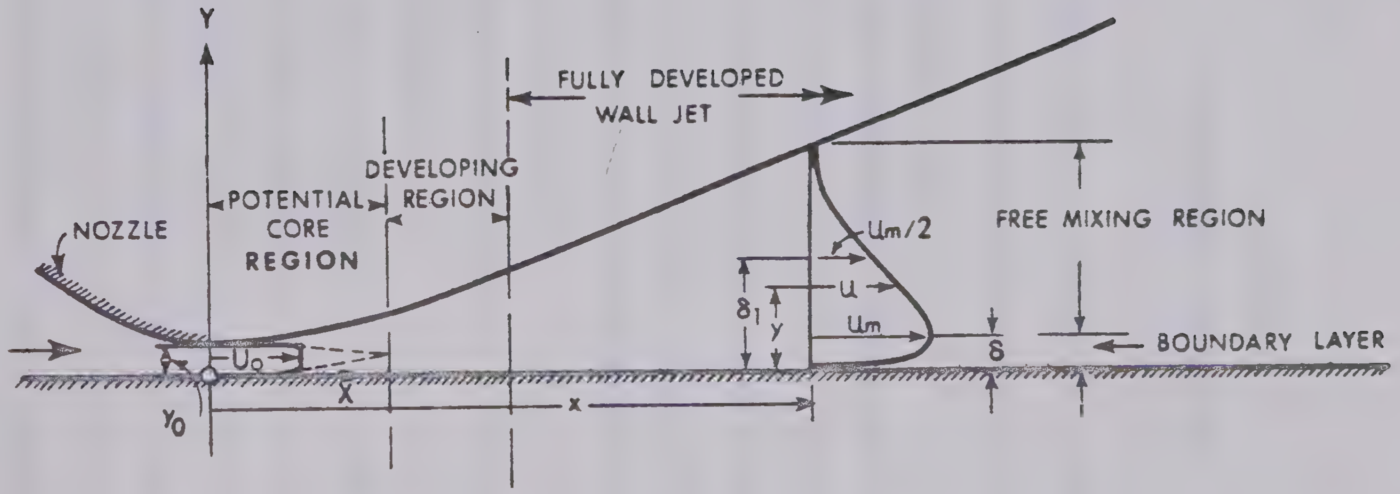

FIG. I- 4. DEFINITION SKETCH OF A WALL JET

CHAPTER II

EXPERIMENTAL FACILITIES

2.1 General

This chapter describes the experimental arrangement, instruments used and the limitations of the observed data.

2.2 Experimental Set-up

The experimental investigation was carried out in three flumes, Flume A, Flume B and Flume C. Flume A was 18 in. wide, 36 in. deep and 16 ft. long with a horizontal aluminum bottom and plexiglass sides. Fig. II-1 gives a schematic representation of Flume A. The setup consisted of a recirculating system with a head tank with stilling arrangements, an upstream control gate, a downstream control gate and a sump. A calibrated orifice meter in the supply line was used to measure the discharge.

The upstream gate-slot was used to install any desired type of outlet, for example, a nozzle, a sluice gate etc. The downstream gate was used for controlling the tailwater elevation. Piezometer holes of 1/8 in. diameter were provided along the center line of the flume at 3 in. intervals. Bed pressures were recorded by connecting the piezometers to a manometer board. Baffle walls of 1 in. and 2 in. heights were used in the flume to measure the form drag.

Flume B was used to measure the mean flow characteristics of forced hydraulic jumps on horizontal beds and the free and submerged hydraulic jumps on bed slopes 15% and 25%. It consisted of a flume 12.25 in. wide, 24 in. high and 16 ft. long with glass walls and smooth brass bed. Fig. II-2 shows the set-up. The flume was fed by the laboratory main supply line and discharged into the sump. The tail water level was controlled by a downstream flap gate. The discharge was measured by a calibrated orifice meter.

Flume C was used to observe the mean flow characteristics of free and submerged hydraulic jumps formed on sloping channels of 5% and 10% slope. It consisted of a 6 in. wide, 12 in. deep and 8 ft. long flume with plexiglass bottom and sides. This flume has got tilting arrangement to set it at slopes of 5%, 10% and 15%. The flume consisted of a recirculation system with a head tank with stilling arrangements, an upstream valve to control the discharge, a downstream flap gate and a sump.

2.3 Measurements

The main instruments used in collecting the data are, point gauges for depth, Prandtl -type Pitot-static tubes and pitch probe for velocity and Preston tube (Preston 1954) for boundary shear measurements. The instruments were mounted on a traverse which could be positioned with an accuracy of 1/1000 ft.in the longitudinal direction and 1/1000 ft. in the transverse direction.

2.3.1 Depth

The depth measurements were made using point gauges which could be read to an accuracy of 1/1000 ft. The water surface elevations were normally measured along the centre line.

2.3.2 Velocity

The velocity observations were made with commercial Prandtl - type Pitot-static tubes of 3 mm. external diameter. No corrections were made for turbulence, displacement and viscous effects.

A Pitot-static tube is insensitive to angle of attack less than about 5 degrees and gives an error of about 4% at 15 degrees. To measure the velocity vector in a highly inclined flow region, a pitch probe made of three 3 mm. tubes with a total nose angle of 90 degrees was used.

2.3.3 Discharge

The discharge was measured with the commercial orifice meter located in the supply line (Flumes A & B)

2.3.4 Bed Shear Stress

Bed shear stress along the centre line of the jumps was measured using a Preston tube [29] 3 mm. external diameter and having a ratio of internal to external diameter of 0.67. Some shear stress measurements were made with a Prandtl -type Pitot tube, as it was observed by Rajaratnam [37] that a Prandtl -type Pitot-static tube can

also be used for bed shear measurements like a Preston tube. The calibration curve used for calculating the bed shear stress τ_o, was that computed by Patel [26] which is slightly different from that computed originally by Preston [29]. The use of the Preston tube for shear measurements is based on the fact that, in all shear flows past a wall, there is a region of local dynamical similarity near the wall such that when a tube of small diameter is placed on the surface, the dynamic pressure recorded by the tube is related to the local shear by the relation,

$$\frac{\nabla p d^2}{4\rho\nu^2} = f\left[\frac{\tau_o d^2}{4\rho\nu^2}\right] \qquad (2.1)$$

where d is external diameter of Preston tube

ρ is mass density

ν is kinematic viscosity of fluid

∇p is differential pressure between the Preston tube and the static pressure on the wall

For the present purpose, equation (2.1) as evaluated by Patel [26] shown in Fig. II-3 was used in preparing a simple plot showing the relationship between τ_o and ∇p in inches depth of water.

2.3.5 Pressure Field

In order to measure the pressure distribution along the centre line of the channel, the piezometer holes were connected to a manometer

board and the corresponding pressures were computed.

2.3.6 Flow Visualisation

Colour injection and tuft probes were used for flow visualisation and qualitative descriptions.

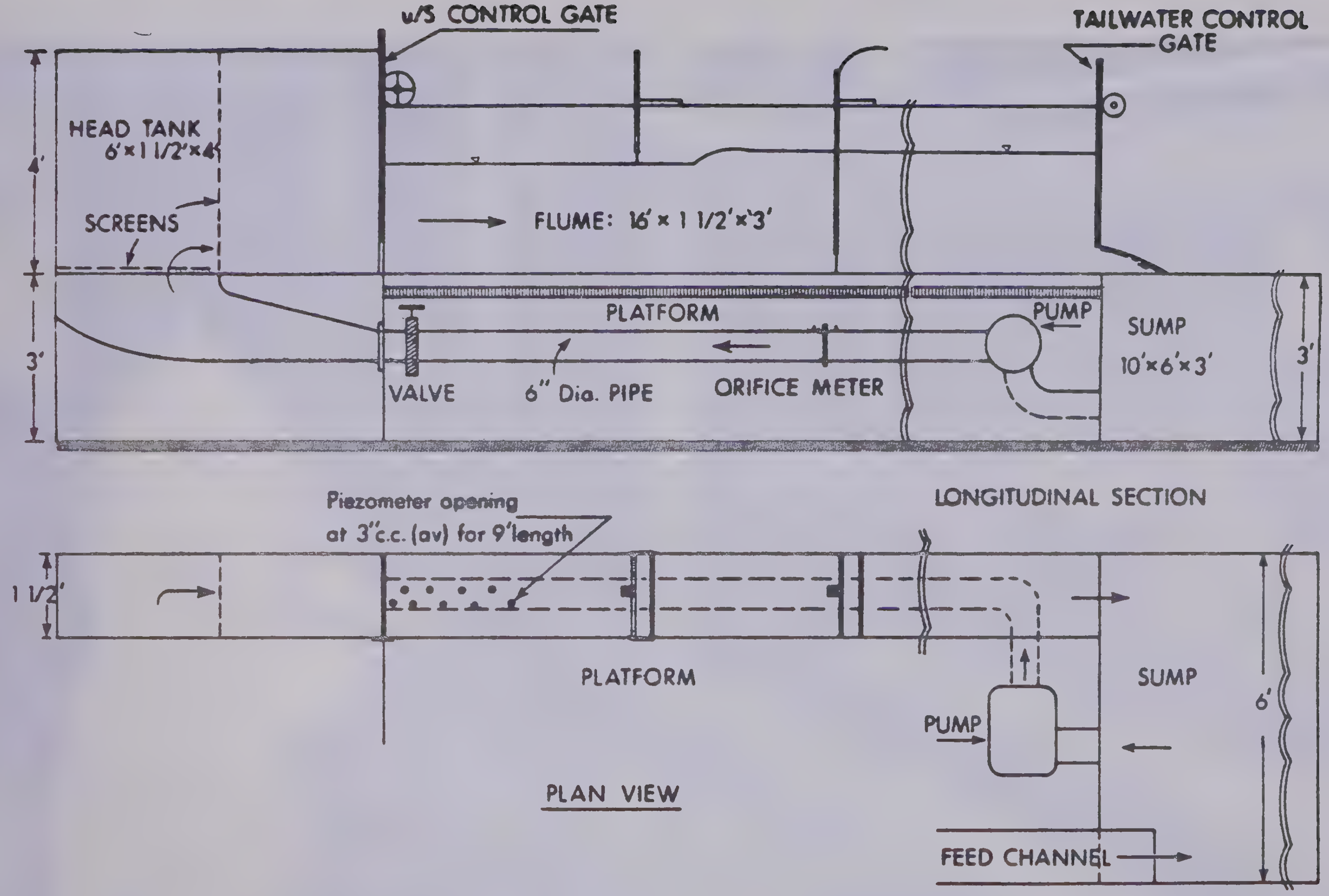

FIG. II-1. SCHEMATIC VIEWS OF THE EXPERIMENTAL SET-UP FLUME : A.

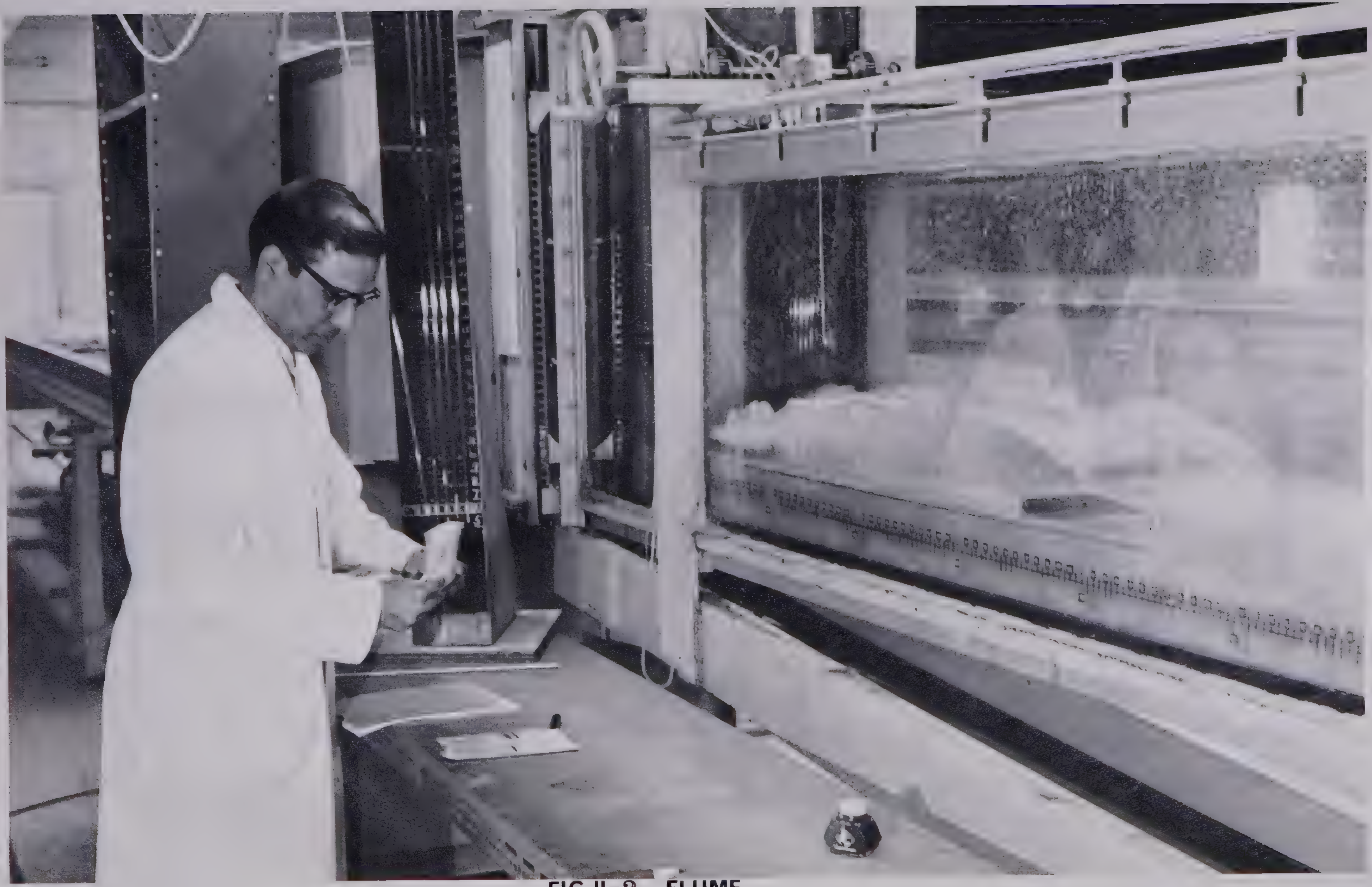

FIG.II-2 FLUME

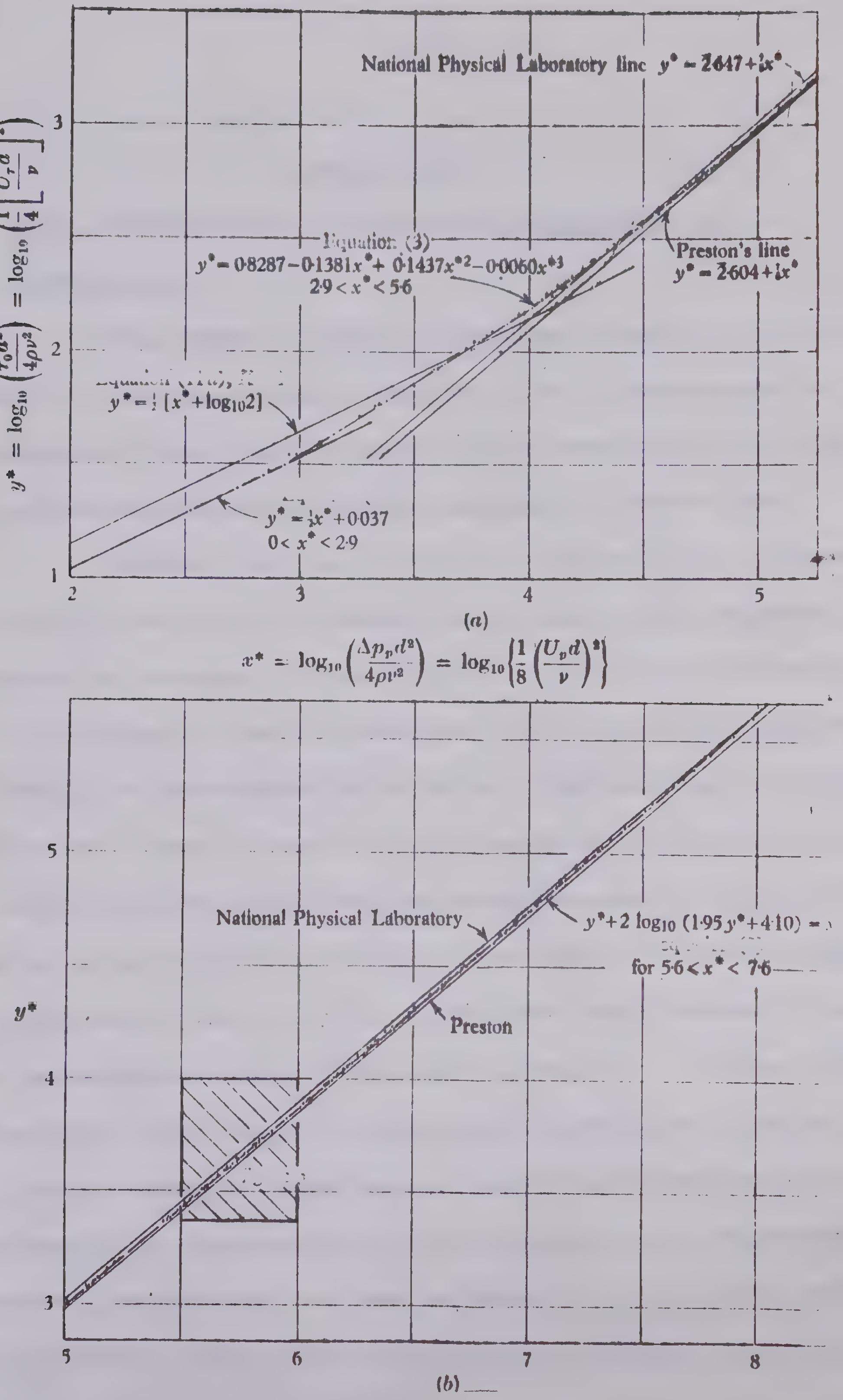

FIG. II-3. CALIBRATION OF PRESTON TUBES

CHAPTER III

PLANE TURBULENT WALL JETS WITH FINITE SUBMERGENCE

3.1 Introduction

This chapter presents an analytical basis for the diffusion of wall jets issuing through sluice gates into a finite depth of standing water downstream. The theoretical developments have also been correlated with the available experimental observations.

Consider the case of a plane turbulent jet of uniform velocity U_o, and depth y_o, issuing from a sluice gate tangential to the horizontal bed as shown in Fig. III-1(a). The outlet is submerged under finite depth of water downstream. The flow picture consists of a diffusing jet superimposed by a roller. The behaviour of plane turbulent wall jets in semi infinite expanse of the same fluid and with zero pressure gradient has been extensively studied [14,32,44,46] whereas the wall jet problems occurring in the field of hydraulic engineering often have a finite depth of submergence which induces, in some cases appreciable backward flow above the wall jet. Further, these problems more often impose adverse pressure gradients on the wall jet. Even though a number of experimental studies have been conducted on these aspects in the recent years [30.31,32,34,35], a comphrehensive theoretical analysis has not been performed and this chapter presents such an analysis along with a correlation of the above theory with the available experimental observations.

3.2 Theoretical Considerations

3.2.1 Plane Turbulent Wall Jets with Zero Pressure Gradient

Considering plane turbulent wall jets with finite submergence but with an essentially zero pressure gradient, i.e. a level water surface in the direction of flow, firstly the reverse flow near the water surface is neglected and the forward flow is analysed. In the last section the shear on the bed is relaxed and the reverse flow is included in the analysis.

For the first analysis, neglecting the reverse flow, and with reference to Fig. III-1(a), the relevant Reynolds equations could be written as

$$u \frac{\partial u}{\partial x} + v \frac{\partial u}{\partial y} = - \frac{1}{\rho} \frac{\partial p}{\partial x} + \frac{1}{\rho} \frac{\partial}{\partial y} [\tau_1 + \tau_t] - \frac{\partial \overline{u'^2}}{\partial x} \tag{3.1}$$

$$u \frac{\partial v}{\partial x} + v \frac{\partial v}{\partial y} = - \frac{1}{\rho} \frac{\partial p}{\partial y} - \frac{\partial \overline{u'v'}}{\partial x} - \frac{\partial \overline{v'^2}}{\partial y} \tag{3.2}$$

$$\frac{\partial u}{\partial x} + \frac{\partial v}{\partial y} = 0 \tag{3.3}$$

where certain obviously negligible terms have been left out and u and v are the turbulent mean velocities in the x (longitudinal) and y (normal) directions, u' and v' are the corresponding velocity fluctuations, $\tau_1 = \mu \frac{\partial u}{\partial y}$ and $\tau_t = - \rho \overline{u'v'}$, p is the mean turbulent piezometric pressure, ρ is the mass density of the fluid and μ is the coefficient of dynamic viscosity.

From the nature of the flow and from earlier experimental observations, one could assume that v<<u and gradients in the x direction are much smaller than the corresponding gradients in the y direction in a major portion of the flow. With these assumptions, Eq. (3.2) reduces to

$$\frac{\partial p}{\partial y} = - \frac{\partial}{\partial y} \rho \overline{v'^2} \qquad (3.4)$$

Integrating

$$p = p_o - \rho \overline{v'^2} \qquad (3.5)$$

where p_o is the piezometric pressure on the bed. Substituting Eq. (3.5) into Eq. (3.2) and rearranging

$$u \frac{\partial u}{\partial x} + v \frac{\partial u}{\partial y} = - \frac{1}{\rho} \frac{dp_o}{dx} + \nu \frac{\partial^2 u}{\partial y^2} + \frac{1}{\rho} \frac{\partial \tau_t}{\partial y} - \frac{\partial}{\partial x} [\overline{u'^2} - \overline{v'^2}] \qquad (3.6)$$

It appears reasonable to neglect the last term and hence the equations of motion for the zero pressure gradient case become

$$u \frac{\partial u}{\partial x} + v \frac{\partial u}{\partial y} = \nu \frac{\partial^2 u}{\partial y^2} + \frac{1}{\rho} \frac{\partial \tau_t}{\partial y} \qquad (3.7)$$

$$\frac{\partial u}{\partial x} + \frac{\partial v}{\partial y} = 0 \qquad (3.8)$$

Based on available experimental observations (34, 35) one could write

$$\frac{u}{u_m} = f\left[\frac{y}{b}\right] = f(\eta) \qquad (3.9)$$

where u_m is the maximum velocity at any section, known as the velocity scale, b is the length scale, defined here as the value of y where $u = \frac{1}{2} u_m$ and $\frac{\partial u}{\partial y}$ is negative. Using the continuity equation, one could show that

$$v = u_m b' \int_o^\eta \eta f' \, d\eta - b u_m' \int_o^\eta f \, d\eta \qquad (3.10)$$

where the primes on b and u_m denote differentiation with respect to x. Based on the observations on turbulent jets and wall jets, one could further assume

$$\frac{\tau_t}{\rho u_m^2} = g(\eta) \qquad (3.11)$$

Using the above expressions, the equation of motion could be reduced to the form

$$g' = \frac{b u_m'}{u_m} f^2 - b' \eta f f' + b' f' \int_o^\eta \eta f' \, d\eta$$
$$- \frac{b u_m'}{u_m} f' \int_o^\eta f \, d\eta - \frac{\nu}{b u_m} f'' \qquad (3.12)$$

where the primes on f and g denote differentiation with respect to η. In most of the problems of practical interest, $\frac{bu_m}{\nu}$ is bound to be very large and hence the last term in Eq. 3.12 could be neglected in a major portion of the wall jet.

From Eq. 3.12, one could write

$$b' \propto x^o \tag{3.13}$$

$$\frac{bu_m'}{u_m} \propto x^o \tag{3.14}$$

If

$$u_m \propto x^p \tag{3.15}$$

$$b \propto x^q \tag{3.16}$$

Eq. 3.13 gives q = 1. Eq. 3.14 also gives q = 1. To evaluate the second exponent p, one could develop the integral momentum equation.

Integrating Eq. 3.7 with respect to y from y = 0 to y_* which is above the level where u is assumed to become zero, [see Fig. III-1(a)].

$$\frac{d}{dx}\int_o^{y_*} \rho u^2 \, dy = - \tau_o \tag{3.17}$$

where τ_o is the bed shear stress. Neglecting τ_o,

$$\frac{d}{dx} \int_{o}^{y_*} \rho u^2 \, dy = 0 \tag{3.18}$$

Eq. 3.18 could be rewritten as

$$\frac{d}{dx} \rho \, b u_m^2 \int_{o}^{y_*} f^2 \, d\eta = 0 \tag{3.19}$$

Eq. 3.19 gives

$$b u_m^2 \propto x^o \tag{3.20}$$

or

$$\text{i.e.} \quad \left.\begin{array}{l} q + 2p = 0 \\ \\ p = -\frac{1}{2} \end{array}\right\} \tag{3.21}$$

The above analysis is essentially the same as that of Schwarz and Cosart (44) for the wall jet with large submergence.

At this stage, it is interesting to use some dimensional arguments to derive once again some expressions for the scales. As in the case of jet problems, the momentum flux M_o, which is preserved in the x direction (if τ_o is neglected) appears to be the dominant factor in this phenomenon. Hence, one could possibly write

$$u_m = f\ [M_o, \rho,\ x] \qquad (3.22)$$

Using the π- theorem, one could show that

$$\frac{u_m}{\sqrt{M_o/\rho x}} = \text{constant } C \qquad (3.23)$$

or

$$\frac{u_m}{U_o} = \frac{C_1}{\sqrt{x/b_o}} \qquad (3.24)$$

where b_o is the height of the nozzle producing the wall jet, U_o is the uniform velocity at the nozzle and C_1 is an empirical constant. Similarly one could show

$$b = C_2\ x \qquad (3.25)$$

and

$$\frac{\tau_o}{M_o/x} = C \qquad (3.26)$$

or

$$\frac{\tau_o}{\rho U_o^2/2} = \frac{C_3}{x/b_o} \qquad (3.27)$$

where C, C_2 and C_3 are empirical coefficients. Strictly speaking C_3 is a function of the Reynolds number. The experimental observations of Rajaratnam and Subramanya (34,35) on plane turbulent wall jets with zero pressure gradient but with finite depth of submergence have shown that the velocity distribution is similar [See Fig. III-2]. The variation of b with $\overline{x}$ has been found to be linear as shown in Fig. III-3(a) and is described by the equation

$$b = 0.097\ x \tag{3.28}$$

where x is the distance measured from the virtual origin, located at a distance of about $5b_o$ behind the nozzle and $\overline{x}$ is the distance measured from the nozzle. Fig. III-3(b) shows a plot of $[U_o/u_m]^2$ versus $\overline{x}/b_o$ where again the relationship is linear as predicted by the analytical considerations and the equation for the velocity scale could be written as

$$\frac{u_m}{U_o} = \frac{4.0}{\sqrt{\overline{x}/b_o}} \tag{3.29}$$

Fig. III-3(c) shows the variation of $1/\tau_o$ with $\overline{x}/b_o$ and it is seen that the points could be described by a straight line having the equation

$$\tau_o = 0.075 \frac{\rho U_o^2}{2} \cdot \frac{1}{x/b_o} \qquad (3.30)$$

for Reynolds number R_1 in the range $10^4 - 10^5$

3.3 Plane Turbulent Wall Jet with Pressure Gradient

Fig. III-1(b) is a schematic representation of a submerged jump [with a moderate value of the submergence factor (16)] which is a good example of the plane turbulent wall jet with finite submergence and adverse pressure gradient. The free jump [Fig. III-1(c) could also be studied under this category. Once again neglecting the backward flow in the surface roller and making the boundary layer type assumptions as in the earlier section, the equations of motion simplify to the form

$$u \frac{\partial u}{\partial x} + v \frac{\partial u}{\partial y} = - \frac{1}{\rho} \frac{dp_o}{dx} + \nu \frac{\partial 2_u}{\partial y^2} + \frac{1}{\rho} \frac{\partial \tau_t}{\partial y} \qquad (3.31)$$

and

$$\frac{\partial u}{\partial x} + \frac{\partial v}{\partial y} = 0 \qquad (3.32)$$

The velocity distribution in the submerged jumps has been found to be similar (31) and hence one could write

$$\frac{u}{u_m} = f \left[\frac{y}{b}\right] = f \left[\eta\right] \qquad (3.33)$$

Further, assume

$$\frac{\tau_t}{\rho u_m^2} = g\ (\eta) \tag{3.34}$$

The pressure profile on the bed is known to be essentially the same as the surface profile and if $\bar{y}$ is the depth of flow at any section, i.e.

$$p_o(x) = \gamma\ \bar{y} \tag{3.35}$$

Let

$$p_o = \gamma\ [y_t - \overset{*}{y}] \tag{3.36}$$

where $\overset{*}{y} = \overset{*}{y}\ (x)$ [see Fig. III-1 (b and c)] and y_t is the tailwater depth.

Substituting the above expressions into the equation of motion and simplifying

$$g' = \frac{bu_m'}{u_m}\ f^2 - b'\ \eta ff' + b'f' \int_0^\eta \eta f'\ d\eta - \frac{bu_m'}{u_m}\ f' \int_0^\eta f\ d\eta$$

$$- \frac{b}{u_m^2}\ \frac{\gamma}{\rho}\ \overset{*}{y}{}' + \frac{\nu}{bu_m}\ f'' \tag{3.37}$$

The last term in Eq. 3.37 is neglected as before. Then for similarity,

$$b' \propto x^0 \tag{3.38}$$

$$\frac{b u_m'}{u_m} \propto x^0 \tag{3.39}$$

$$\frac{b}{u_m^2} \overset{*}{y}' \propto x^0 \tag{3.40}$$

If,

$$u_m \propto x^p \tag{3.41}$$

$$b \propto x^q \tag{3.42}$$

and

$$\overset{*}{y} \propto x^r \tag{3.43}$$

Eqs. 3.38 and 39 give $q = 1$. Considering Eq. 3.40,

$$\left.\begin{array}{l} x^{q - 2p + r - 1} \propto x^0 \\ \text{or} \\ r = 2p \end{array}\right\} \tag{3.44}$$

Dimensional considerations (as shown later in this section) indicate that p = - 1/2. Then, using Eq. 3.44, r = - 1.0. Hence for similarity

$$u_m \propto \frac{1}{\sqrt{x}}$$

$$b \propto x \qquad (3.45)$$

$$y^* \propto \frac{1}{x}$$

A consideration of the integral momentum equation (neglecting the bed shear stress) showed that the prediction of the exponents based on the integral momentum equation would agree with Eq. 3.45 only when the momentum flux is much larger than the piezometric pressure.

Using dimensional considerations if it is assumed that the pressure plus momentum is the dominant parameter describing the flow, one could obtain the following relations

$$\frac{u_m}{U_o}\sqrt{\frac{x}{b_o}} = C_4\left[1 + \frac{1}{2F_1^2}\right]^{1/2} \qquad (3.46)$$

$$\frac{\tau_o}{\rho U_o^2/2} \cdot \frac{x}{b_o} = C_5\left[2 + \frac{1}{F_1^2}\right] \qquad (3.47)$$

for the free jump and

$$\frac{u_m}{U_o}\sqrt{\frac{x}{b_o}} = C_6\left[1 + \frac{1}{2F_1^{\,2}}\cdot\left(\frac{y_3}{b_o}\right)^2\right]^{1/2} \tag{3.48}$$

and

$$\frac{\tau_o}{\rho U_o^{\,2}/2}\ \frac{x}{b_o} = C_7\left[2 + \frac{1}{F_1^{\,2}}\ \left(\frac{y_3}{b_o}\right)^2\right] \tag{3.49}$$

for the submerged jump, where y_3 is the backed-up depth at the nozzle and C_4 to C_7 are empirical coefficients and F_1 is the supercritical Froude number. It should be noted that $b_o = y_1$, and y_1 is retained because of its frequent use in describing hydraulic jumps.

The experimental observations of Rajaratnam [31] have shown that the velocity distribution in the jump is similar [see Fig. III-4] and the length has been found to vary linearly with the distance from the beginning of the jump, Fig. III-7. Data from three typical runs of Ref. 31 are plotted in Fig. III-5(a) with $^1/y^*$ versus $\overline{x}$, which is indeed linear in the region under consideration. A detailed discussion regarding the profile of the jump could be found in (36). Fig. III-5(b) shows that in a certain region of the jump (i.e. for $\frac{\overline{x}}{y_1}$ up to about 30, $[\frac{u_o}{u_m}]^2$ varies linearly with $\overline{x}/b_o$, thereby showing that $u_m \propto \frac{1}{\sqrt{x}}$. Fig. III-5(c) shows that τ_o varies as $\frac{1}{x}$ is predicted by the theoretical considerations. Using the results of dimensional analysis and the experimental results of Ref. 31, the following two

equations have been developed

$$\frac{u_m}{U_o} \simeq \frac{2.4}{\sqrt{x/b_o}} \tag{3.49}$$

$$\frac{\tau_o}{\rho U_o^2/2} = \frac{0.01}{x/y_1} \tag{3.50}$$

wherein the term involving the supercritical Froude number has been left out for the sake of simplicity and x is taken as the distance from the nozzle. If more accurate results are needed, one should use the plots of Ref. 31.

For submerged jumps, in the recent years some observations have been made as student projects at the University of Alberta and one set of these results for $F_1 = 4.62$ and submergence factor S = 0.15, 0.34, 0.62, 0.95, 1.41 and 2.18 (1A to 1F) is considered herein. Fig. III-6(a) shows the results of runs 1A - 1C with $\frac{1}{y^*}$ versus $\bar{x}$ and the runs 1D - 1F, fall under the almost zero pressure gradient case. It is seen from Fig. III-6(a) that $\frac{1}{y^*}$ varies linearly with $\bar{x}$. Fig. III-6(b) shows the variation of $[U_o/u_m]^2$ with $\bar{x}/b_o$ and it is seen that over a certain region of $\bar{x}/b_o$, the extent of which increases with the submergence factor, the variation is reasonably linear. The shear stress results are shown in Fig. III-6(c), where τ_o is plotted against $1/\bar{x}$, and the theoretical prediction is indeed found to be true.

For the submerged jump, if the submergence is not large enough to provide a level surface, the following approximate relations were obtained

$$\frac{u_m}{U_o} = \frac{2.40}{\sqrt{x/y_1}} \left[1 + \frac{1}{2F_1^2} \left(\frac{y_3}{y_1}\right)^2 \right]^{1/2} \tag{3.52}$$

$$\frac{\tau_o}{\rho U_o^2/2} = \frac{0.01}{x/y_1} \left[2 + \frac{1}{F_1^2} \cdot \left(\frac{y_3}{y_1} \right)^2 \right] \tag{3.53}$$

The empirical coefficient 2.40 in Eq. 3.52 was found to decrease as the submergence factor increases and in the above equations, $\bar{x}$ has been taken as x.

It should be mentioned that Eqs. 3.50-53 are given only as rough approximations for simple calculations and for more accurate results, one should refer to Ref. 31 for free jumps and Refs. 16 and 30 for submerged jumps.

3.3.1 Analysis including Reverse Flow

To consider the reverse flow above the wall jet for the zero pressure gradient case, the shear on the bed is relaxed thereby allowing a slip at the bed as shown in Fig. III-8(a). If $\bar{u}_m$ is the backward velocity at the surface, let

$$U = u - \bar{u}_m \tag{3.54}$$

where $\bar{u}_m$ is negative. Based on the few experimental results of Liu (22) and also from experience in treating somewhat similar cases, one could write

$$\frac{U}{U_m} = f\left[\frac{y}{b}\right] = f\,[\bar{\eta}] \tag{3.55}$$

where U_m is the maximum value of U and $\bar{b}$ is the value of y where $U = \frac{1}{2}\,U_m$. Assuming further

$$\frac{\tau_t}{\rho U_m^2} = h\,(\bar{\eta}) \tag{3.56}$$

the equations of motion reduce to the form

$$\begin{aligned} h' = {} & -\bar{b}'\, f' \int_0^{\bar{\eta}} f\, d\bar{\eta} + \frac{\bar{b}\,\bar{u}_m'}{U_m}\,[\,f - \bar{\eta} f'\,] \\ & + \frac{\bar{b}\,U_m'}{U_m}\,[f - f' \int_0^{\bar{\eta}} f\, d\bar{\eta}] + \frac{\bar{b}}{U_m^2}\,\bar{u}_m\bar{u}_m' \\ & + \frac{\bar{b}\,\bar{u}_m U_m'}{U_m^2}\, f - \frac{\bar{b}'\,\bar{u}_m}{U_m}\,\bar{\eta} f' \end{aligned} \tag{3.57}$$

For similarity,

$$\overline{b}' \propto x^{o} \tag{3.58}$$

$$\frac{\overline{b}\,\overline{u}_m'}{U_m} \propto x^{o} \tag{3.59}$$

$$\frac{\overline{b}\,U_m'}{U_m} \propto x^{o} \tag{3.60}$$

$$\frac{\overline{b}\,\overline{u}_m\overline{u}_m'}{U_m^2} \propto x^{o} \tag{3.61}$$

$$\frac{\overline{b}\,\overline{u}_m U_m'}{U_m^2} \propto x^{o} \tag{3.62}$$

If

$$u_m \propto x^{p_1} \tag{3.63}$$

$$\overline{b} \propto x^{q_1} \tag{3.64}$$

$$\overline{u}_m \propto x^{p_2} \tag{3.65}$$

$q_1 = 1.0$ from Eq. 3.58. From Eq. 3.59, $p_1 = p_2$. The other equations of this group do not furnish any other information.

The integral momentum equation could be reduced to the form

$$\frac{d}{dx} \int_{o}^{\bar{y}} [U_m^2 f^2 + \bar{u}_m^2 + U_m \bar{u}_m 2f]\, \bar{b}\, d\bar{\eta} = 0 \tag{3.66}$$

where $\bar{y}$ is the constant depth of flow downstream of the nozzle. A consideration of Eq. 3.66 shows that for $\bar{u}_m < U_m$ and for $\bar{u}_m \simeq U_m$, shows that for

$$\left.\begin{aligned} p_1 &= -\frac{1}{2} \\ p_2 &= -\frac{1}{2} \end{aligned}\right\} \tag{3.67}$$

That is, considering the reverse flow,

$$\left.\begin{aligned} U_m &\propto \frac{1}{\sqrt{x}} \\ \bar{u}_m &\propto \frac{1}{\sqrt{x}} \\ \bar{b} &\propto x \end{aligned}\right\} \tag{3.68}$$

The interesting relation of this group is the manner of variation of $\overline{u}_m$. The results of Rajaratnam (31) and that of Liu (22) shown plotted in Fig. III-8(c) indicate that the theoretical prediction for the variation of $\overline{u}_m$ is not supported by experimental observations. This difficulty could not be resolved and hence the reverse flow for the adverse pressure gradient case was not attempted.

3.4 Conclusions

The plane turbulent wall jet with finite submergence and with or without pressure gradient has been analysed theoretically and the theoretical predictions have been correlated with the available experimental observations. The attempt to analyse the reverse flow has not been successful.

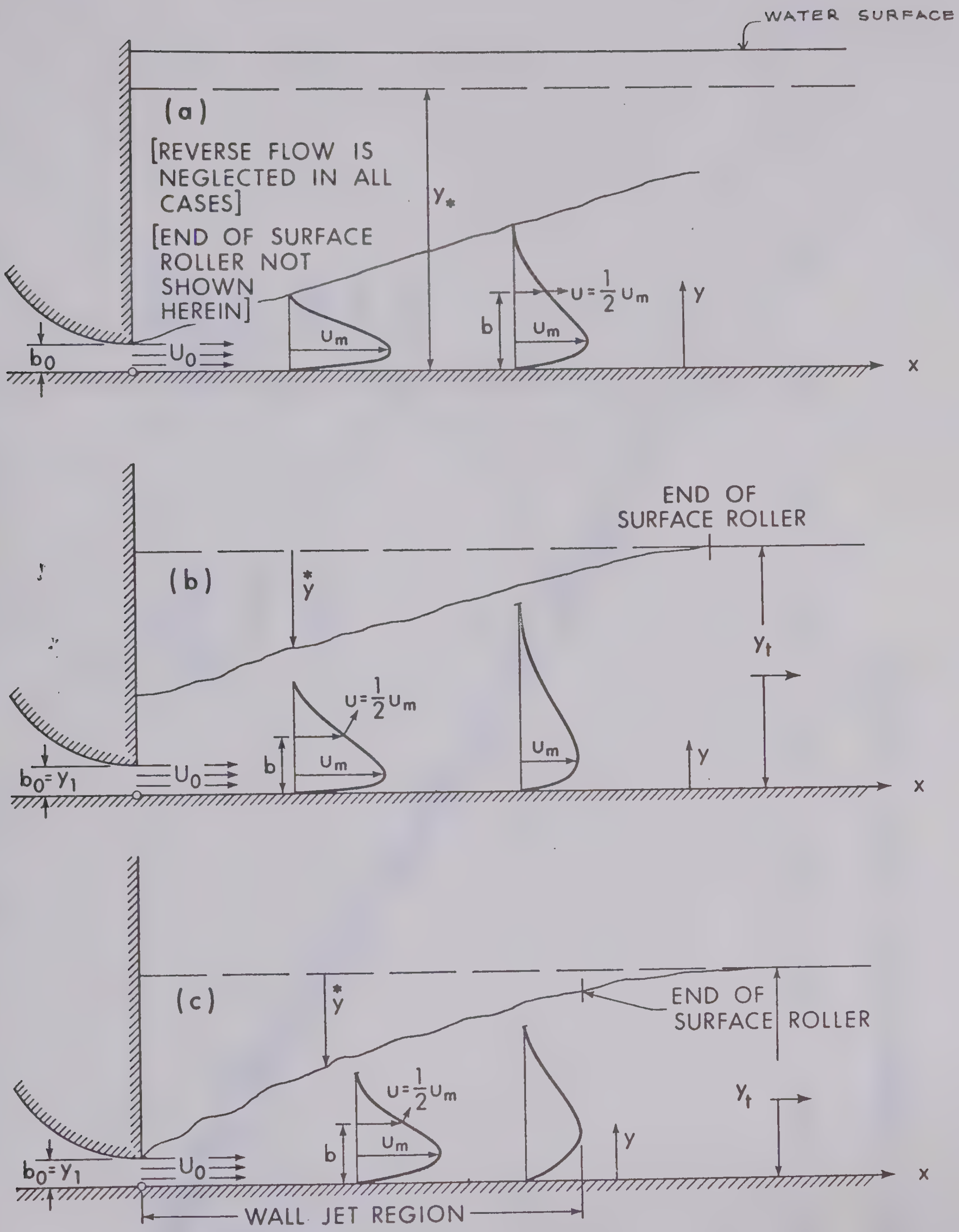

FIG. III-1 DEFINITION SKETCH

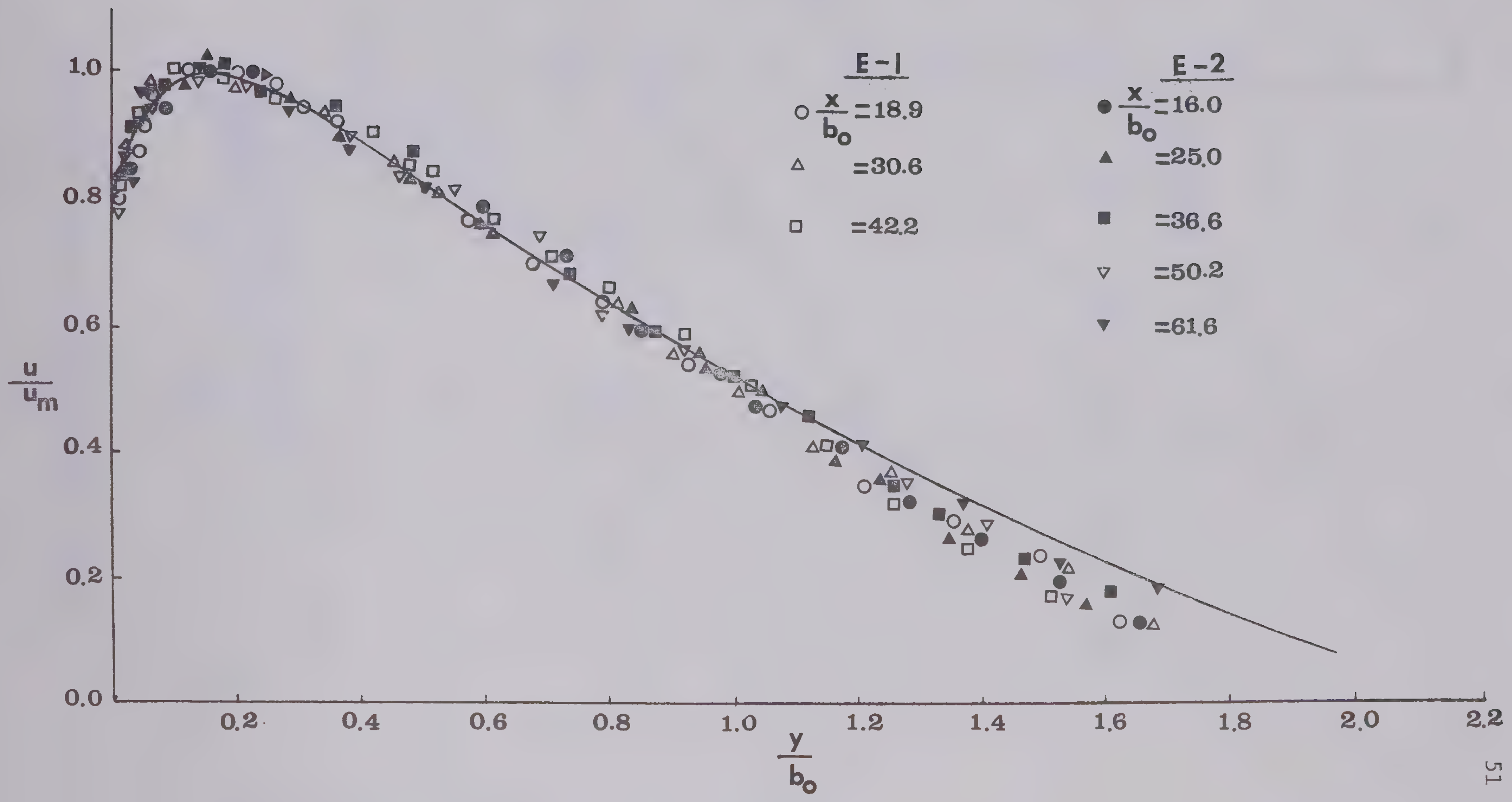

FIG. III-2. DIMENSIONLESS VELOCITY PROFILES

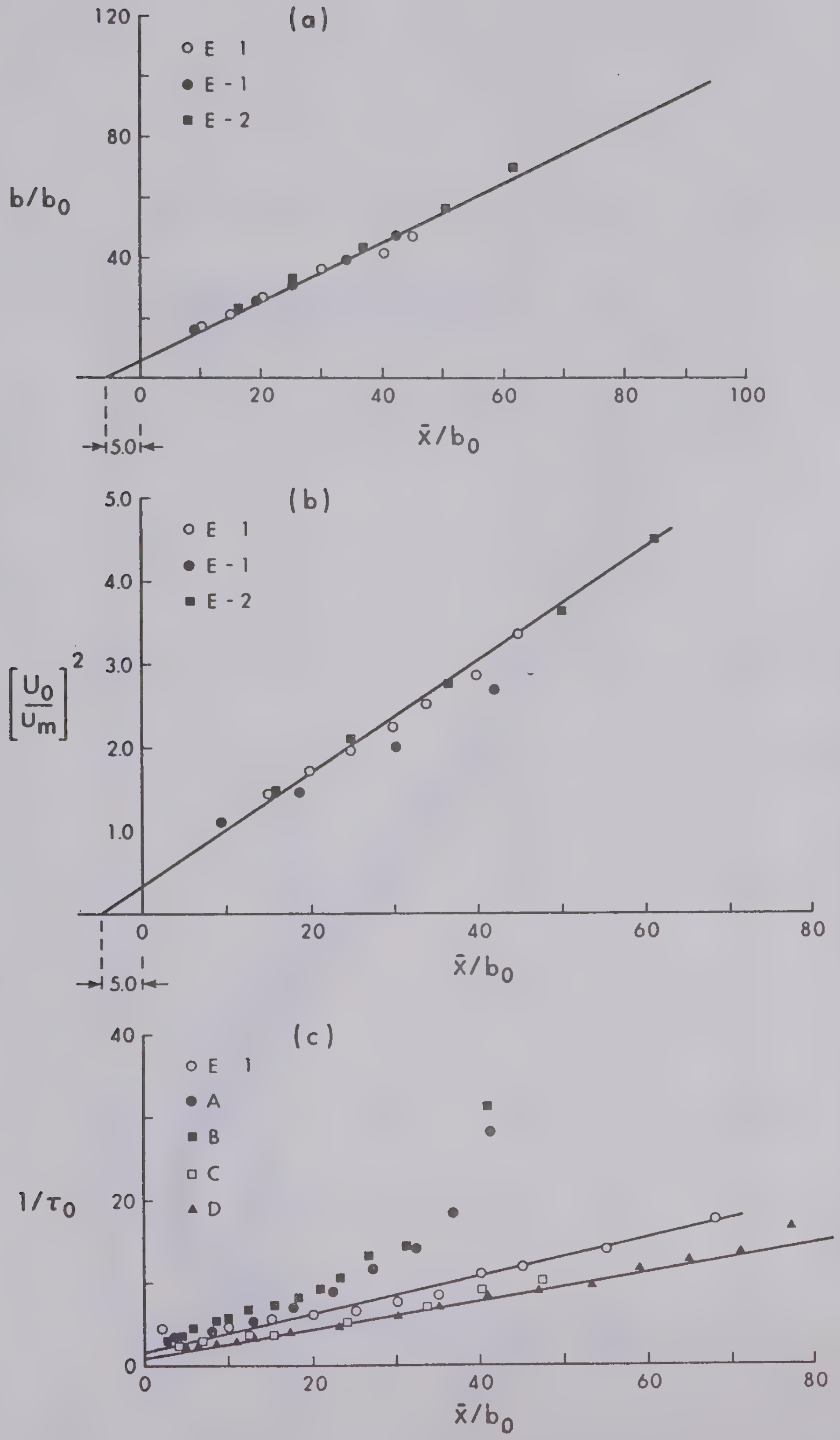

FIG. III-3. DEEPLY SUBMERGED FLOWS

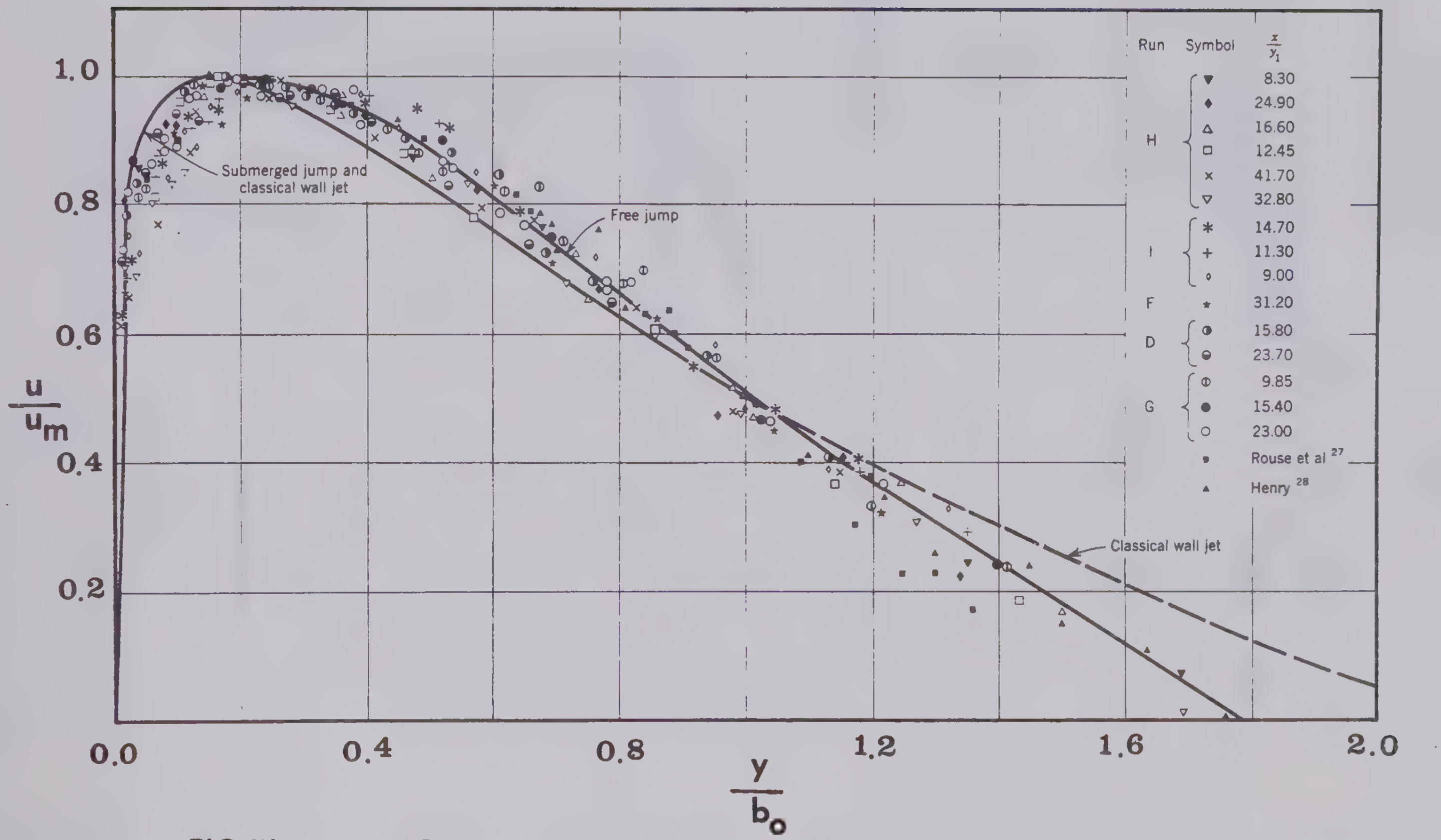

FIG.III-4. VELOCITY DISTRIBUTION IN JUMP

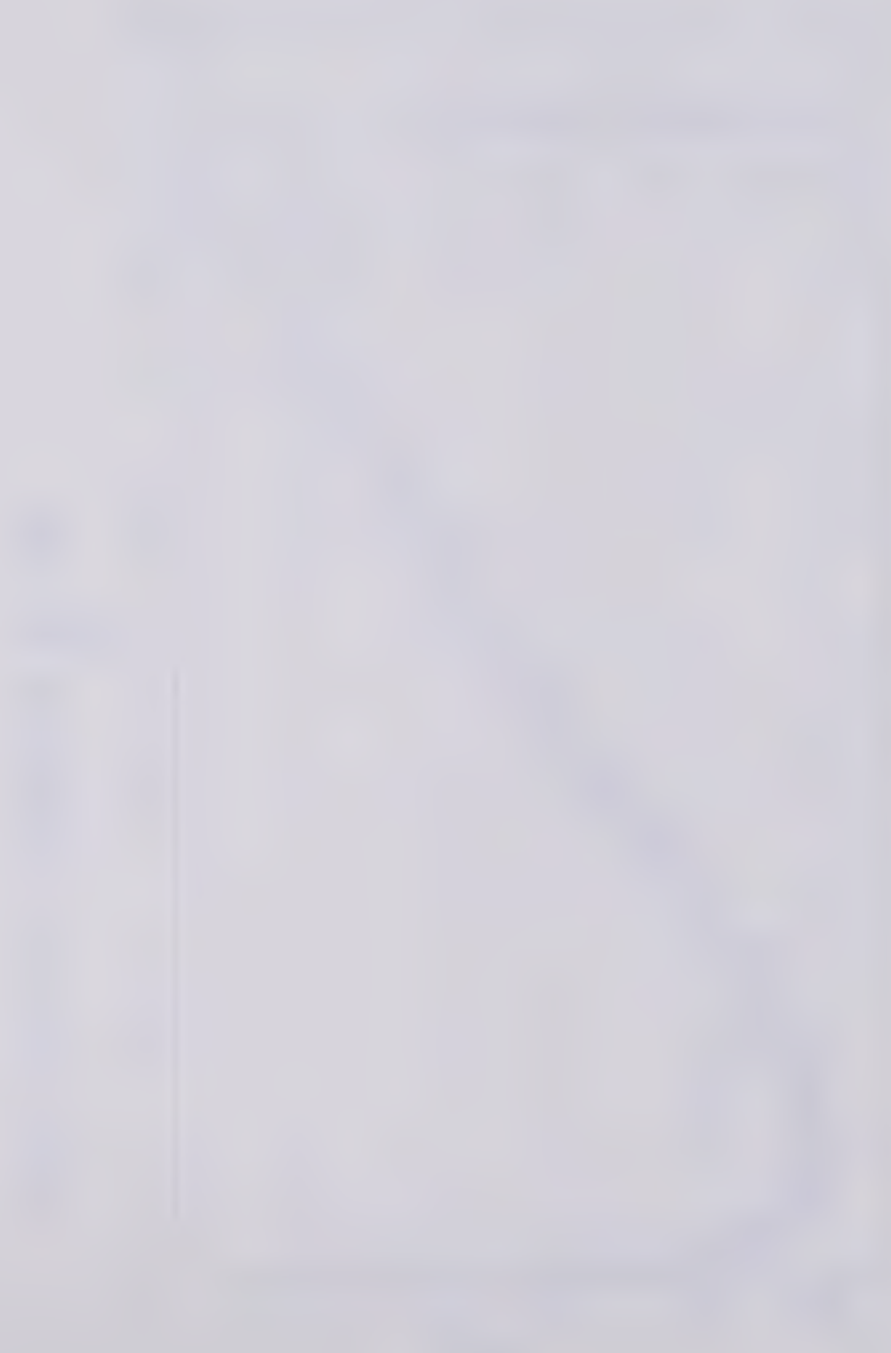

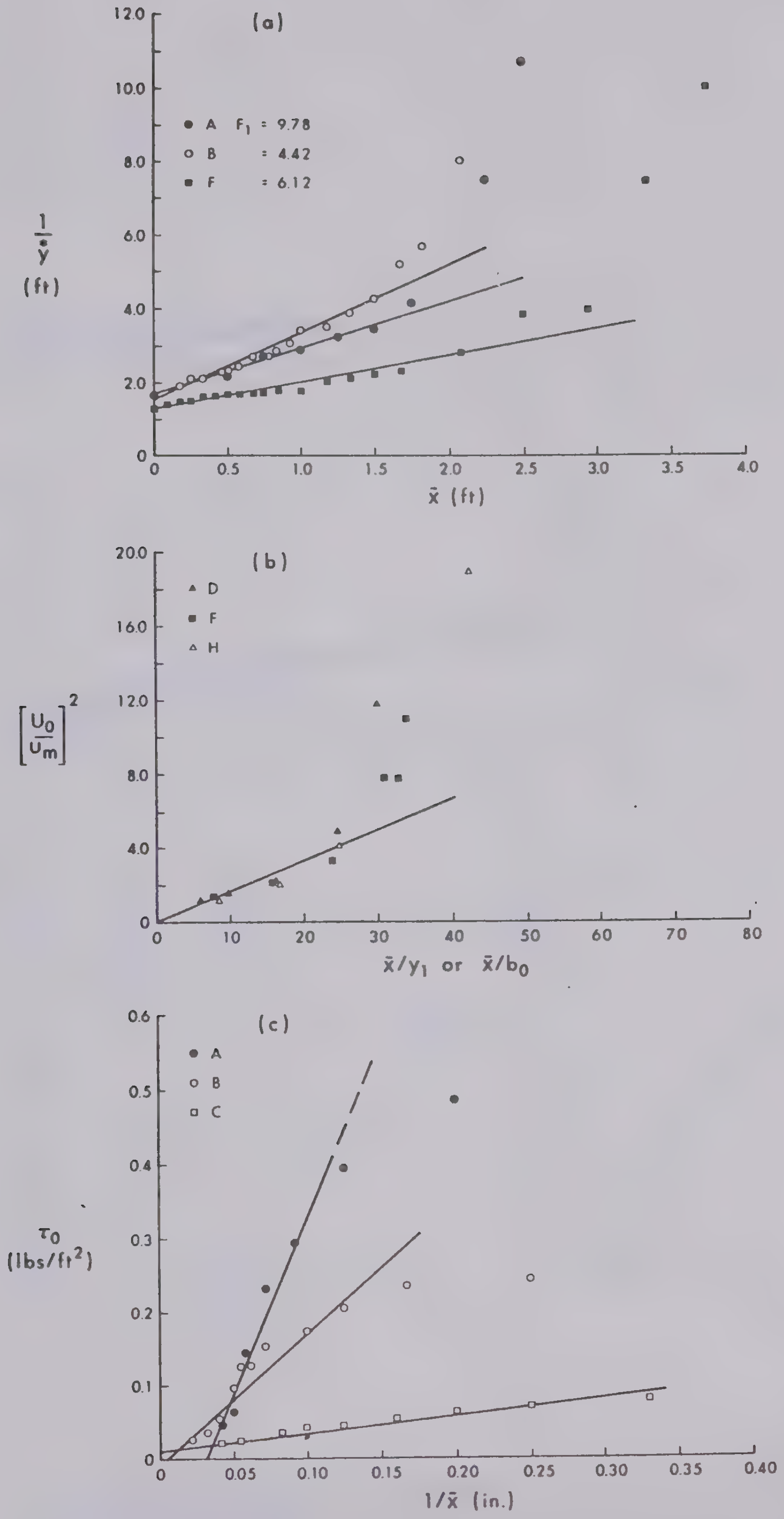

FIG. III-5. THE FREE HYDRAULIC JUMP

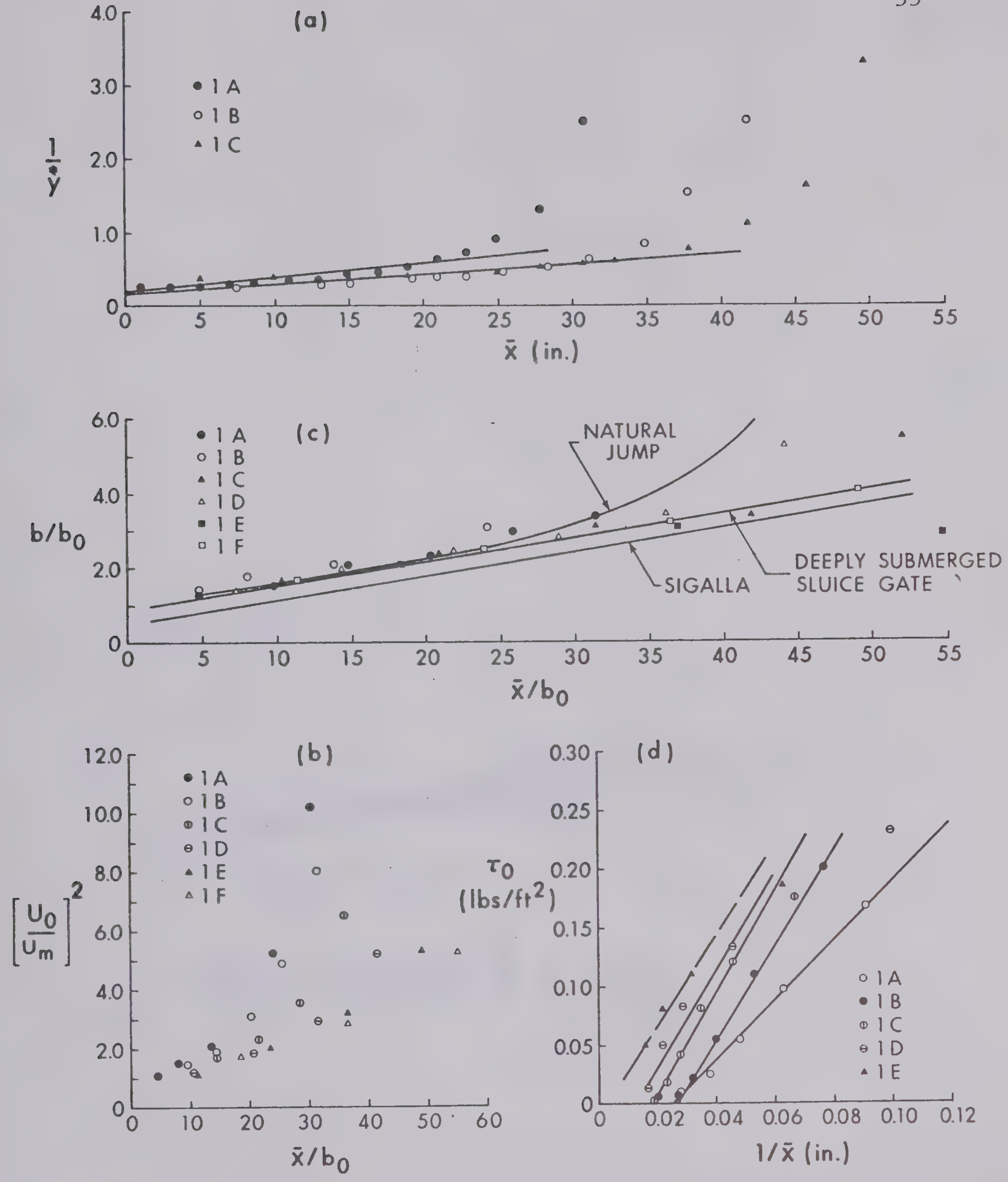

FIG. III-6 SUBMERGED JUMPS

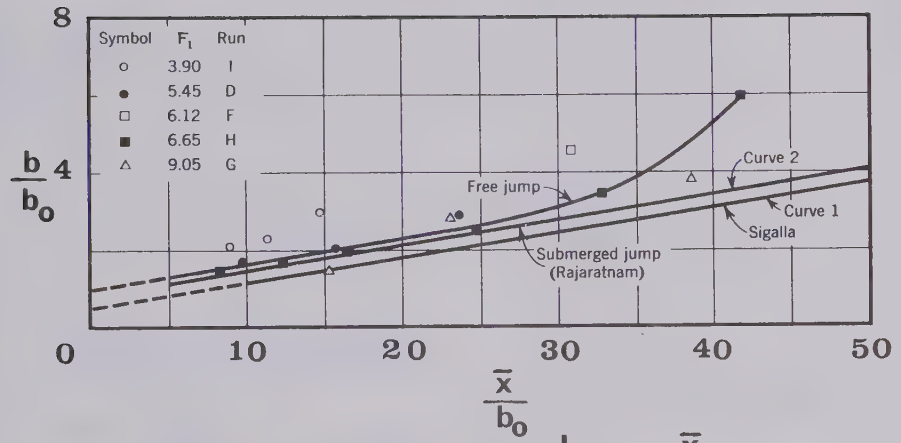

FIG. III-7. VARIATION OF $\frac{b}{b_o}$ with $\frac{\bar{x}}{b_o}$

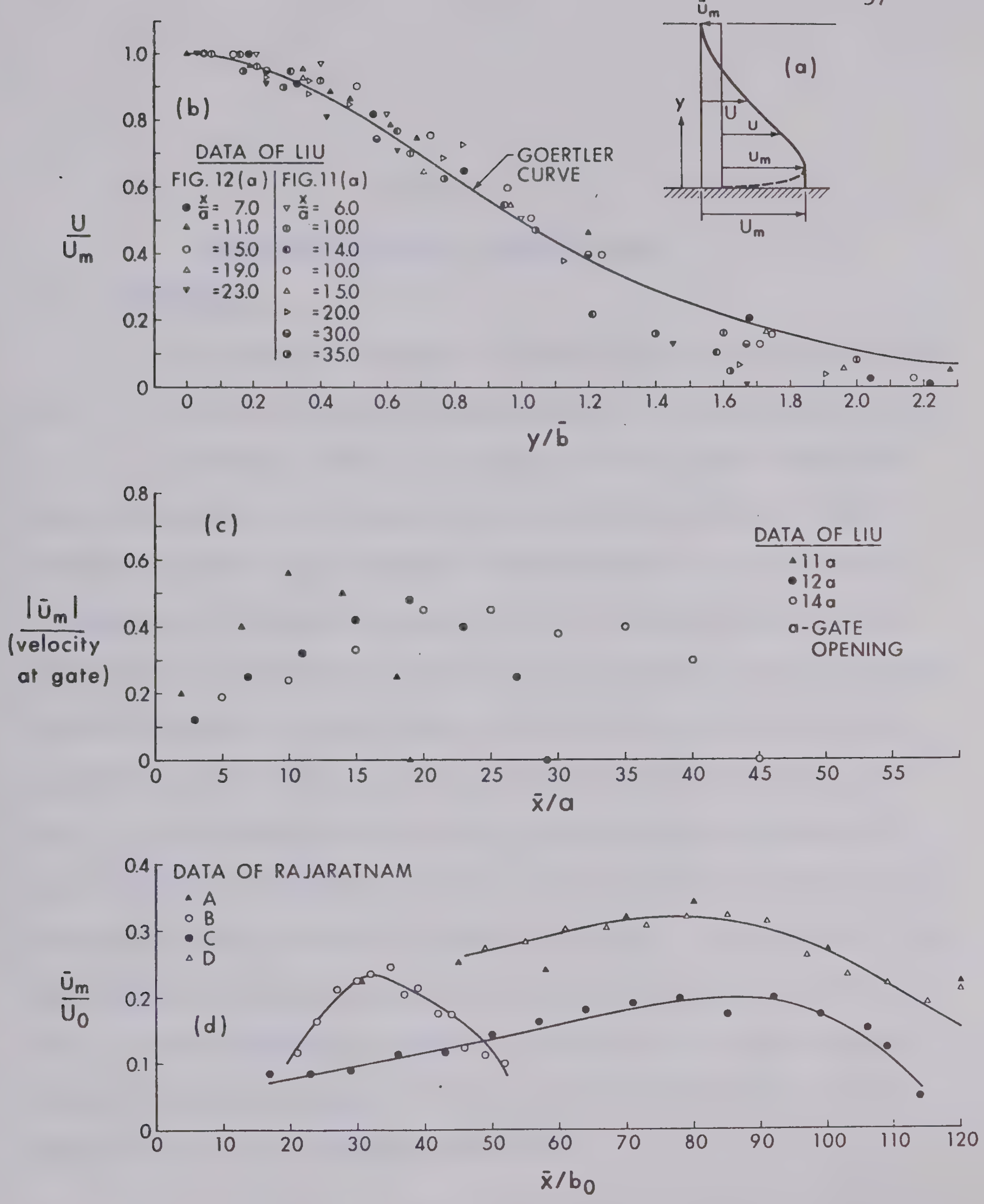

FIG. III-8 DEEPLY SUBMERGED FLOWS WITH REVERSE FLOW

CHAPTER IV

MECHANICS OF SLOPING CHANNEL JUMPS

4.1 Introduction

This chapter presents the study of the mechanics of jumps formed on favourable sloping floors under free and submerged conditions.

Hydraulic jumps on sloping floors are used as hydraulic energy dissipators in a large number of hydraulic structures under suitable tailwater and topographic considerations. A large amount of experimental work has been done on the sloping channel jumps and Kindsvater's semi-empirical equation (20) is generally used for computing the subcritical sequent depth. Fig. IV-1 shows the well-known classification in which y_1 is the supercritical depth normal to the bed, y_1' is its vertical projection, y_2 is the vertical subcritical sequent depth at the end of the jump, taken generally as the end of the surface roller (unless the slope of the bed is very small), y_t is the vertical tailwater depth measured above the horizontal downstream bed, L_j is the horizontal length of the jump and θ is the slope of the bed with the horizontal. For the C-jump, Kindsvater's equation could be written in the Belanger form (38)

$$\frac{y_2}{y_1'} = \frac{1}{2} \left[\sqrt{1 + 8G_1^2} - 1 \right] \tag{4.1}$$

where

$$G_1^2 = \Gamma_1^2 F_1^2$$

and

$$\log_{10} \Gamma_1 = 0.027\,\theta \qquad (4.2)$$

θ being the angle of the bed in degrees and F_1 is the supercritical Froude number at the toe of the jump equal to $U_1/\sqrt{gy_1}$, where U_1 is the mean supercritical velocity and g is the acceleration due to gravity. For the C-jump, $y_2 = y_t$. Eq. 4.1 could be used for D-jumps also with the only difference that $y_t \neq y_2$. The length of the jump has been measured and analysed well by Bradley and Peterka (6).

Apparently no significant attempt has been made to explore the sloping channel jump to study the mean flow patterns, velocity, pressure and bed shear distributions, turbulent fluctuations and turbulent shear. Such a knowledge would be very useful in improving upon the present design methods.

4.2 Review of Previous Work

The problem of hydraulic jump on sloping floors was studied by Riegel and Beebe (1917), Ellms (1927), Yarnell (1934) Rindlaub (1935), Bakhmeteff and Matzke (1936), and Puls (1941). In 1944 a rational approach was presented by Kindsvater. Hickox [18] presented the experimental results of jumps on 1:3 slopes. Dutta (1949) developed design charts for few slopes based on Kindsvater's analysis. An extensive

experimental study of free jumps on sloping floors was made by Bradley and Peterka [6] at U.S.B.R. Flores [11] attempted to develop mathematical solutions for jump characteristics in sloping exponential channels. In 1958 Wigham extended the work of Bradley and Peterka to steeper slopes. Argyropolous [3] presented the experimental results on sloping parabolic and triangular channels. Rajaratnam [38] made a complete reanalysis of the problem with regards to various types of jumps on sloping floors and the available theoretical and experimental developments.

4.3 Experimental Arrangement

The experiments were conducted in two flumes. Flume B and Flume C. The first two series with $\tan\theta = 0.05$ and 0.10 were conducted in Flume C and the last two series with $\tan\theta = 0.15$ and 0.25 conducted in Flume B. Plywood planks were installed to give 15 and 25% slopes. In both the flumes the supercritical stream was provided by sluice gates and necessary tailwater was caused by tailgates.

On the whole thirteen experiments were conducted, five experiments on free jumps and eight experiments on jumps with varied degree of submergence. The Froude number was varied over a range of 6.24 to 8.05 and the Reynolds number $R_1 = \frac{U_1 y_1}{\nu}$ was in the range of 1.93×10^4 to 3.2×10^4. The significant details of the data are given in Table IV-1.

Considering firstly, the sloping channel jump (of the D-type), observations of the water surface profiles showed that as the slope increases, the jump surface appears to become reasonably level, which is distinctly different from the jumps on level floors. Fig. IV-2 shows some typical cases. If the height of the sloping channel jump is taken as h as shown in Fig. IV-1, then h decreases rapidly as the slope increases for a given Froude number. There is a surface roller as in the level channel case. The mean velocity measurements were made only in the forward flow and a few typical velocity distributions are shown in Fig. IV-3.

A careful look at these velocity distributions shows that the supercritical stream diffusing through the jump behaves like a turbulent wall jet (14, 33). To see whether these distributions are similar, they were plotted in the conventional manner in which the dimensionless velocity ${}^{u}/u_m$ is plotted against the dimensionless distance $\lambda={}^{y}/\delta_1$ in Fig. IV-4 where u_m is the maximum velocity at any section and δ_1 is the distance y from the bed where $u = \frac{u_m}{2}$ and $\frac{\partial u}{\partial y}$ is negative. These two non-dimensionalising quantities u_m and δ_1 are known as the velocity and length scales respectively. A study of Fig. IV-4 shows that there is some scatter in the boundary layer portion (i.e. the region close to the wall) for the two flatter slopes. Otherwise, they indicate similarity in velocity distribution even though there is some difference from the corresponding curve of the plane turbulent wall jet on smooth walls with zero pressure gradient referred to normally

as the classical wall jet (44).

From the submerged flow experiments, which were only of an exploratory nature, some typical velocity distributions are shown in Fig. IV-3. The results for the runs with the highest submergence for each slope have been analysed for similarity and presented in Fig. IV-5. Here the agreement with the wall jet curve is very good. Other results will be presented in a later section after presenting a theoretical analysis in the following section.

4.4 Theoretical Analysis

Consider the hydraulic jump in a sloping channel either free (Fig. IV-6(a)) or submerged (Fig. IV-6(b)). Let x be the distance measured along the bed from the so-called virtual origin which may or may not coincide with the outlet and y be the distance in the perpendicular direction with u and v as the turbulent mean velocities and u' and v' the fluctuations in the respective directions. Then one could write the Reynolds equations as

$$u \frac{\partial u}{\partial x} + v \frac{\partial u}{\partial y} = -\frac{1}{\rho}\frac{\partial p}{\partial x} + g \sin\theta + \nu\left\{ \frac{\partial^2 u}{\partial x^2} + \frac{\partial^2 u}{\partial y^2} \right\}$$

$$- \left\{ \frac{\partial \overline{u'^2}}{\partial x} + \frac{\partial \overline{u'v'}}{\partial y} \right\} \qquad (4.3)$$

$$u \frac{\partial v}{\partial x} + v \frac{\partial v}{\partial y} = - \frac{1}{\rho} \frac{\partial p}{\partial y} - g \cos\theta + \nu \left\{ \frac{\partial^2 v}{\partial x^2} + \frac{\partial^2 v}{\partial y^2} \right\}$$

$$- \left\{ \frac{\partial \overline{u'v'}}{\partial x} + \frac{\partial \overline{v'^2}}{\partial y} \right\} \qquad (4.4)$$

$$\frac{\partial u}{\partial x} + \frac{\partial v}{\partial y} = 0 \qquad (4.5)$$

From the nature of the flow in this phenomenon one could make the following assumptions.

In a major portion of the flow u>>v; gradients in the y direction are generally much larger than the gradients of the corresponding quantities in the x direction, for example

$$\frac{\partial u}{\partial y} >> \frac{\partial u}{\partial x} .$$

With these assumptions, Eqs. 4.3 and 4.4 become

$$u \frac{\partial u}{\partial x} + v \frac{\partial u}{\partial y} = - \frac{1}{\rho} \frac{\partial p}{\partial x} + g \cdot \sin\theta + \nu \frac{\partial^2 u}{\partial y^2} - \frac{\partial \overline{u'v'}}{\partial y} - \frac{\partial \overline{u'^2}}{\partial x} \qquad (4.6)$$

$$0 = \frac{1}{\rho} \frac{\partial p}{\partial y} - g \cos\theta - \frac{\partial \overline{v'^2}}{\partial y} \qquad (4.7)$$

Integrating Eq. 4.7 after some rearrangement, from y = 0 to y

$$\int_0^y \frac{\partial}{\partial y} (p + \gamma y \cos\theta)\, dy = - \int_0^y \frac{\partial\, \overline{\rho v'^2}}{\partial y}\, dy \tag{4.8}$$

$$p + \gamma y \cos\theta - p_o = - \overline{\rho v'^2} \tag{4.9}$$

or:

$$p + \gamma y \cos\theta = p_o - \overline{\rho v'^2} \tag{4.10}$$

where p_o is the pressure on the bed.

Substituting Eq. 4.10 into Eq. 4.6;

$$u \frac{\partial u}{\partial x} + v \frac{\partial u}{\partial y} = - \frac{1}{\rho} \frac{dp_o}{dx} + \nu \frac{\partial^2 u}{\partial y^2} - \frac{\partial \overline{u'v'}}{\partial y}$$

$$- \frac{\partial}{\partial x} [\overline{u'^2} - \overline{v'^2}] + g \sin\theta \tag{4.11}$$

Without much error, the last but one term in Eq. 4.11 could be neglected. Hence, the final simplified equations of motion for the sloping channel jump could be written as

$$u \frac{\partial u}{\partial x} + v \frac{\partial u}{\partial y} = - \frac{1}{\rho} \frac{dp_o}{dx} + \nu \frac{\partial^2 u}{\partial y^2}$$

$$- \frac{\partial \overline{u'v'}}{\partial y} + g \sin\theta \tag{4.12}$$

$$\frac{\partial u}{\partial x} + \frac{\partial v}{\partial y} = 0 \tag{4.5}$$

From the experimental observations, mentioned in the early part of this part, one could write

$$\frac{u}{u_m} = f \left[\frac{y}{\delta_1} \right] = f (\lambda) \tag{4.13}$$

From the knowledge of the experimental measurements and theory for similar turbulent flows like jets and wall jets, one could further write

$$- \frac{\overline{u'v'}}{u_m^2} = G (\lambda) \tag{4.14}$$

With these assumptions and using the continuity equation, Eq. 4.12 could be reduced to the form

$$G' = \frac{\delta_1 u_m'}{u_m} f^2 - \delta_1' \lambda f f' + \delta_1' f' \int_0^\lambda \lambda f' d\lambda - \frac{\delta_1 u_m'}{u_m} f' \int_0^\lambda f d\lambda$$

$$- \frac{\nu}{\delta_1 u_m} f'' + [\frac{1}{\rho} \frac{dp_o}{dx} - g \sin\theta] \tag{4.15}$$

Where the primes on f and G denote differentiation with respect to λ and the primes on u_m and δ_1 denote differentiation with respect to x. Since $\frac{\delta_1 u_m}{\nu}$ is generally very large, the term $\frac{\nu}{\delta_1 u_m}$ f'' could be neglected. Rearranging, Eq. 4.15 becomes

$$G' = \frac{\delta_1 u_m'}{u_m} [f^2 - f' \int_0^\lambda f d\lambda] - \delta_1' [\lambda f f' - f' \int_0^\lambda \lambda f' d\lambda]$$

$$+ [\frac{1}{\rho} \frac{dp_o}{dx} - g \sin\theta] \tag{4.16}$$

Regarding the last term in Eq. 4.16; one could write for level water surface

$$p_o = \gamma Y \cos\theta = \gamma \overline{y} \tag{4.17}$$

Where Y is the normal depth of flow and $\bar{y}$ is the vertical depth. Further

$$\frac{1}{\rho}\frac{dp_o}{dx} - g\sin\theta = \frac{1}{\rho}\gamma\frac{d\bar{y}}{dx} - g\sin\theta = 0 \qquad (4.18)$$

Then, in Eq. 4.16, since the left hand side is a function of only λ, the right hand side should only be a function of λ. Hence, one could write

$$\frac{\delta_1 u_m'}{u_m} \quad \alpha \quad x^o \qquad (4.19)$$

$$\delta_1' \quad \alpha\ x^o \qquad (4.20)$$

If

$$u_m\ \alpha\ x^p$$

$$\delta_1\ \alpha\ x^q \qquad (4.21)$$

From Eq. 19

$$q + p - 1 - p = 0$$

or

$$q = 1 \qquad (4.22)$$

Eq. 4.20 also gives q = 1. To evaluate the other unknown exponent, one could use an integral form of Eq. 4.12.

For the horizontal water surface, integrating Eq. 4.12 with respect to y from y = 0 to y = Y and neglecting the backward flow on the surface, one could obtain

$$\frac{d}{dx}\int_{o}^{Y} \rho\, u^{2} dy = -\, \tau_{o} \qquad (4.23)$$

where the shear stress on the surface of the water has been neglected and τ_o is the bed shear stress.

For the present neglecting the shear stress on the bed, Eq. 4.23 becomes,

$$\frac{d}{dx}\int_{o}^{Y} \rho\, u^{2} dy = 0 \qquad (4.24)$$

That is, the momentum flux in the x direction is preserved.

Equation 4.24 could be written as

$$\frac{d}{dx} \rho \delta_1 u_m^2 \int_0^{Y/\delta_1} f^2 d\lambda = 0 \qquad (4.25)$$

Since the integral will be a number, Eq. 4.25 could be rewritten as

$$\delta_1 u_m^2 \alpha x^0 \qquad (4.26)$$

or

$$q + 2p = 0 \qquad (4.27)$$

or

$$p = \frac{1}{2} \qquad (4.28)$$

Hence,

$$\delta_1 \alpha x \qquad (4.29)$$

$$u_m \alpha \frac{1}{\sqrt{x}} \qquad (4.30)$$

Equations 4.29 and 4.30 could be verified using dimensional analysis as shown below.

Since in this problem, the momentum flux M_1 is preserved and appears to be the dominant parameter, one could write

$$u_m = f_1 \; [M_1, \rho, x] \tag{4.31}$$

Using the π theorem, Eq. 4.31 could be reduced to the form

$$\frac{u_m}{\sqrt{M_1/\rho x}} = \text{const } C_1 \tag{4.32}$$

Since $M_1 = \rho y_1 U_1^2$, Eq. 4.32 becomes

$$\frac{u_m}{U_1} = \frac{C_1}{\sqrt{x/y_1}} \tag{4.33}$$

The constant C_1 has to be determined experimentally. The length scale could be easily written as

$$\delta_1 = C_2 x \tag{4.34}$$

or

$$\frac{\delta_1}{y_1} = C_2 \frac{x}{y_1} \tag{4.35}$$

Again C_2 is another coefficient to be determined experimentally.

$$\tau_o = f_1 \ [M_1, \rho, x] \tag{4.36}$$

Using the π theorem, Eq. 4.36 could be reduced to

$$\frac{\tau_o/\rho}{M_1 \frac{1}{\rho} \frac{1}{x}} = \text{const} \quad C_3 \tag{4.37}$$

or

$$\frac{\tau_o}{\rho U_1^{\,2}/2} = \frac{2C_3}{x/y_1} \tag{4.38}$$

or

$$\frac{\tau_o}{\rho u_m^{\,2}/2} = \frac{2C_3}{C_1^{\,2}} = C_4 \tag{4.39}$$

For plane turbulent wall jets, Sigalla (46) found that $\tau_o/\rho u_m^{\,2}$ is a function of some type of Reynolds number and Myers et al (23) found that

$$\frac{\tau_o}{\rho U_1^{\,2}/2} \cdot \frac{x}{y_1} \cdot \left[\frac{U_1 Y_1}{\nu}\right]^{\frac{1}{2}}$$ is a constant equal to 0.20. The

relationship of Myers et al could be shown to agree with the predictions of Eq. 4.31.

The foregoing analysis was confined to a case where the water surface in the jump was horizontal. It could be applied for free as well as submerged jumps. If the water surface is not level, then

the term $\frac{1}{\rho}\frac{dp_o}{dx} - g \sin\theta$ will be different from zero. But, if it is still small in comparison with the other terms of Eq. 4.15, similarity of velocity distribution will still be satisfied along with the other relations for the scale factors. These points will be considered again while discussing the relevant experimental data.

4.5 Analysis of Experimental Results

Considering the velocity distribution, Fig. IV-4 shows a plot of the dimensionless velocity distribution along with the curve of the classical wall jet. It is seen that the results for the 15 and 25 percent slopes indicate well the existence of similarity, whereas those of the 5 and 10 percent slopes show some scatter in the region near the bed, similar to the bahaviour of jumps on level floors (28). For practical purposes like computing the momentum and energy, the difference from the curve of the classical wall jet could possibly be neglected for the sake of simplicity and the classical wall jet curve itself be used.

The variation of the dimensionless velocity scale u_m/U_1 against x/y_1 is shown in Fig. IV-7. All the data points are confined between the curves of the classical wall jet (34) and the jump on a level rectangular channel known as the classical jump (31). These data are replotted in Fig. IV-8 in accordance with the prediction of the results of the similarity analysis and dimensional arguments. It

is seen that for larger values of x/y_1, $\frac{u_m}{U_1}$ indeed varies linearly with $\frac{1}{\sqrt{x/y_1}}$. The value of the coefficient C_1 has been found to increase from 2.6 for $\theta = 0$ to about 3.5 for $\theta = 90$ degrees. It will be useful to obtain some information for steeper slopes in the future investigations.

Experimental results for the length scale are shown in Fig. IV-9 where δ_1/y_1 is plotted against x/y_1 along with the other two curves. For the two flatter slopes, the variation is linear for $\frac{x}{y_1} \gtrsim 12$, whereas for the steeper slopes, it becomes linear for $x/y_1 \gtrsim 25$. The interesting observation is that in general the length scale is much larger than that for the two standard cases. For slopes greater than 5%, for any x/y_1, δ_1/y_1 decreases with increase in slope. Then for the slopes flatter than about 5%, it should be increasing with slope. This aspect also should be given consideration in future studies.

Regarding the variation of the bed shear stress τ_o with $^1/x$, dimensional analysis and similarity analysis predicted a linear variation of τ_o with $^1/x$ or $c_f = {}^{\tau}o/\rho u_m{}^2/_2$ should be a constant with respect to x. Fig. IV-10 shows the variation of τ_o against x for all the experiments. When c_f is plotted against x, it is found that for the steepest slope, for x/y_1 greater than 18, c_f becomes almost independent of x or x/y_1. For the smaller slopes, c_f varies strongly with x/y_1. Fig. IV-11 shows the effect of bed slope on the bed shear in which y_2* is the subcritical sequent depth of the corresponding classical jump.

The velocity distribution data for the submerged cases (with the highest submergence for each slope) are shown plotted in the standard non-dimensional manner in Fig. IV-5. It is interesting to find that the distribution is fairly well described by the curve of the classical wall jet. The variation of the velocity scale is shown in Fig. IV-13 for all the submerged cases and in Fig. IV-14 for the extreme in each slope. Fig. IV-14 shows that in most of the cases the data approach the linear variation asymptotically and the value of the coefficient C_1 is indicated in the relevent places. In Fig. IV-13, it is found that in some cases $\frac{u_m}{U_1}$ is larger than the zero pressure gradient wall jet curve. The reason seems to be that in those cases the water surface is not level and possibly $\frac{1}{\rho}\frac{dp}{dx} - \sin\theta$ was negative, thereby accelerating the flow.

The variation of the length scale is studied in Fig. IV-15. The variation appears to be generally linear and the lines shift towards the wall jet line as the submergence increases. The variation of the skin friction coefficient c_f with x/y_1, is shown in Fig. IV-16 for the case of extreme submergence for each slope. For the two steeper slopes, c_f appears to be independent of x whereas for the two flatter slopes, c_f decreases as x increases. It is reasonable to conclude that as the slope and submergence increase, c_f will become invariant with x. Based on the observations on wall jets, it could be said that c_f will

be a function of the Reynolds number of the flow.

4.6 Boundary Layer

Fig. IV-17 (a to d) shows the velocity distribution in boundary layer part of the forward flow for free jumps on different slopes. It is quite interesting to observe the profiles exhibiting the decay of the effect of pressure gradient with increased bed slopes.

Fig. IV-18 shows the velocity distribution in the boundary layer for submerged jumps on different bed slopes. The data for all the cases shows good correlation between u/u_m and y/δ drawn on arithmetic scale with some scatter near the bed. Fig. IV-19 shows the relationship between U/u^* and yu^*/ν for the same data showing the functional form

$$\frac{u}{u^*} = 3.8 \log \frac{y\,u^*}{\nu} + 9.5 \qquad (4.40)$$

The values of constants in Eq. 4.40 are different from that of well known boundary layer equation. This is justified because the turbulent structure of the boundary layer flow is different from the well known boundary layer formed on a smooth flat plate. The boundary layer in a jet flow is growing under a turbulent decelerating flow rather than potential flow.

Fig. IV-20 shows the velocity distribution in the inner layer (boundary layer) of the forward flow for submerged jumps formed on different bed slopes. The correlation is shown between $u/_{u_m}$ and $y/_{\delta_1}$ plotted on logarithmic scales. It can be observed that over the range of experiments conducted for submerged jumps, the correlation with velocity scale u_m and length scale δ_1 is very good with an expected scatter near the bed (submergences not being same and appreciable). This correlation once again indicates the fact that the flow under appreciable submergences can be analysed as a wall jet.

4.7 Conclusions

Based on a theoretical and experimental study of sloping channel jumps with and without submergence on four slopes of 5 to 25%, it could be concluded that,

1. The theoretical analysis, inspite of some simplifying assumptions predicts the scale variations reasonably well. Prediction for c_f was successful only for the steeper slopes indicating the influence of pressure gradient for smaller slopes.
2. The turbulent wall jet model is quite useful for predicting some of the mean flow characteristics.
3. The velocity distribution in the boundary layer for free jumps was found to exhibit the decay of adverse pressure gradient effects with increasing bed slopes. In the submerged jumps, the boundary layer velocity distribution when correlated with u_m and δ_1 was found good indicating the existence of similarity.

TABLE IV-1

EXPERIMENTAL DETAILS

Expt. No.	Bed Slope	y_1 (inch)	U_1 ft/sec.	$F_1 = \frac{U_1}{\sqrt{gy_1}}$	$R = \frac{U_1 Y_1}{\nu}$	Comments
S-5-2	5%	0.40	8.23	7.95	2.38×10^4	Free (F)
S-5-3	5%	0.40	8.10	7.82	2.34×10^4	Submerged (S)
S-5-4	5%	0.40	8.10	7.82	2.34×10^4	S
S-5-5	5%	0.40	8.00	7.75	2.32×10^4	S
S-5-7	5%	0.40	6.68	6.45	1.93×10^4	S
S-10-1	10%	0.40	8.33	8.05	2.41×10^4	F
S-10-2	10%	0.40	7.96	7.70	2.30×10^4	S
S-15-1-1	15%	0.50	7.37	6.37	2.67×10^4	F
S-15-1-2	15%	0.50	8.82	7.63	3.20×10^4	F
S-15-2	15%	0.50	7.31	6.31	2.65×10^4	S
S-15-4	15%	0.50	7.37	6.37	2.67×10^4	S
S-25-1	25%	0.50	7.55	6.53	2.74×10^4	F
S-25-2	25%	0.50	7.22	6.24	2.62×10^4	S

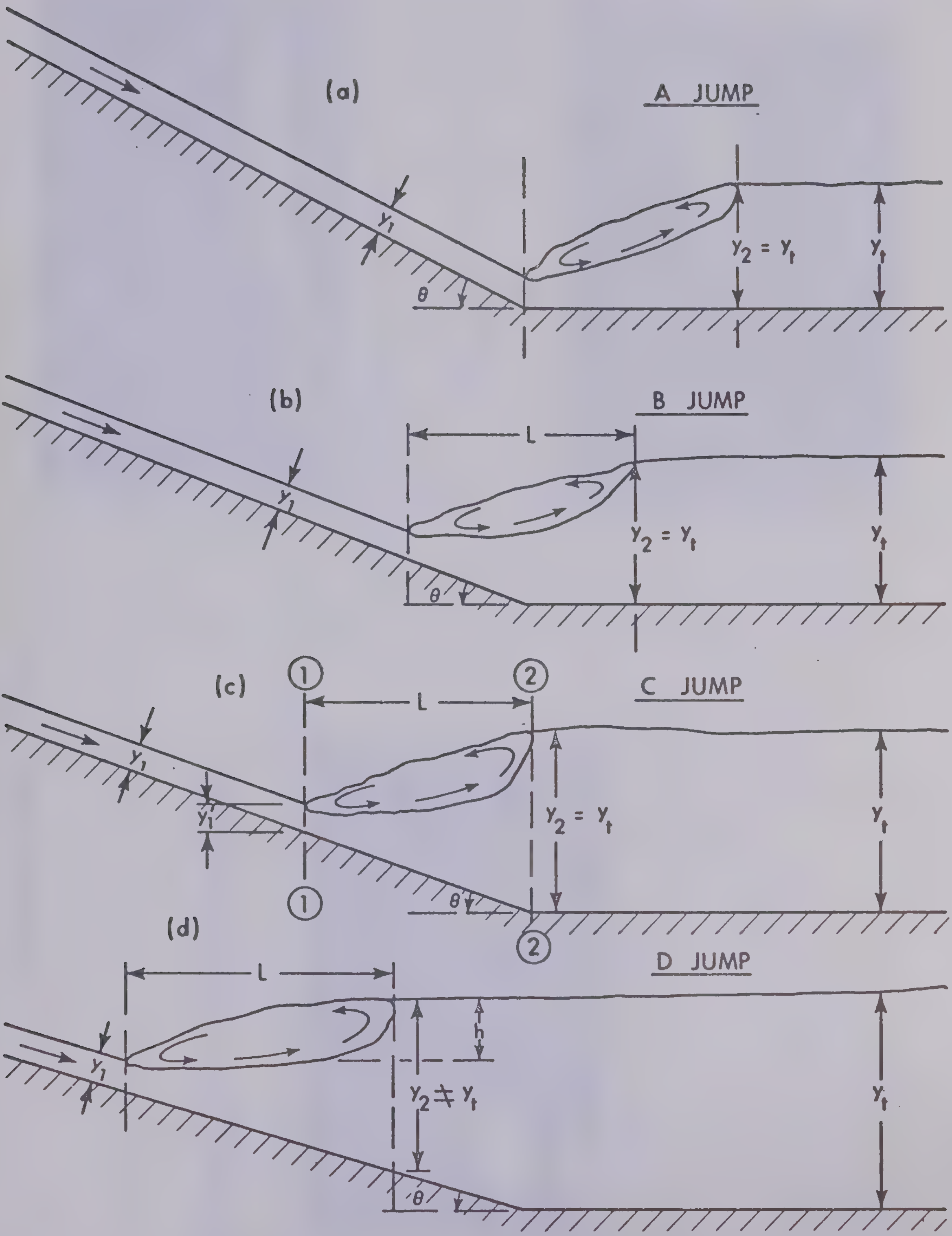

FIG·IV-1. HYDRAULIC JUMP IN SLOPING CHANNELS

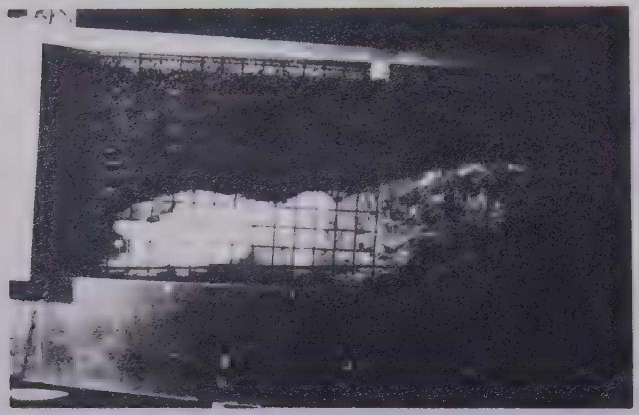

Jump on 5% bed slope

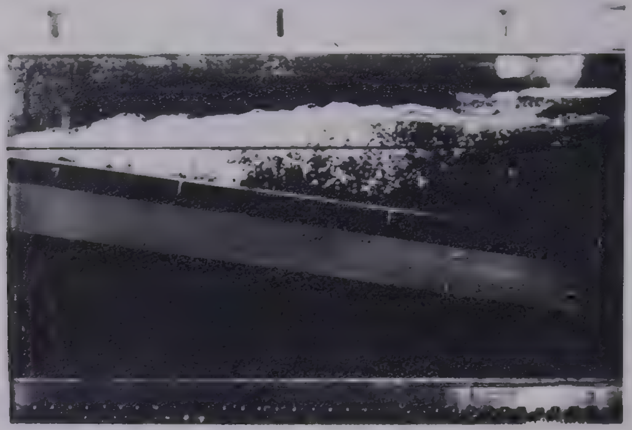

Jump on 25% bed slope

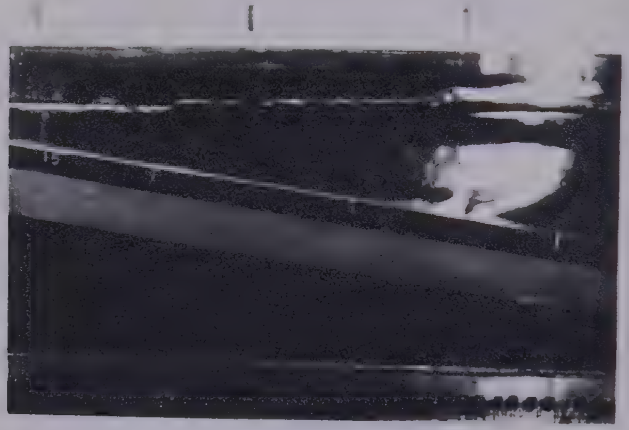

Submerged Jump on 25% bed slope

FIG. 2. FLOW PROFILES

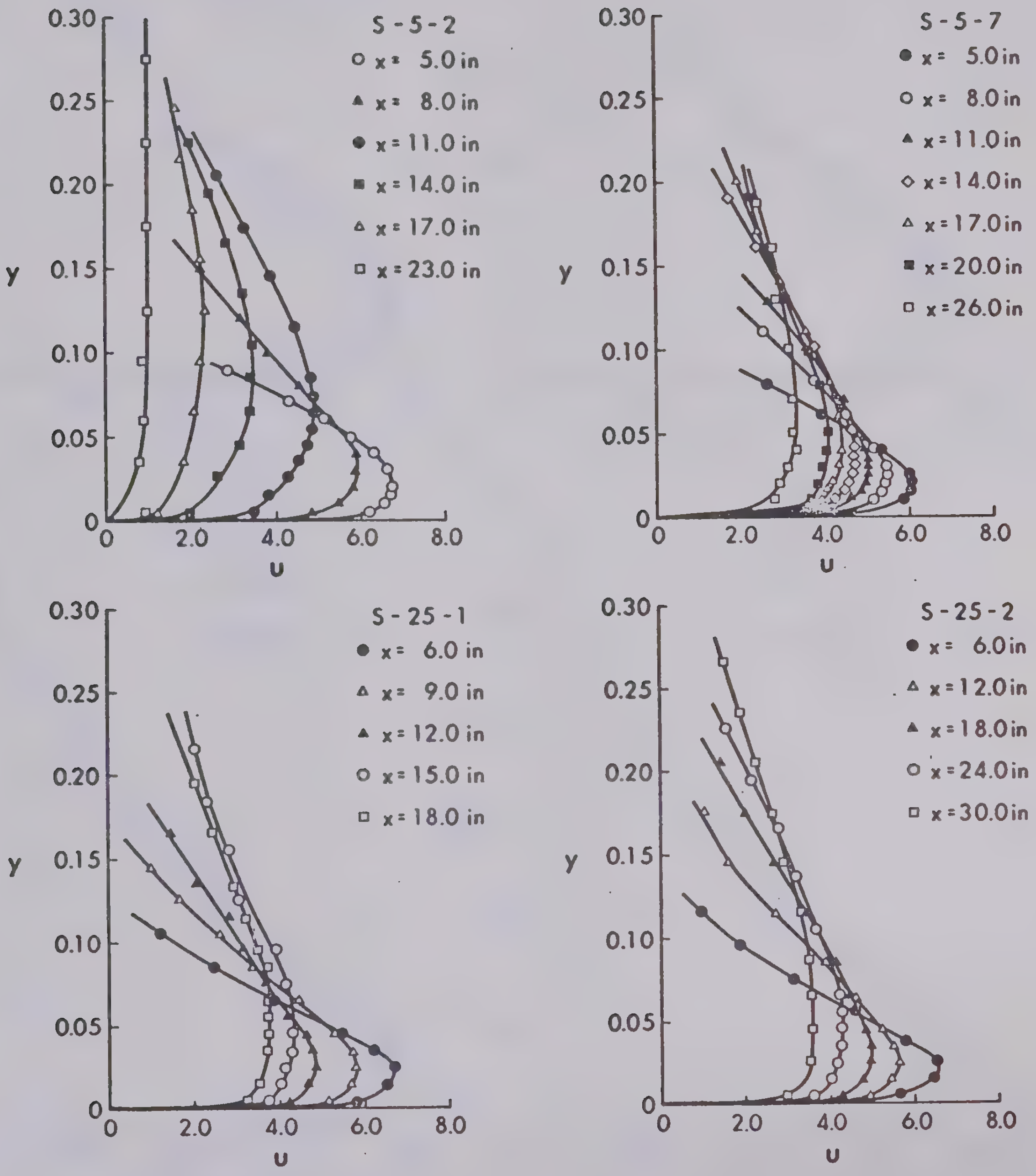

FIG·IV-3. TYPICAL VELOCITY DISTRIBUTIONS

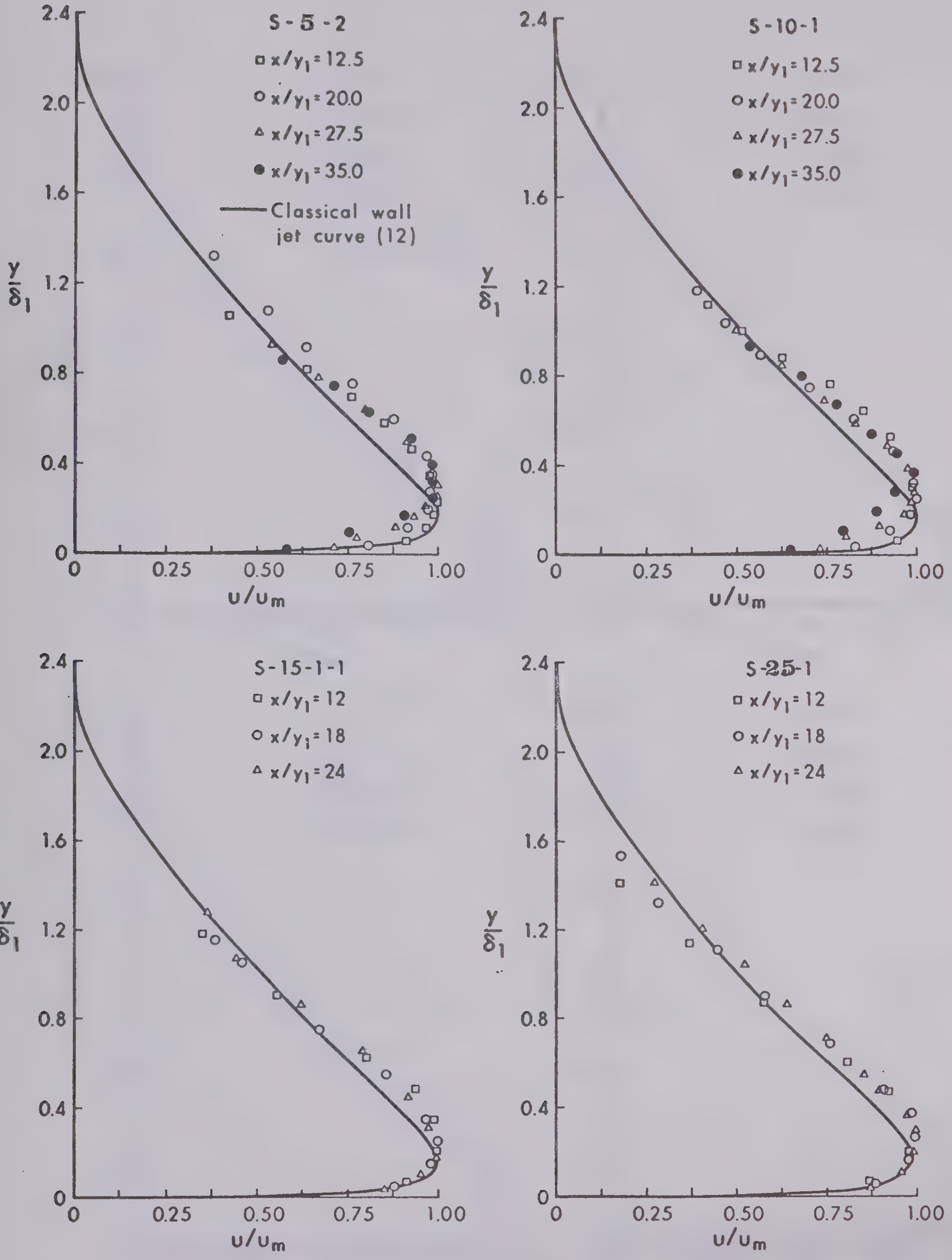

FIG. IV-4. SIMILARITY OF VELOCITY PROFILES - FREE JUMPS.

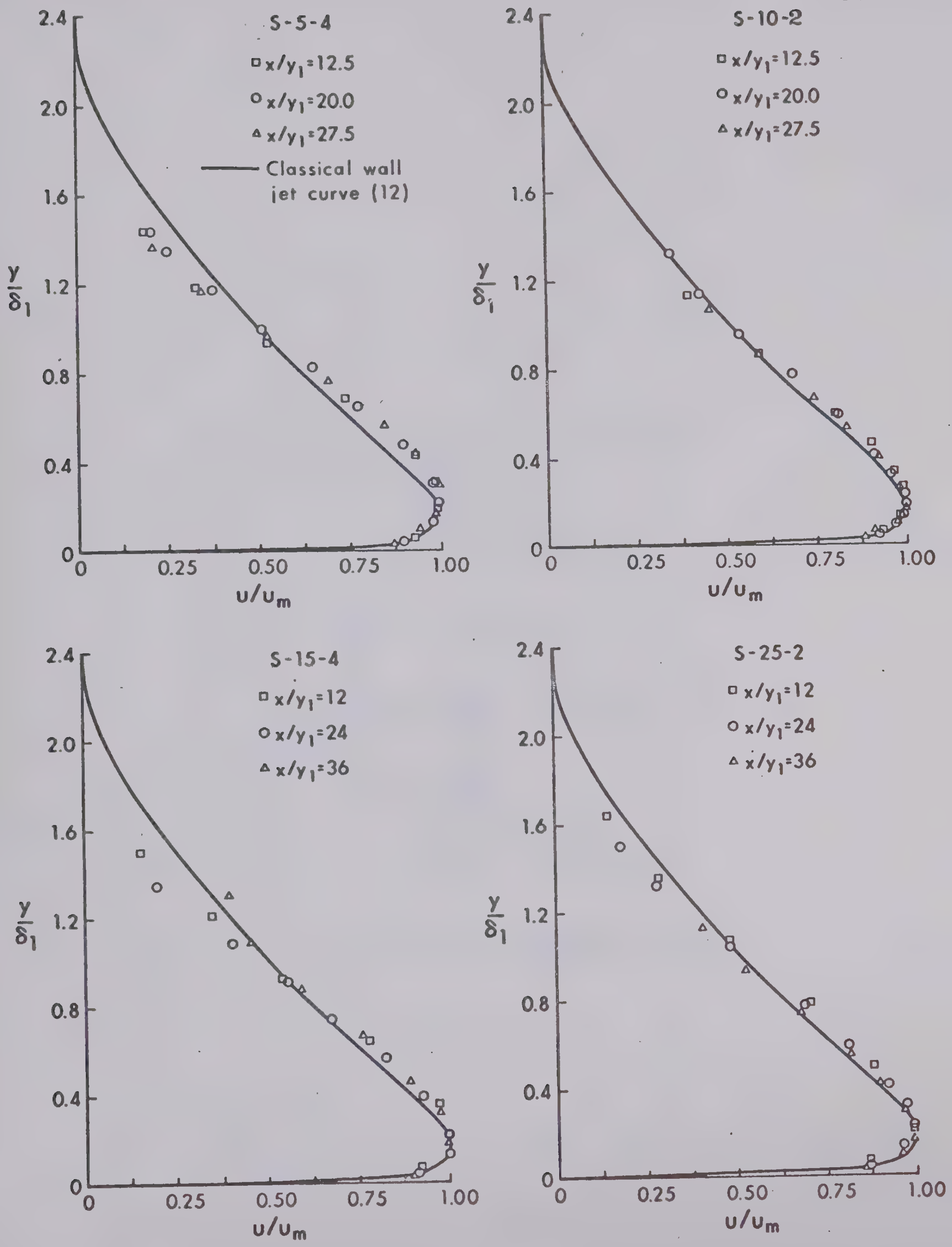

FIG·IV-5. SIMILARITY OF VELOCITY PROFILES – SUBMERGED JUMPS.

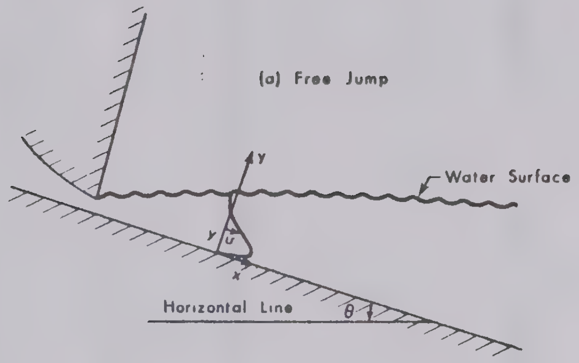

(a) Free Jump

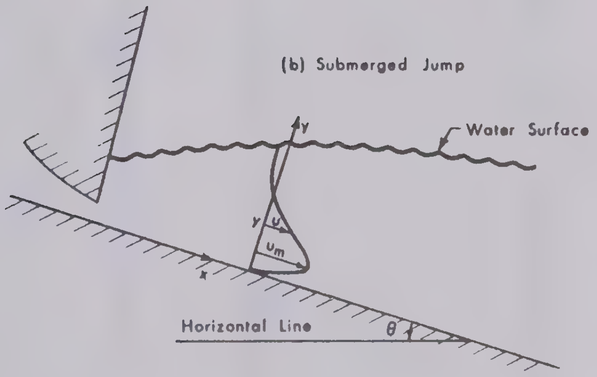

(b) Submerged Jump

FIG.IV-6 DEFINITION SKETCH

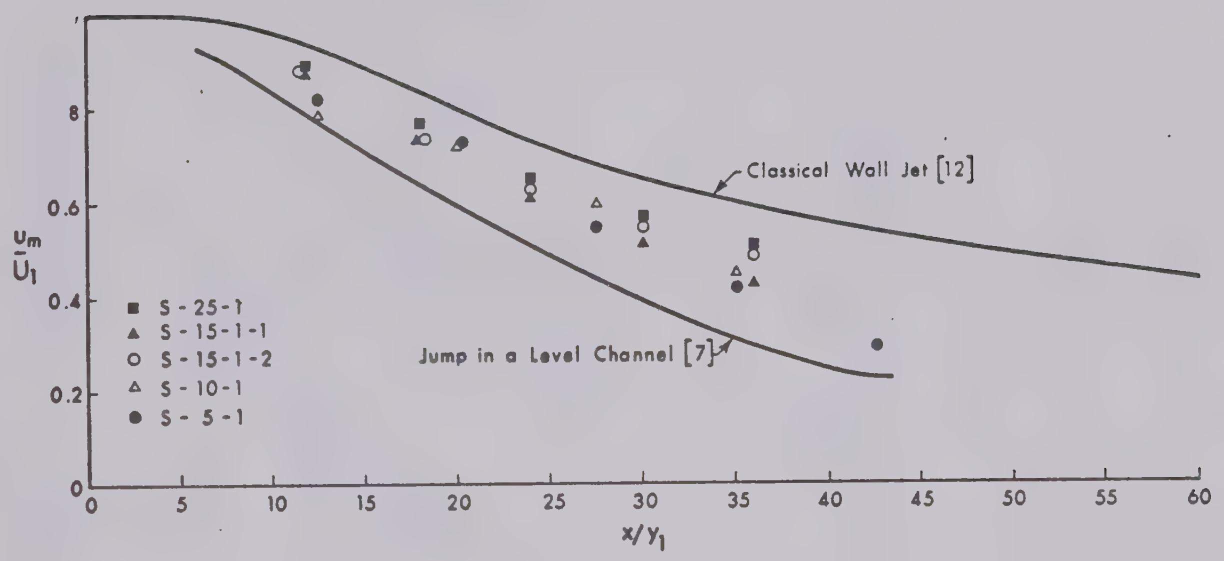

FIG·IV-7. VARIATION OF u_m/U_1 WITH x/y_1 - FREE JUMPS.

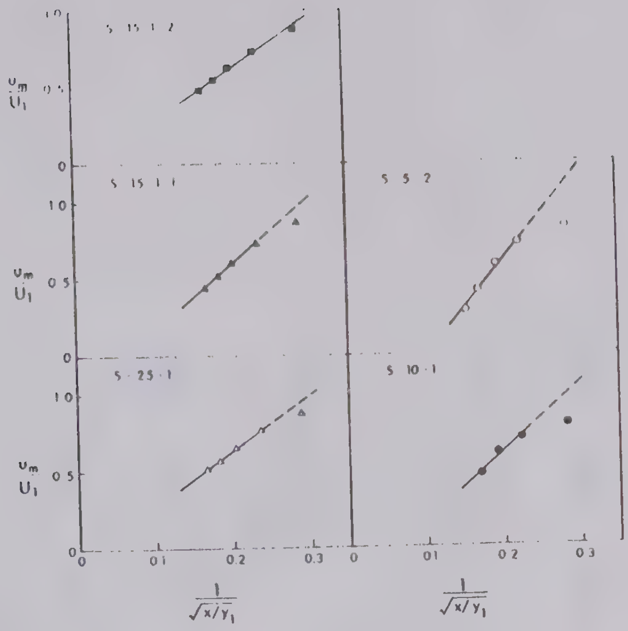

FIG.IV-8 VARIATION OF u_m/U_1 WITH $1/x/y_1$ -FREE JUMPS

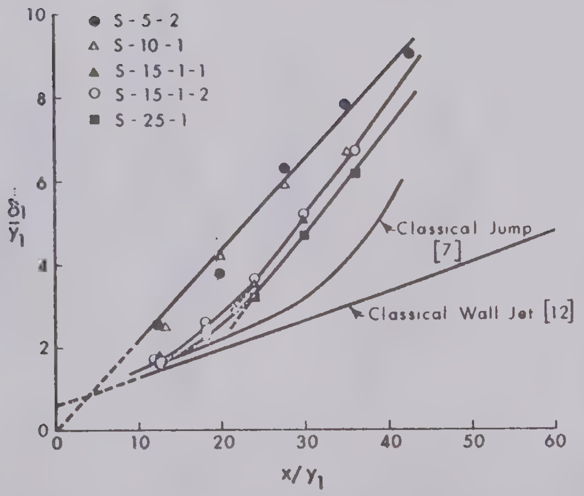

FIG.IV-9 STUDY OF LENGTH SCALE -FREE JUMPS

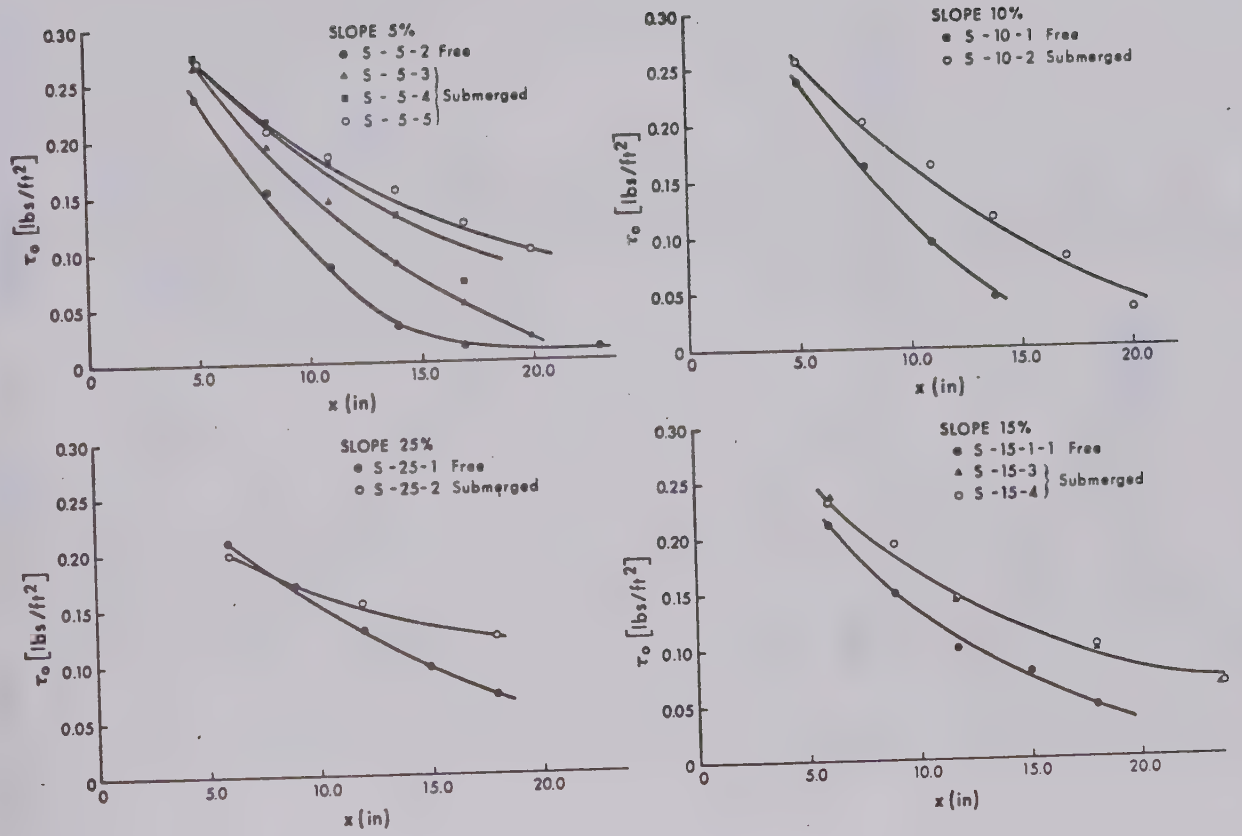

FIG·IV-10. VARIATION OF τ_0 WITH X.

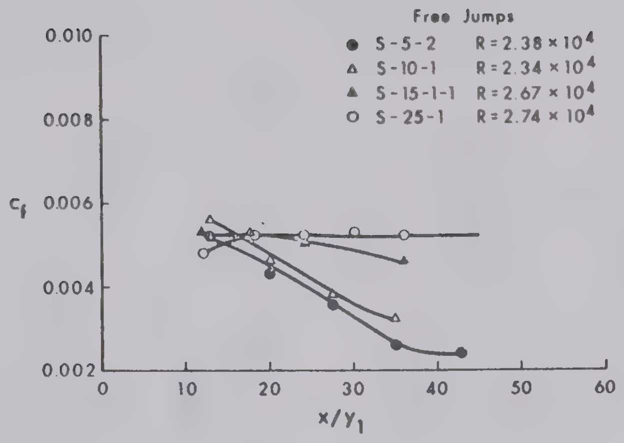

FIG.IV-11.VARIATION OF c_f WITH x/y_1

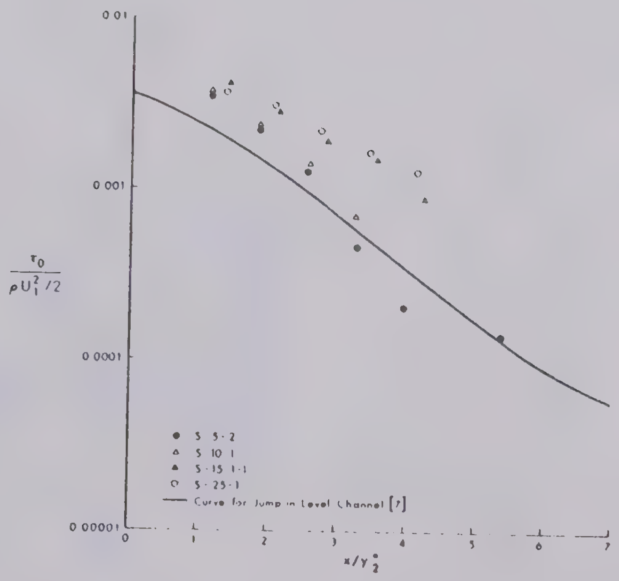

FIG.IV-12.EFFECT OF SLOPE ON BED SHEAR
-FREE JUMPS

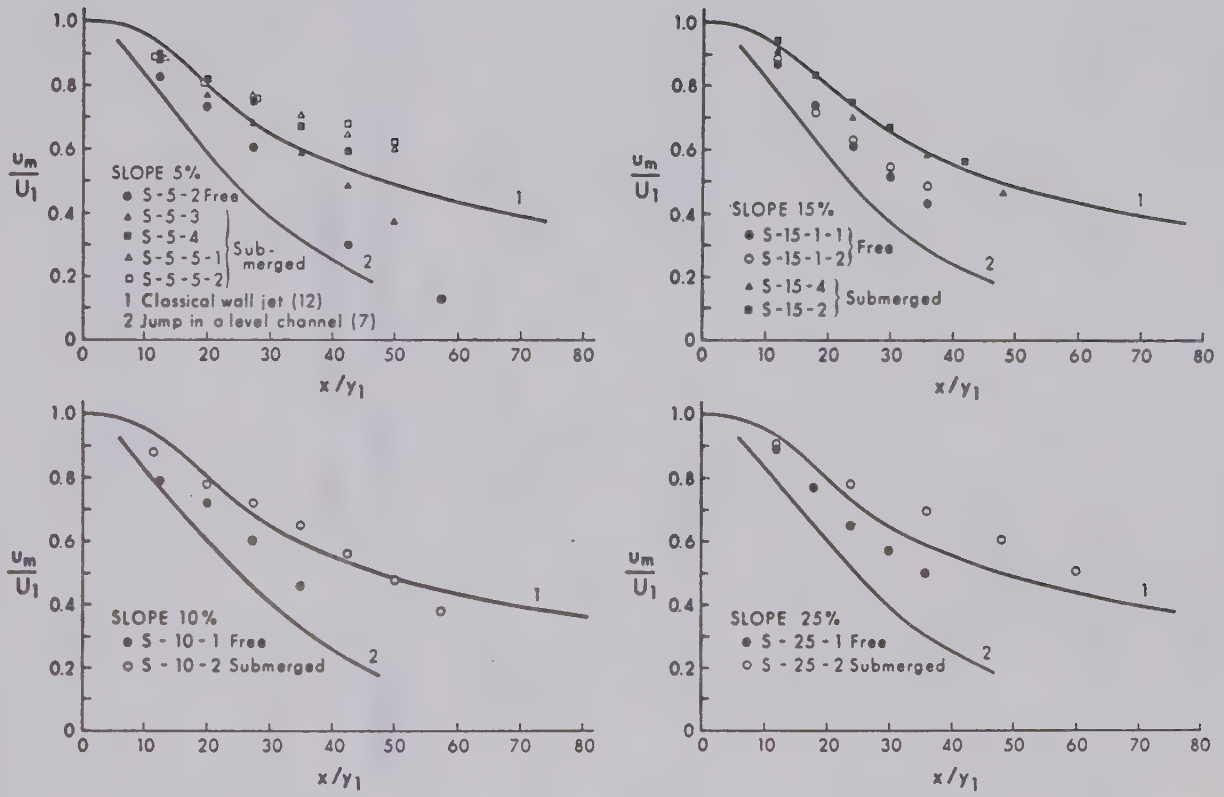

FIG. IV-43 VELOCITY SCALE FOR SUBMERGED JUMPS.

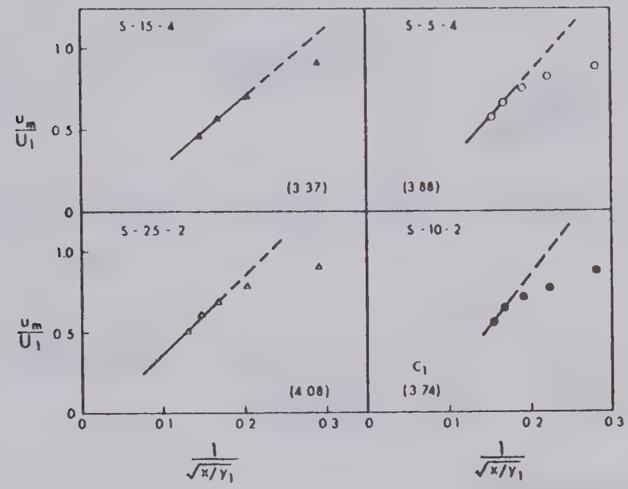

FIG.IV-14 VELOCITY SCALES FOR EXTREME -SUBMERGENCE CASES

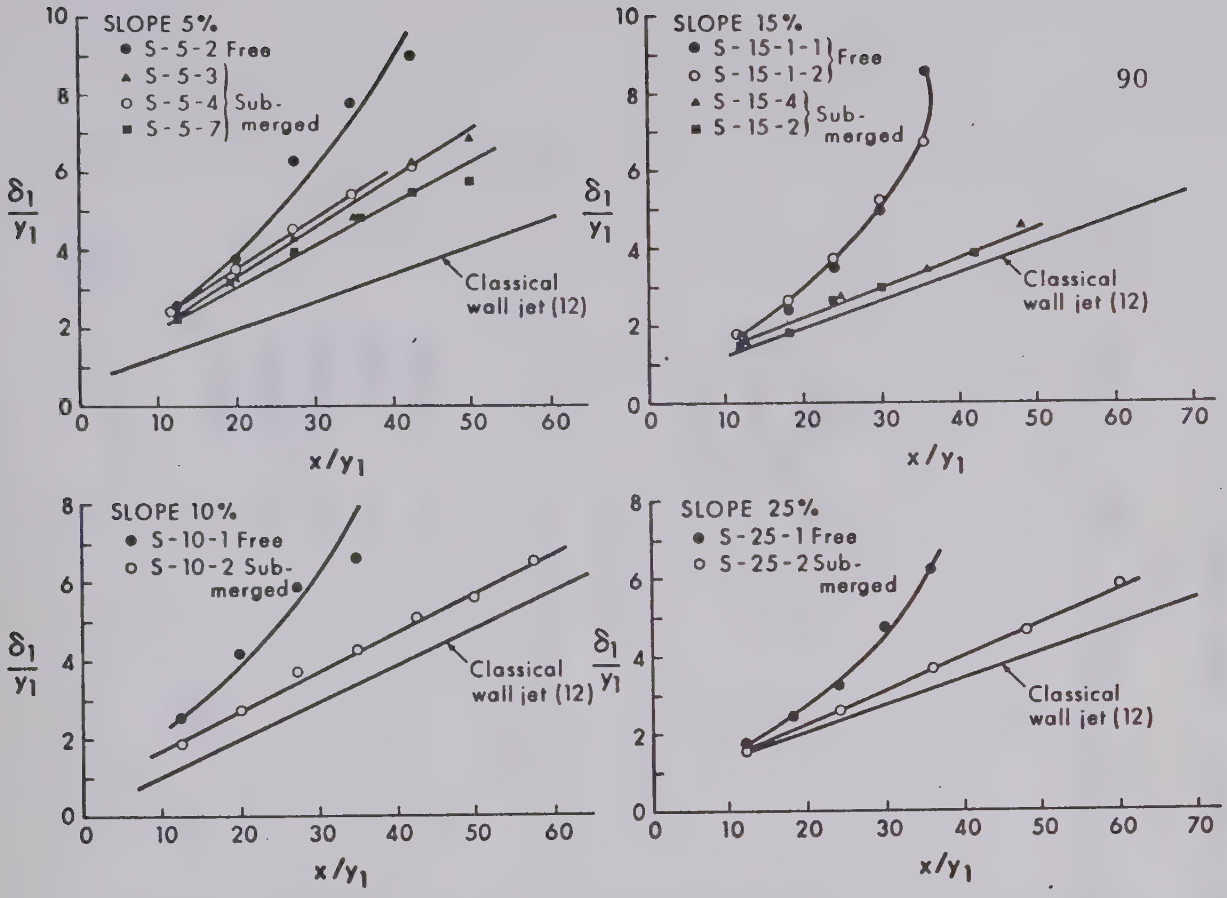

FIG. IV-15. STUDY OF LENGTH SCALE FOR SUBMERGED JUMPS.

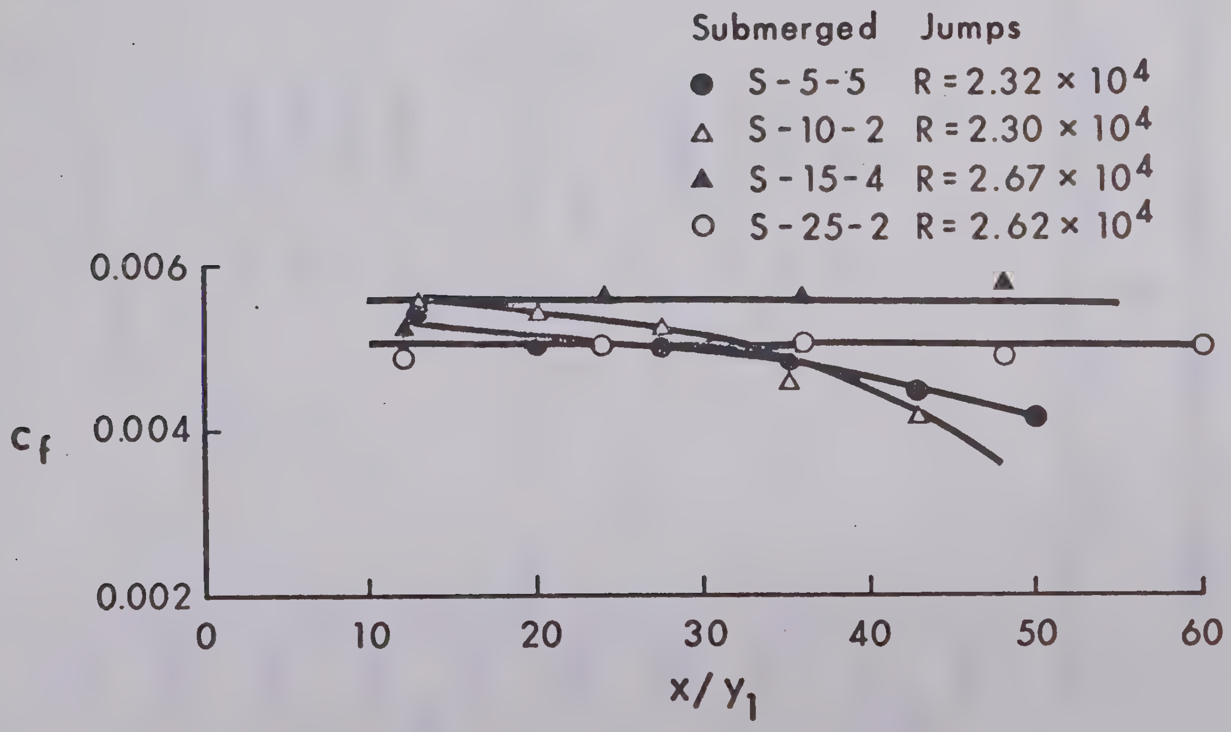

FIG. IV-16. STUDY OF c_f FOR EXTREME SUBMERGENCES.

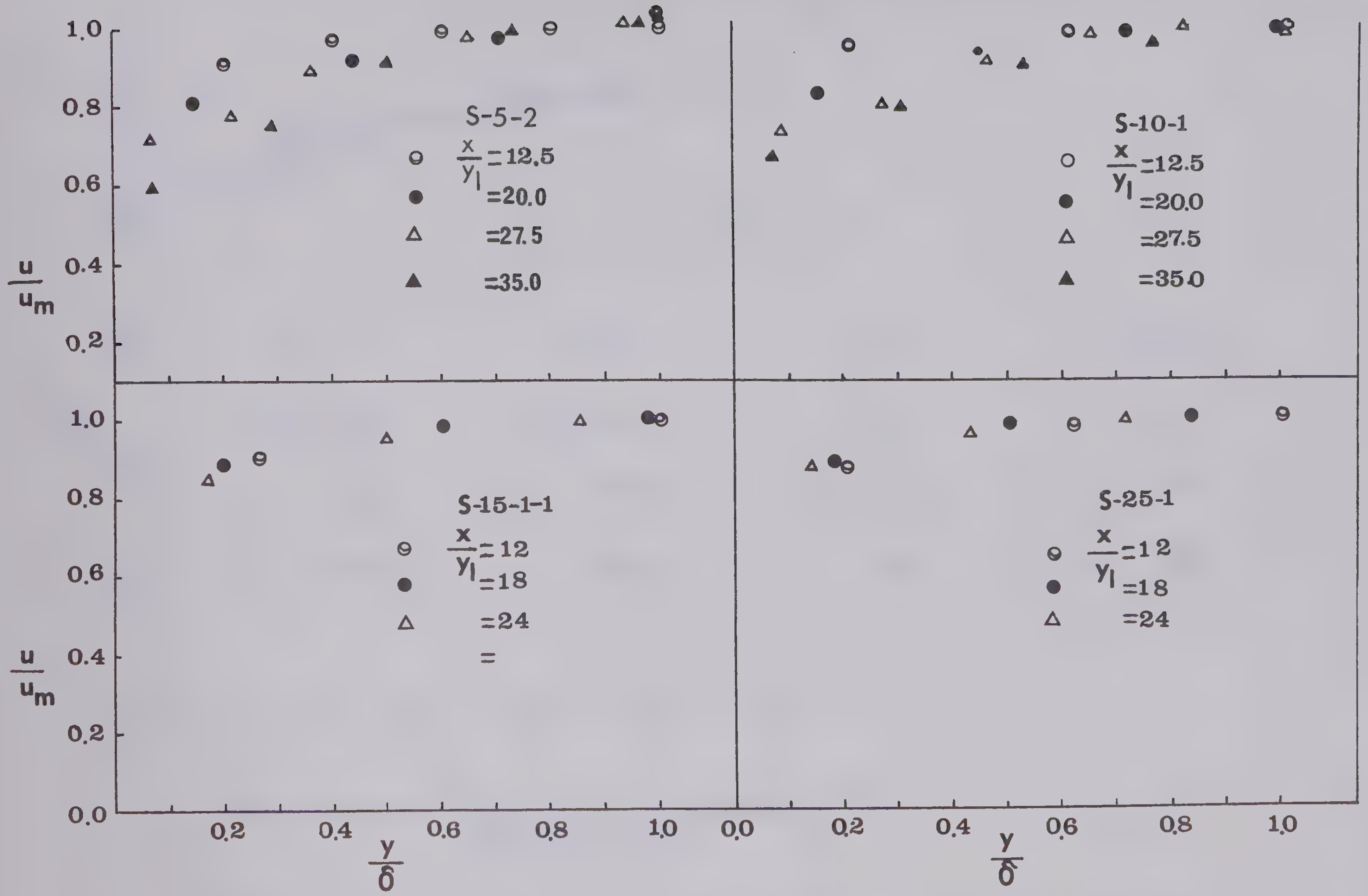

FIG. IV–17. VELOCITY DISTRIBUTION IN BOUNDARY LAYER – FREE JUMPS

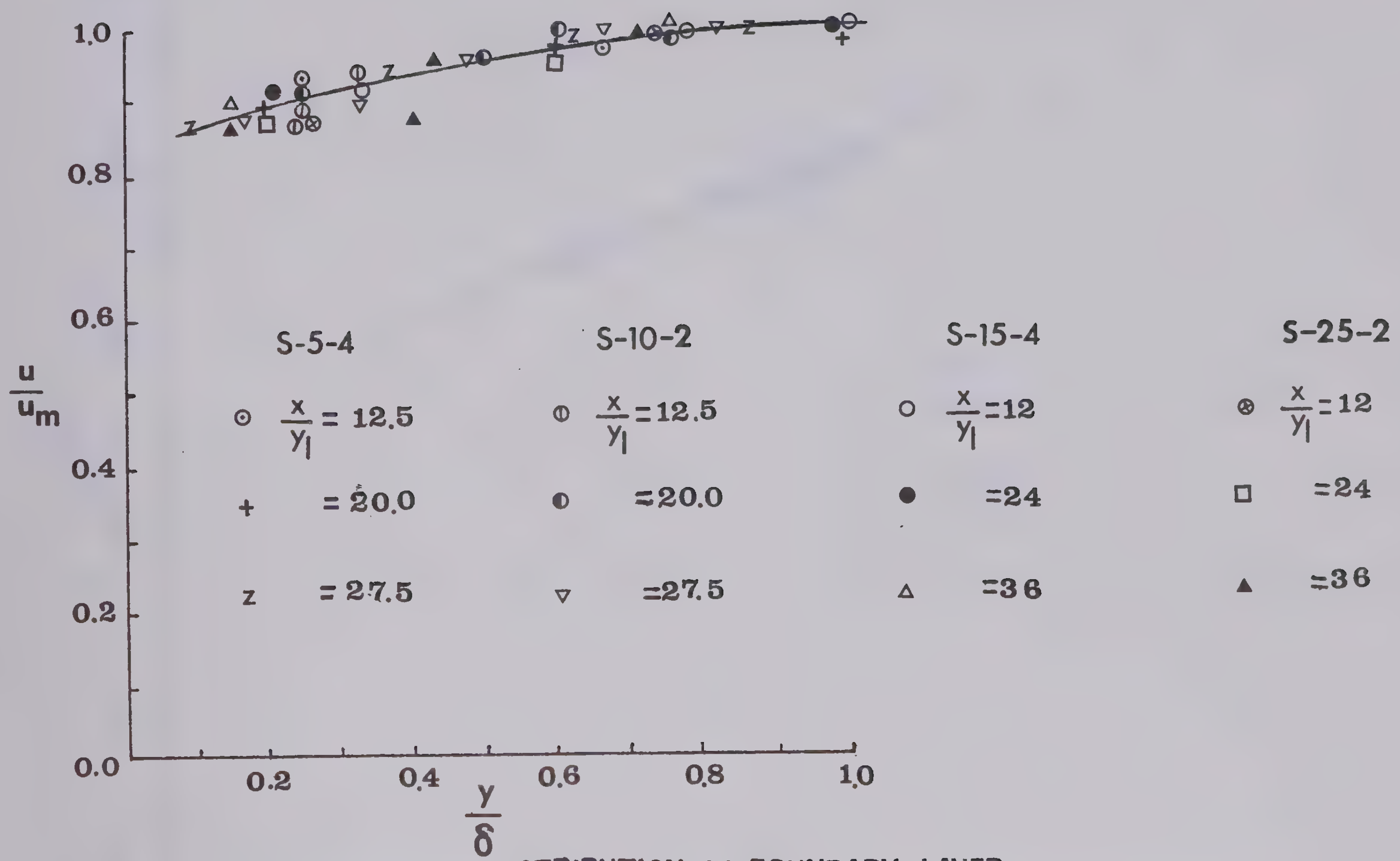

FIG.IV-18. VELOCITY DISTRIBUTION IN BOUNDARY LAYER SUBMERGED JUMPS

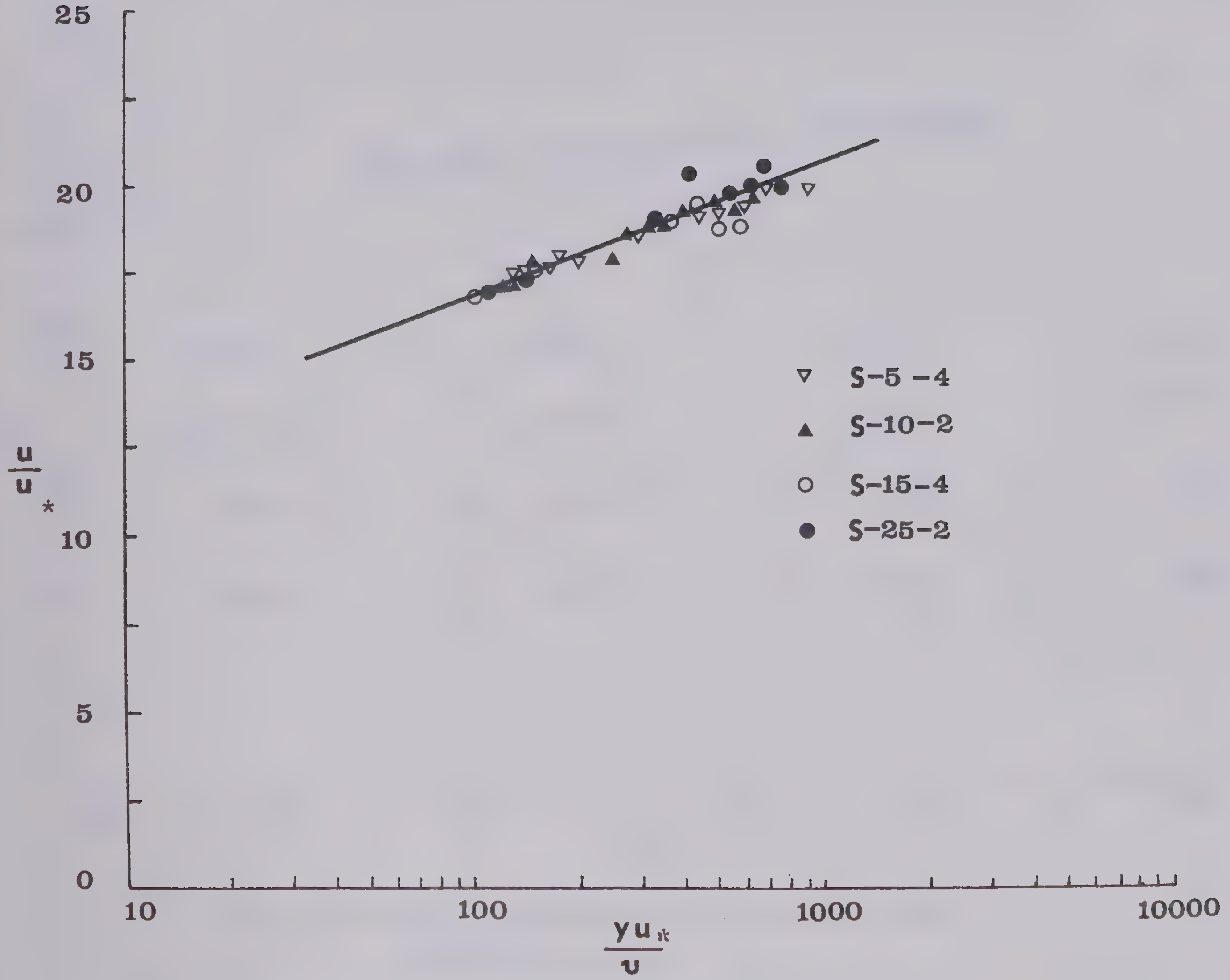

FIG. IV-19. VELOCITY DISTRIBUTION IN BOUNDARY LAYER - SUBMERGED JUMPS

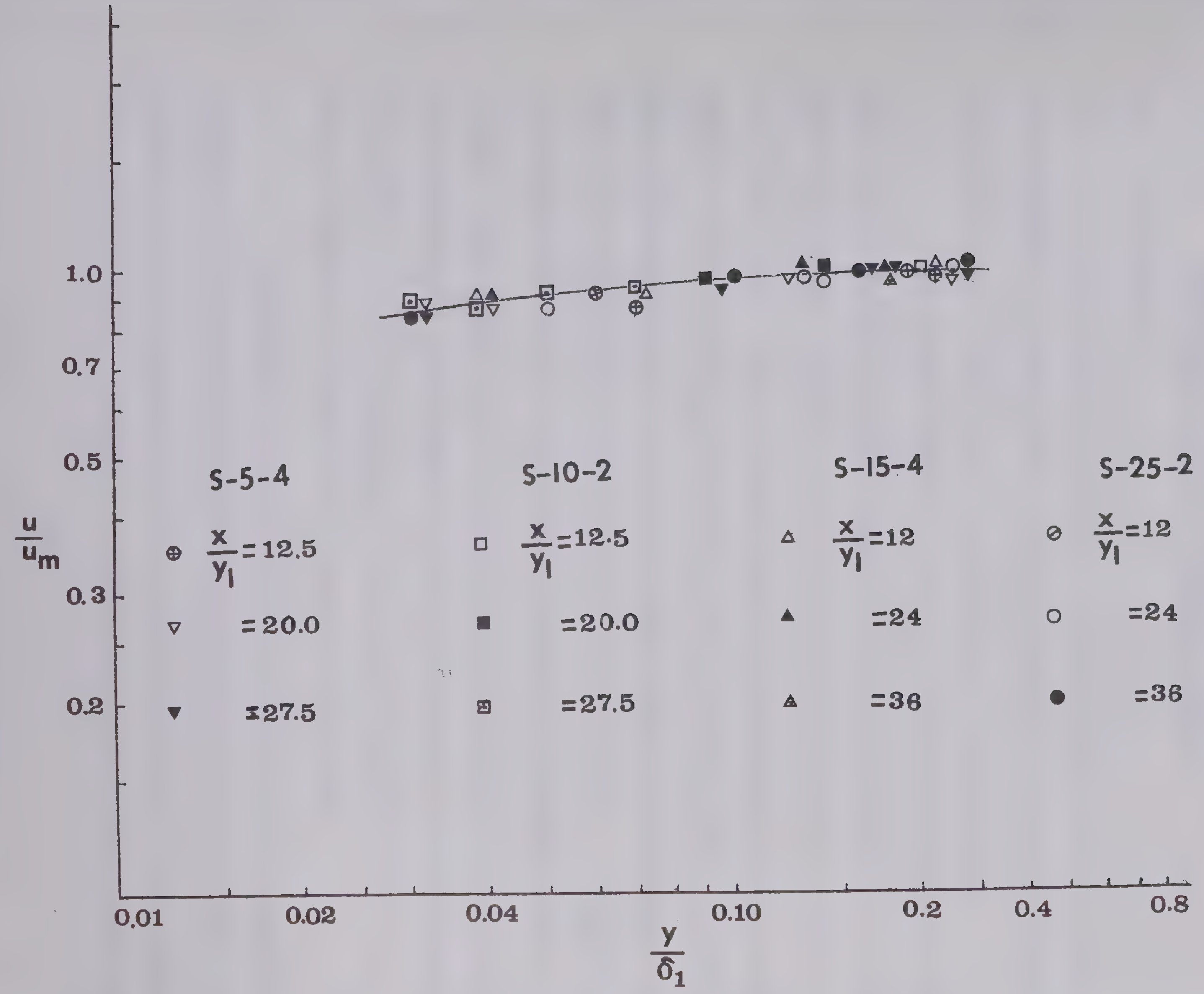

FIG. IV-20. VELOCITY DISTRIBUTION IN INNER LAYER SUBMERGED JUMPS

CHAPTER V

MECHANICS OF FORCED HYDRAULIC JUMPS

5.1 Introduction

This chapter presents the experimental results of drag distributions on baffle walls and the mechanics of some types of forced hydraulic jumps formed with the assistance of baffle walls.

The forced hydraulic jump is a jump formed with the assistance of baffles (or baffle piers) with or without a subcritical tail-water and is the basic design element of most of the hydraulic jump type stilling basins. A considerable amount of experimental work has been done on forced jumps in the course of the hydraulic model studies for the stilling basins for the large number of dams that have been constructed all around the world. But the first attempt at organising a reasonable theory for forced jumps appears to have been made by Forster and Skrinde [13] in 1950. This case followed by the studies of Harleman [17], Rajaratnam [41] and more recently my McCorquodale and Regts [24]. On the experimental side, careful studies have been made by Bradley and Peterka (6), Rand (43) and others.

In general, in all the above studies, only the gross characteristics of the forced jump have been studied with very little attention being given to the detailed flow processes that occur in the phenomenon. It is believed that a better understanding of these will enable better

control of the forced jump, giving rise to more rational and economical design procedures for the hydraulic jump-type stilling basins. As a first step in this direction, the mean flow patterns inside forced jumps created by baffle walls have been studied and described using the flow models of the turbulent wall jet and turbulent free jet in the appropriate regions. In addition, the form drag on the baffle wall has been measured using a large number of suitably placed pressure tappings and analysed. Further, this analysis has been used to develop preliminary design procedure for stilling basins.

5.2 Drag on the Baffle Wall

Fig. V-1 is a schematic representation of a forced jump, in which y_1 is the depth and U_1 is the mean velocity of the supercritical stream before the jump, y_t is the tailwater depth after the jump, h is the height of the baffle wall located at a distance of x_o from the toe of the jump and y_m is the maximum depth in the forced jump. If D is drag on unit length of the baffle wall, one could write

$$D = f_1 \, [y_1, U_1, g, y_t, x_o, h, \rho, \nu] \tag{5.1}$$

where g is the acceleration due to gravity, ρ is the mass density and ν is the kinematic viscosity of the fluid. Using the π - theorem, Eq. 5.1 could be reduced to

$$C_d = \frac{D}{\frac{\rho U_1^{\,2}}{2}.h} = f_2\left[F_1 = \frac{U_1}{gy_1},\ R = \frac{U_1 y_1}{\nu},\ \frac{h}{y_1},\ \frac{x_o}{y_1},\ \frac{y_t}{y_1}\right] \tag{5.2}$$

where C_d is some type of a drag coefficient, F_1 is the Froude number and R is the Reynolds number of the supercritical stream. In the forced jump, if R is very large, say greater than about 10^4, the effect of viscosity on the turbulent diffusion and hence on the gross characteristics could be assumed to be negligible and Eq. 5.2 would then reduce to the form

$$C_d = f_3\left[F_1,\ \frac{h}{y_1},\ \frac{x_o}{y_1},\ \frac{y_t}{y_1}\right] \tag{5.3}$$

Applying the integral momentum equation along with the continuity equation to the forced jump, one could obtain, as shown in (41)

$$C_d = \frac{\left[\frac{y_t}{y_1} - 1\right]\left[2F_1^{\,2} - \frac{y_t}{y_1}\left(1 + \frac{y_t}{y_1}\right)\right]}{F_1^{\,2} \cdot \frac{y_t}{y_1} \cdot \frac{h}{y_1}} \tag{5.4}$$

From Eq. 5.4, it is seen that, $\frac{y_t}{y_1}$ is specified for given values of the set of C_d, F_1 and $\frac{h}{y_1}$. Hence, Eq. 5.3 could be further reduced to the form

$$C_d = f_4 \left[F_1, \frac{h}{y_1}, \frac{x_o}{y_1} \right] \tag{5.5}$$

At the present state of knowledge of turbulent flows, it does not appear to be possible to evaluate Eq. 5.5 theoretically and hence it has to be evaluated only experimentally. To evaluate the drag coefficient, Rajaratnam (41) used Eq. 5.4 and measured values of F_1, h, y_t and y_1. In this process it was found that C_d was very sensitive to even small errors in measurement of y_t, which is quite difficult to measure accurately due to the fluctuating nature of the tailwater. The best solution would be to measure the drag force directly as was done by Harleman (17) and by McCorquodale and Regts (24). Due to the non-availability of such a device, the pressure drag on the baffle wall was measured by providing a large number of piezometric holes in the baffle wall. The skin friction drag on the baffle wall is assumed to be neglible and hence the pressure drag will constitute the total drag. This method has of course got the superiority of furnishing the pressure distribution on the baffle wall.

The first series of experiments were devised to evaluate Eq. 5.5. These experiments were done in Flume B. Different types of forced jumps could be created by adjusting the tailwater with another control gate located at the downstream end of the flume. Baffle walls of heights of one and two inches shown in Fig. V -2 were used in this study. The pressure distribution on the baffle walls was obtained from

water manometers. Depths of flow were measured by means of precision point gauges.

Fig. V -3 shows some typical piezometric pressure distributions on the baffle wall. On the front face, for $x_o = 11.0$ inches, the piezometric pressure decreases from a certain value on the bottom to some minimum value and then increases to a maximum value at $\frac{y}{h} \simeq 0.85$ and would drop down to some low value at the crest, where the flow separates from the baffle wall. For large values of x_o, the piezometric pressure on the front face becomes almost uniform. The base pressure on the rear side of the baffle wall was uniform for all values of x_o.

From these pressure distributions, the drag and the drag coefficient were computed. The variation of C_d with x_o/y_1 for $\frac{h}{y_1} = 0.625$, 0.954, 1.25 and 1.90 are shown in Fig. V -4 (a) to (d). The first conclusion is that for a given value of h/y_1, the variation of C_d with x_o/y_1 appears to be independent of F_1. In Fig. V -4 (b) and (d), the results for the one inch and two inch baffle walls do not agree and it is difficult to imagine that the absolute height difference would be responsible for this difference and hence no special significance is given to this disagreement.

For the purpose of developing a design procedure for the baffle wall, it appears to be more convenient to plot the variation of the quantity $\Lambda = C_d \cdot \frac{h}{y_1}$ with x_o/y_1 as is done in Fig. V -5(a) to (d).

The mean curves are all collected together in Fig. V -6. Using Fig. V -6 and Eq. 5.4 which is displayed in a graphical form in Fig. V -7, stilling basins could be designed using the procedure suggested earlier by Rajaratnam (41). Discussing this procedure further, from the work of Rand (43) it appears that for a given supercritical stream and any baffle height, there is a minimum position for the forced jump and let x_o for this minimum position be denoted by L_1. The variation of L_1/y_1 with F_1 has been obtained by Rand (43). Using this minimum position any other forced jump could be defined by a parameter ξ defined as

$$\xi = \frac{x_o - L_1}{L_1} \tag{5.6}$$

From the work of Rand (43), it is found that for the range of F_1 from 2 to 10, L_1/y_1 varies from 5 to about 10. Hence, L_1/y_1 is given an average value of 7.5 for further use. Then

$$\xi = \frac{\frac{x_o}{y_1} - 7.5}{7.5} = \frac{1}{7.5} \frac{x_o}{y_1} - 1 \tag{5.7}$$

Using the above equation, lines of $\xi = 0$, to 5.0 are drawn in Fig. V -6. If ξ_o is the value of ξ when x_o is equal to the length of the corresponding natural jump, i.e. the jump formed without a baffle, using the data

of Bradley and Peterka (7), the variation of ξ_o with F_1 is shown in Fig. V -8. For any forced jump with any given F_1, if its ξ is close to zero the forced jump is very similar to the minimum jump; if ξ is closer to ξ_o, then it approaches the corresponding natural jump.

5.3 Flow Characteristics of the Forced Jump

When the forced hydraulic jump is formed in the minimum position, it is very violent and is considerably different from the corresponding natural jump with the same supercritical Froude number. On the other hand, when the baffle wall is placed far away from the toe so that $\xi \to \xi_o$, then as mentioned in the previous section the resulting phenomenon is approximately the same as the corresponding natural jump. In the intermediate range of $0 < \xi < \xi_o$, the geometrical configuration of the forced jump and the violence of flow changes continuously. The geometrical configurations have been qualitatively studied earlier by Rajaratnam (41), who connected certain forms with certain ranges of the drag coefficient. Rand (43) classified these flow patterns with the parameter K defined as

$$K = \frac{x_o - L_1}{1.25\ L_j - L_1} \tag{5.8}$$

where L_j is the length of the natural jump. For the minimum jump $K = 0$ and when K approaches unity, the forced jump approaches the natural jump. The two parameters K and ξ are connected by the relation

$$K = \frac{7.5\xi}{1.25 \frac{L_j}{y_1} - 7.5} \tag{5.9}$$

and Eq. 5.9 is shown plotted in Fig. V-9.

Six forced jumps were studied to obtain the mean flow characteristics as given in Table V-1 (second series). For three experiments K = 0, with supercritical and subcritical tailwater, for two runs K = 0.4 with subcritical tailwater and for one experiment K = 1.0, with subcritical tailwater. The supercritical Froude number was varied from 4.30 to 7.15.

Fig. V-10 shows the forced jump with K = 1.0 with the surface profile, velocity distribution in the region between the toe of the jump and the baffle wall (Region 1) and in the region beyond the baffle wall (Region 2). The velocity distribution before the baffles indicates that the flow could possibly be analysed using model of the plane turbulent wall jet (14, 44, 34). It appears that the forward flow downstream of the wall (Region 2) could be analysed, using the model of the curved free turbulent jet. The above comments apply reasonably well to Fig. V-11 for K = 0.4, and Fig. V-12 for K = 0 and to Fig. V-13 for K = 0 with supercritical tailwater.

5.4 Flow Characteristics of Region 1

The velocity distribution to Region 1 which appeared to be amenable for analysis using the model of the wall jet was tested for

similarity of velocity distribution in the conventional manner by plotting the dimensionless velocity $\frac{u}{u_m}$ against the dimensionless ordinate $\frac{y}{\delta_1}$ where u is the turbulent mean velocity in the x direction at a distance of y normal to the bed, u_m is the maximum value of u at any x station and δ_1 is the value of y where $u = \frac{u_m}{2}$ and $\frac{\partial u}{\partial y}$ is negative. Generally, u_m and δ_1 are known respectively as the velocity and length scales. It was found that there was considerable amount of scatter, especially in the layer in which u increases from zero to u_m, this being known as the boundary layer zone. The region above this is the so-called free-mixing zone, and, the velocity distribution in this region was tested for similarity by plotting u/u_m against $\frac{y-\delta}{\delta_1-\delta}$ where δ is the thickness of the boundary layer. This operation is shown in Fig. V-14 for a few typical runs. For the jumps with K = 0.4 and 1.0, the similarity is reasonably good and the data agree reasonably well with the corresponding curve of the plane turbulent wall jet with zero pressure gradient, known as the classical wall jet. For the cases with K = 0, there appears to be more scatter in the experimental observations.

In the boundary layer region, the velocity distribution is satisfactorily described by the power laws as shown in Fig. V-15, with the exponent n in the power law written as

$$\frac{u}{u_m} = [\frac{y}{\delta}]^{1/n} \tag{5.10}$$

varying from 5.0 to 8.65.

The variation of the boundary layer thickness δ is studied in Fig. V-16. It is seen that in the forced jump due to the additional adverse pressure gradient created by the baffle wall, the boundary layer grows faster than that in the natural jump. The length scale for the free mixing region is plotted in Fig V-17 with $\frac{\delta_1-\delta}{y_1}$ against x/y_1. It is interesting to find that this scale factor grows at the same rate as that in the natural jump showing that the effect of the baffle wall on the growth of the free mixing region is negligible.

The next important parameter is the velocity scale u_m. The data for u_m are shown plotted in Fig V-18 along with the curve for the jump in a level rectangular channel known as the classical jump (31). The data points for forced jumps with K equal to and greater than 0.4 lie on the curve of the classical or natural jump whereas the points for $K = 0$ are located much lower thereby indicating more violent turbulent mixing of the supercritical stream. In conclusion it could be said that the forward flow in region 1 could be described by the turbulent wall jet model with some modifications to the classical case.

5.5 Flow Characteristics of Region 2

With reference to Fig V-1, it could be seen that behind the baffle wall there is a region of circulation which could be termed a standing eddy, the length of which is denoted as L_e. On top of this

eddy there is a region of forward flow which is similar to a plane turbulent curved free jet. The surface roller in cases with small values of K would extend beyond the baffle wall, but the reverse flow in this region was not measured.

Studies on curved jets are mainly of a empirical nature (for example see 27, 19, 28) and the velocity distributions are normally correlated with the solutions for straight jets. The velocity distribution in region 2 is plotted in Fig. V-19 with u/u_m against the nondimensional distance y/δ_1 where y is measured from the axis of the curved jet (which is taken as the line of maximum velocity) and δ_1 is the length scale defined as the value of y where $u = \frac{u_m}{2}$. The data for all the cases studied agree reasonably well with the Tollmien curve for the plane straight jet (45).

The variation of the velocity scale is studied in Fig. V-20, in which $\frac{u_m}{u_{mj}}$ is plotted against $\bar{x}/y_1$ where u_{mj} is the maximum velocity in the plane of the baffle wall and $\bar{x}$ is the longitudinal distance from the baffle wall. The variation appears to be roughly linear, with u_m/u_{mj} decreasing to about 0.57 at $\frac{\bar{x}}{y_1} = 12.0$. A study of the length scale showed that $\frac{\delta_1}{x} \simeq 0.23$ which is considerably greater than the corresponding straight jet value.

The backward flow in the eddy close to the bed appears to be fairly uniform. If u_{m*} is the maximum backward velocity in the eddy, $\frac{u_{m*}}{U_1} \simeq 0.25$ for $K = 0$ and decreases to about 0.1 for $K \simeq 1.0$.

Rough estimates of the bed shear stress in forced jump were obtained using the Preston technique (26, 29) and a typical variation is shown in Fig.V-10 & 12. If τ_{o*} is the maximum bed shear stress in the eddy, $\tau_{o*}/\rho\ U_1^2/2$ was found to be about 3×10^{-4} for $K = 0$ and 0.5×10^{-4} for $K \simeq 1.0$. The length of the eddy L_e was found to vary from 4 to 12 times the height of the baffle wall.

5.6 Conclusions

This chapter presents an experimental study of forced hydraulic jumps formed with two dimensional baffles or baffle walls. Using dimensional analysis, the integral momentum equation and experimental results, the drag on the baffle wall has been analysed and a design chart for a preliminary design of stilling basins has been presented. Further, the mean flow characteristics in the forced jump have been analysed using the model of turbulent wall jet and plane turbulent curved free jet in the proper regions. Some observations have also been made regarding the flow in the eddying region behind the baffle wall.

DETAILS OF SECOND SERIES OF EXPERIMENTS

Expt. No.	y_1 (in)	U_1 (ft/sec)	F_1	y_t (in)	K	Remarks
2 - 1	1.2	11.8	6.60	8.85	0	Subcritical Tail water (Sub TW)
2 - 2	1.2	11.8	6.60	8.85	0.4	Sub TW
2 - 3	1.2	11.80	6.60	8.85	$\simeq$1.0	Sub TW
2 - 4	1.00	7.3	4.30	5.6	0	Supercritical Tail water (Sup TW)
2 - 5	1.15	10.00	5.72	7.6	0	Sub TW
2 - 6	1.00	11.65	7.15	7.15	0.4	Sub TW

TABLE V.-1

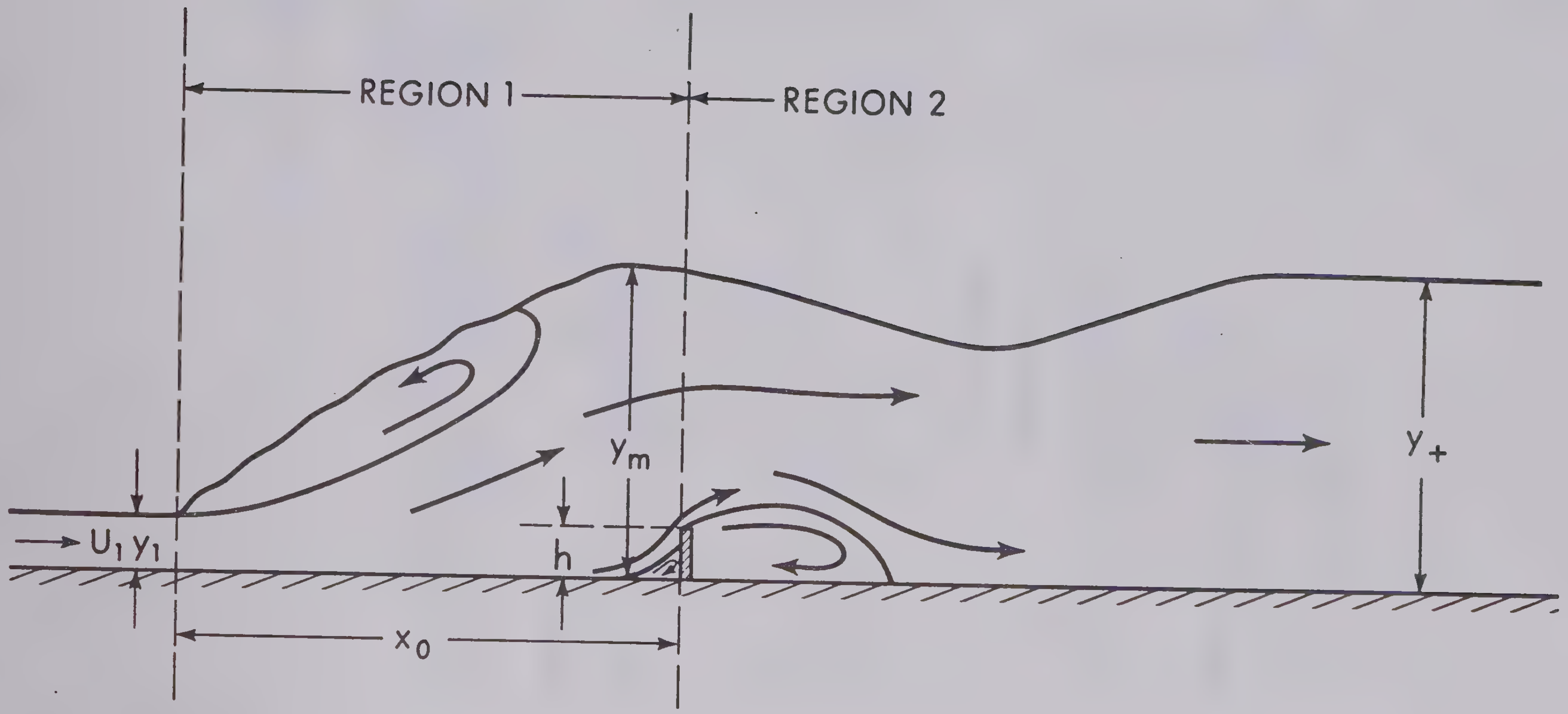

FIG.V-1. FORCED HYDRAULIC JUMP – DEFINITION SKETCH.

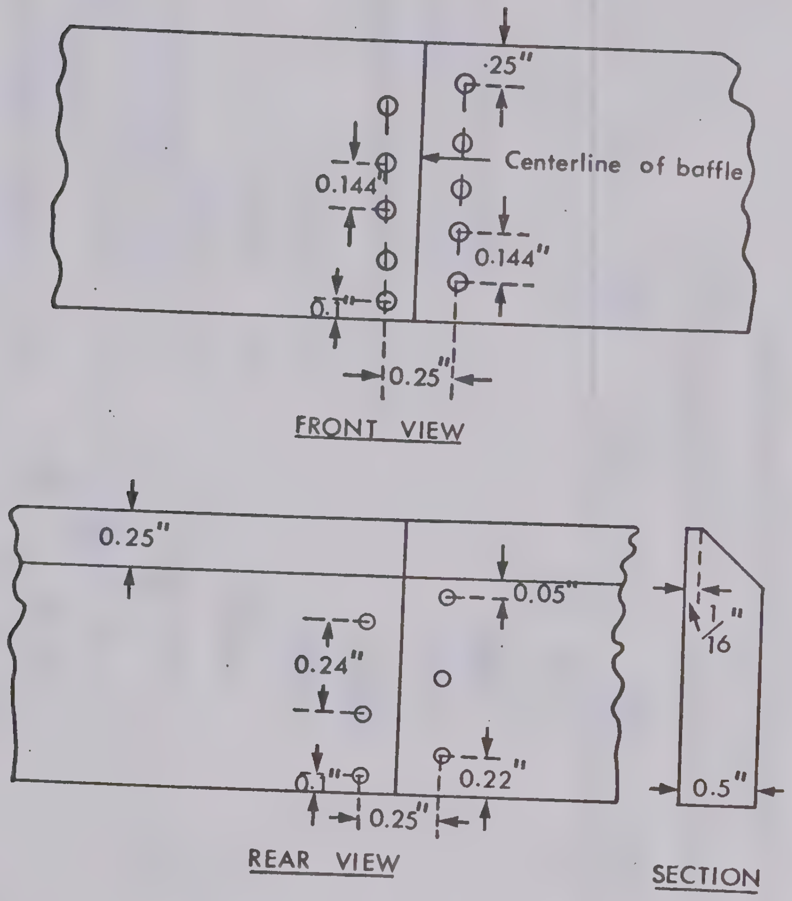

Note: The above details of the 1 inch wall are not shown to scale. For the 2 inch wall, there were 10 holes in the front and 6 holes in the rear. All the holes are 1.5 mm in diameter.

FIG.V-2. BAFFLE PIER DETAILS.

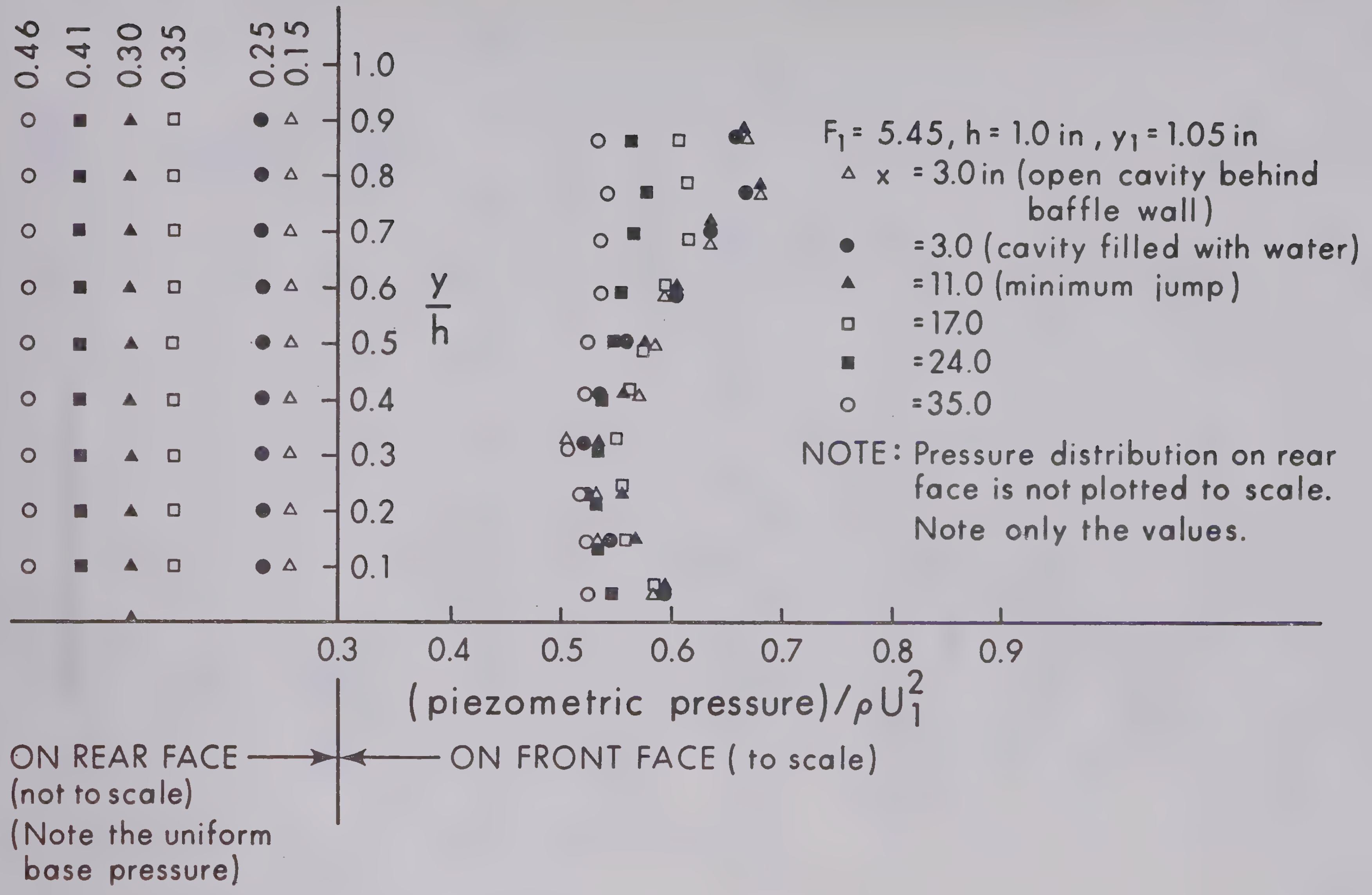

FIG.V-3. TYPICAL PRESSURE DISTRIBUTION ON BAFFLE WALL.

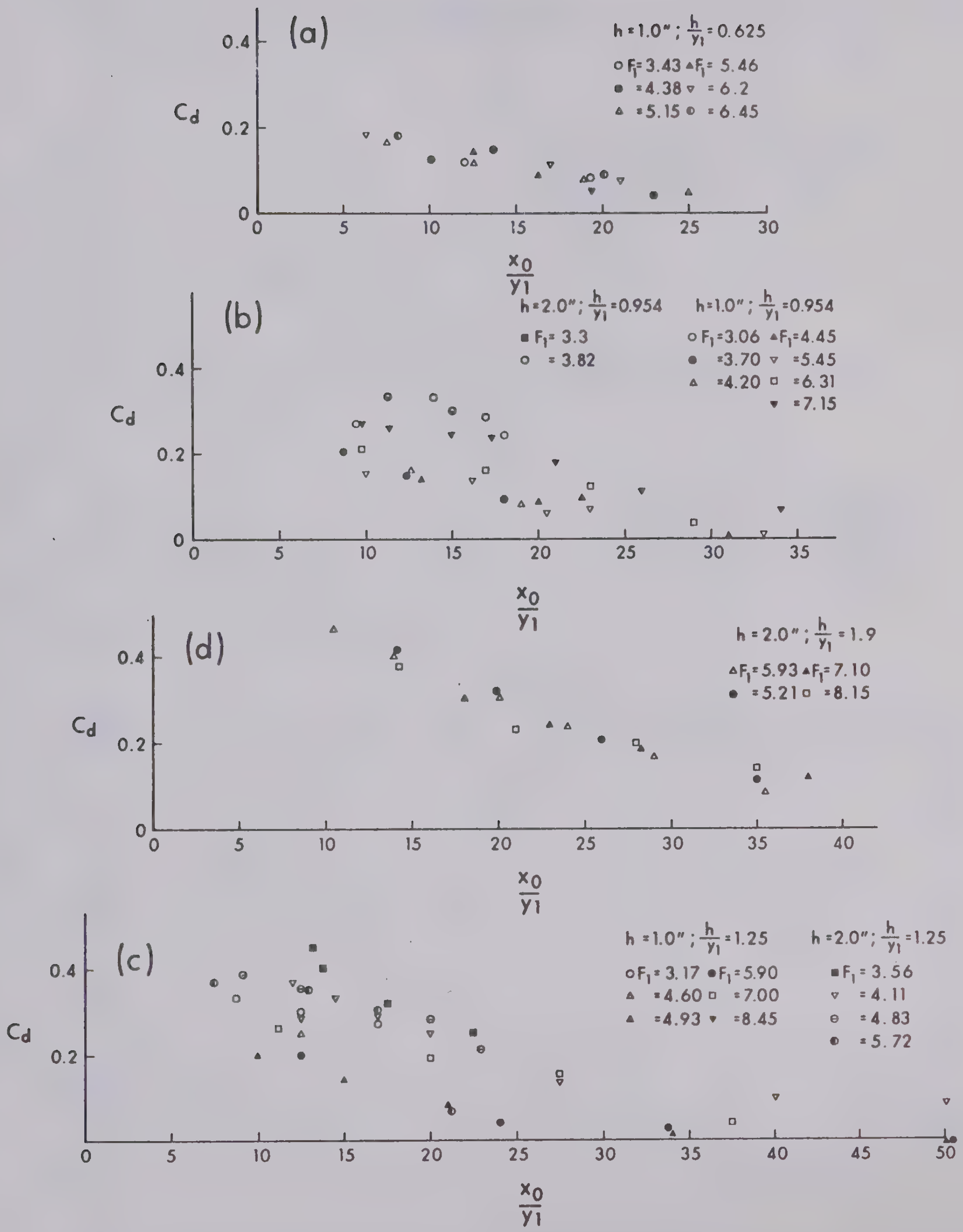

FIG. V-4. PLOT OF THE DRAG COEFFICIENT.

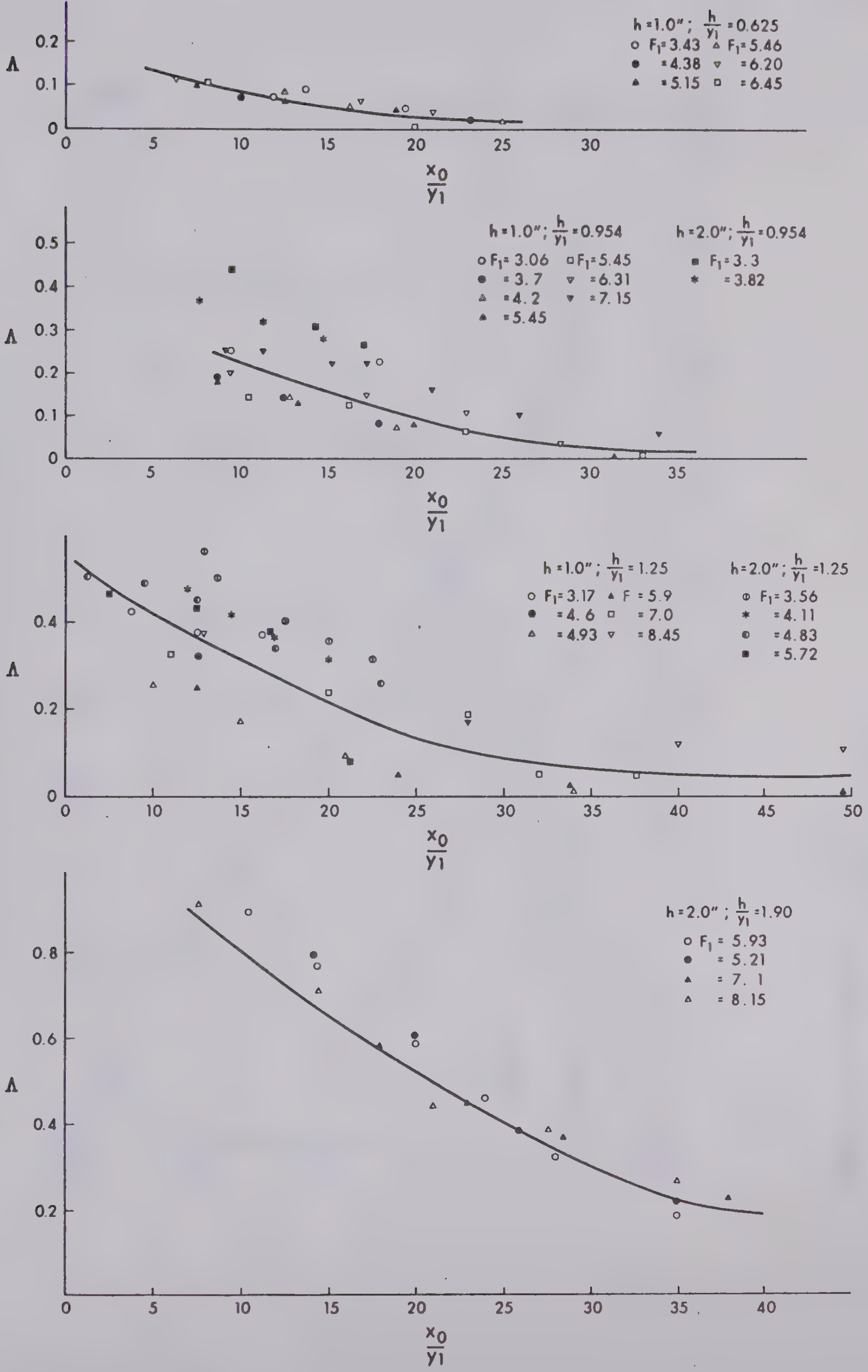

FIG. V–5 VARIATION OF THE PARAMETER Λ.

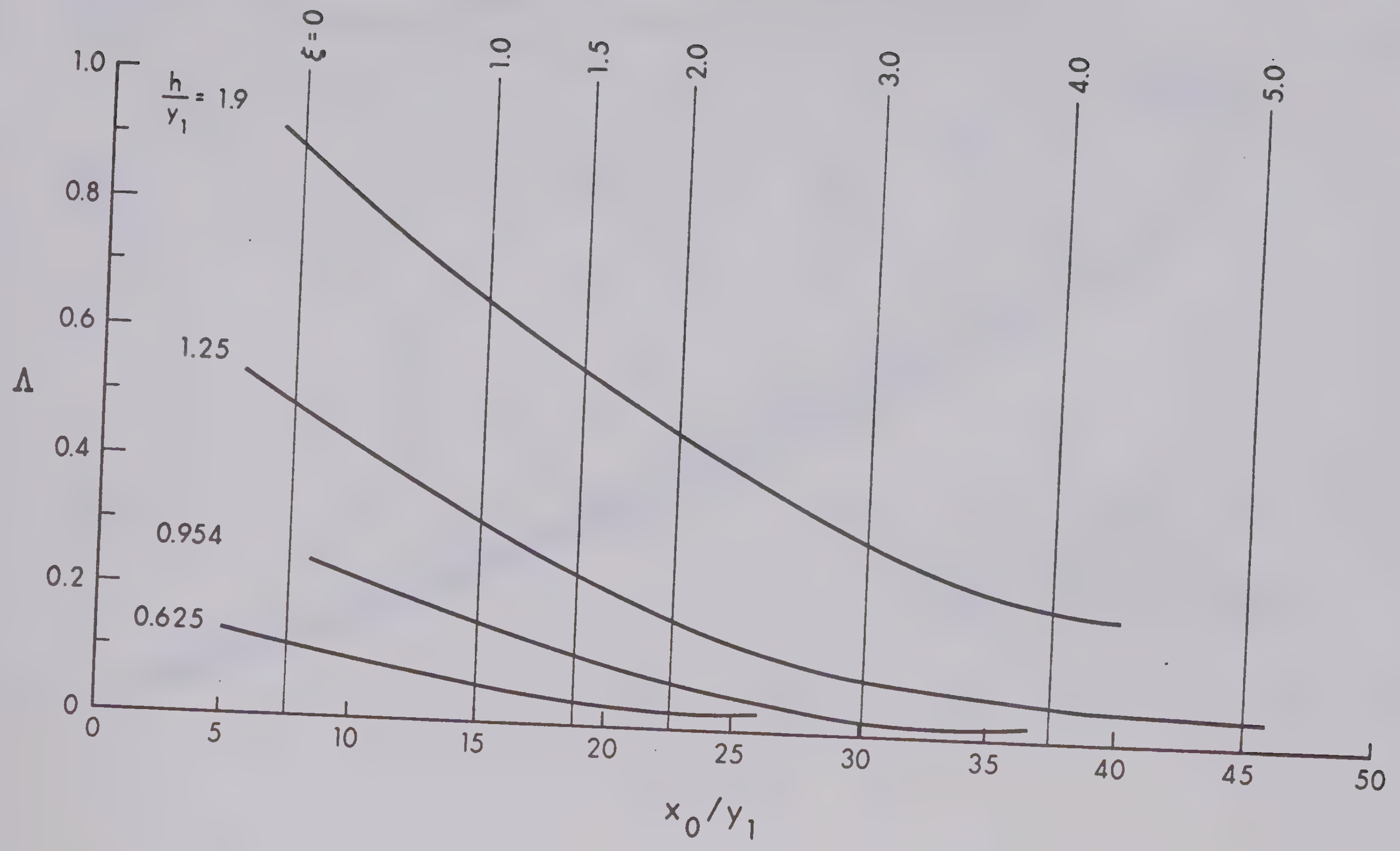

FIG. V-6. DESIGN CURVES FOR Λ .

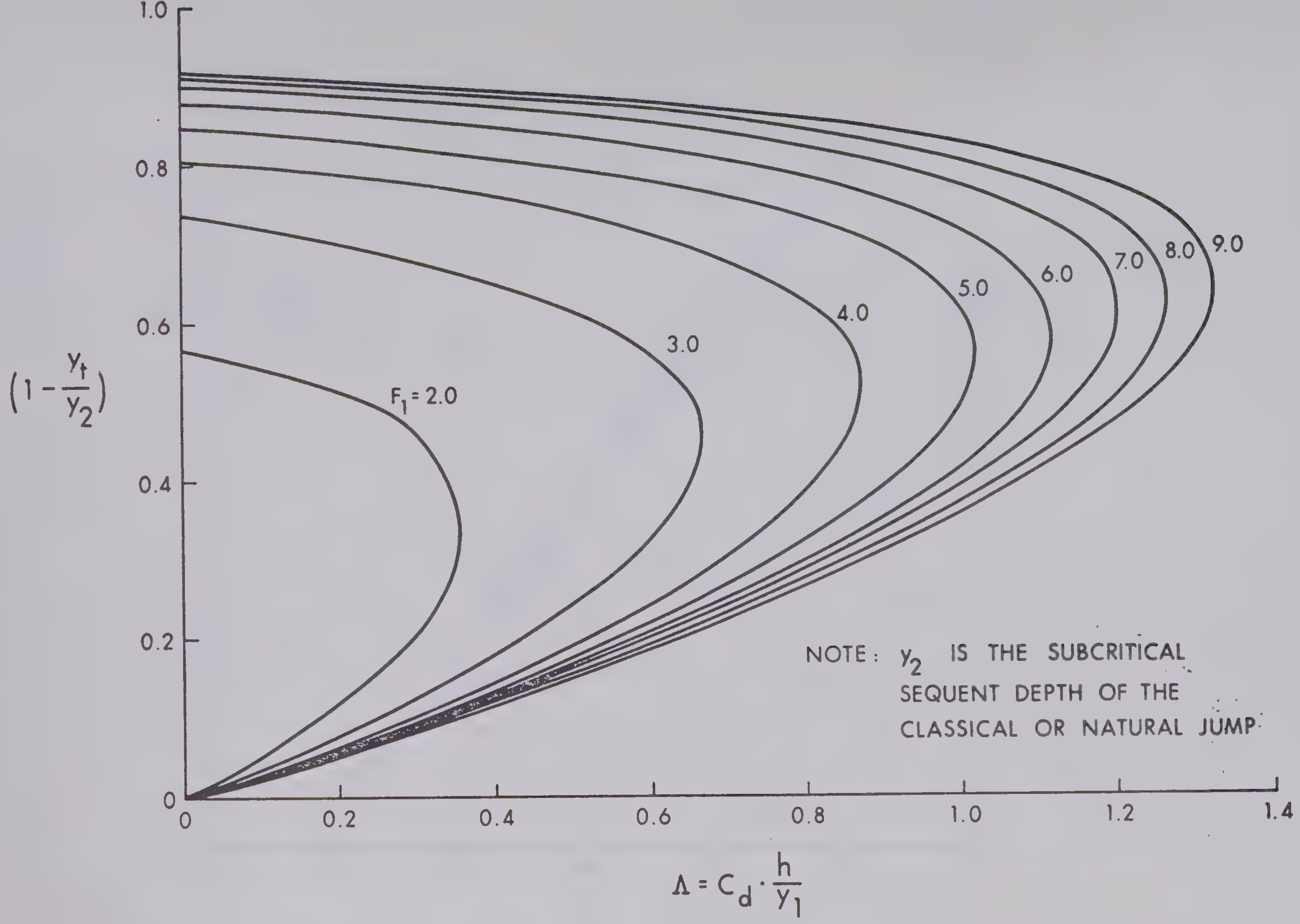

FIG.V-7. PLOT OF EQ.5.4

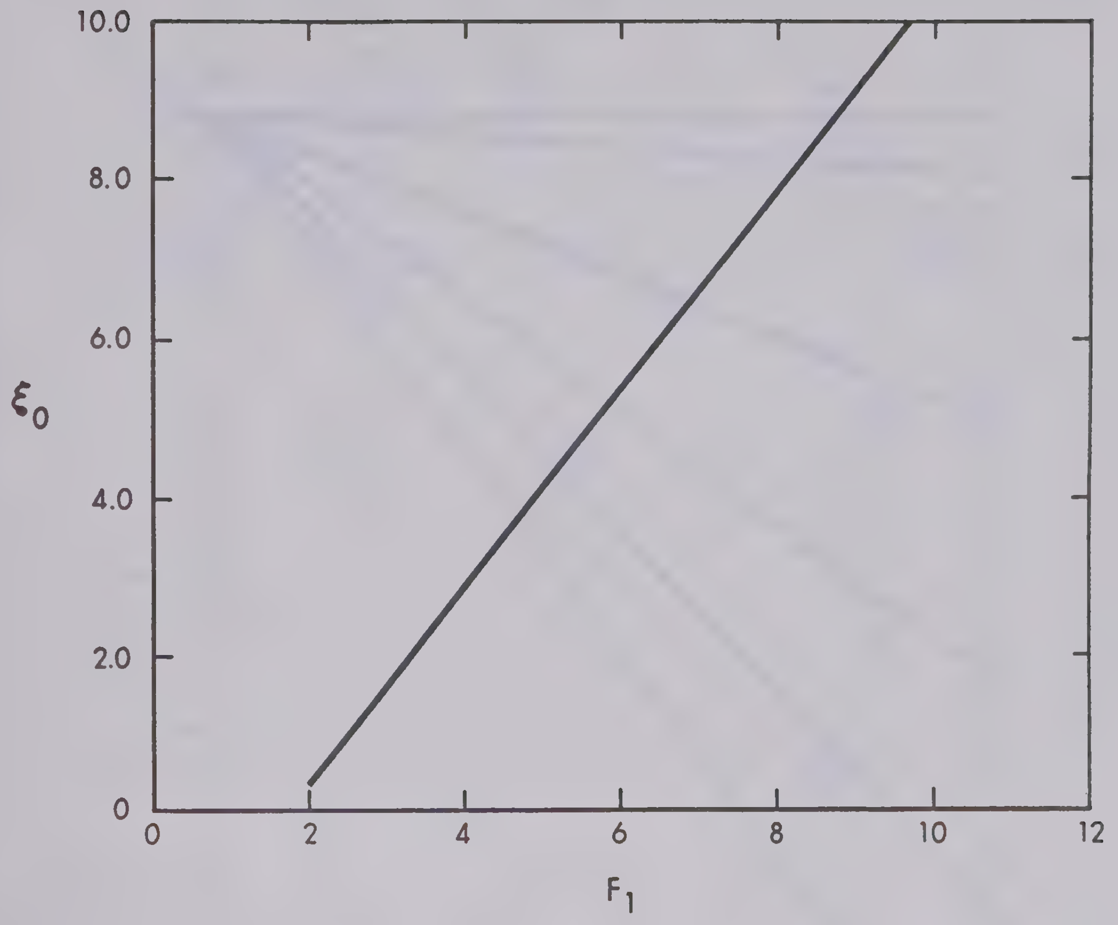

FIG.V-8 VARIATION OF ξ_0 WITH F_1 .

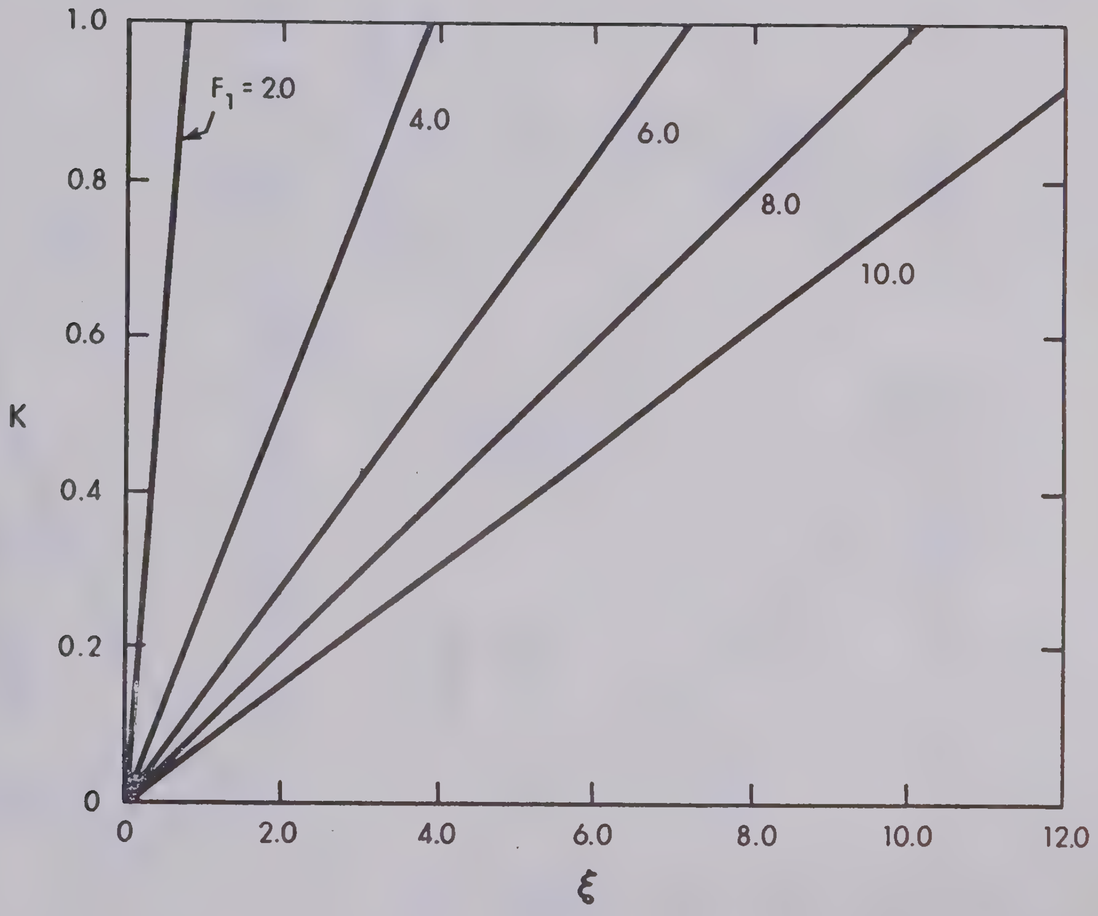

FIG.V-9. PLOT OF EQ.5.9.

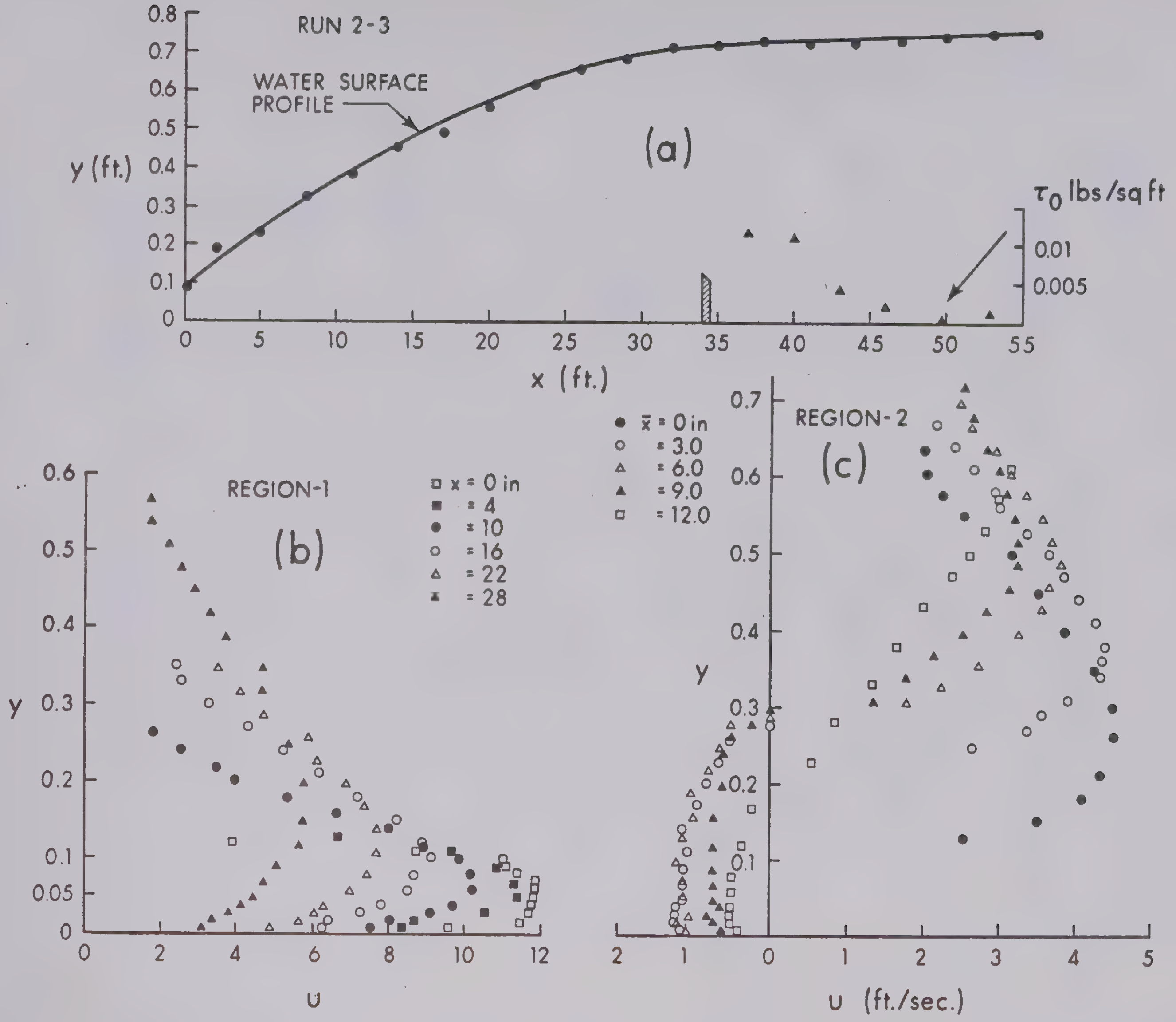

FIG.V-10. FLOW PATTERNS FOR K ≃ 1.0.

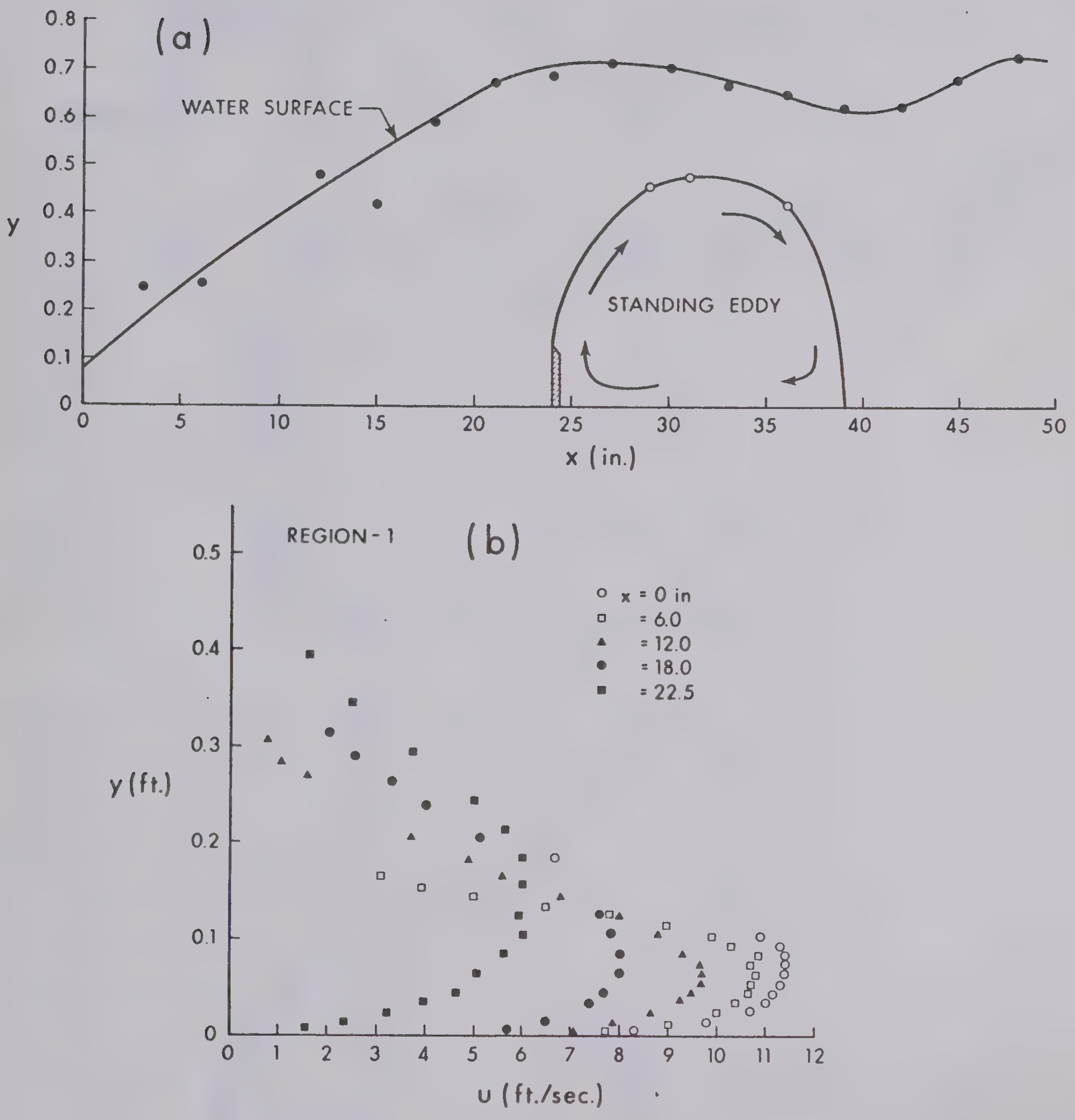

FIG.V-11. FLOW PATTERNS FOR K = 0.4.

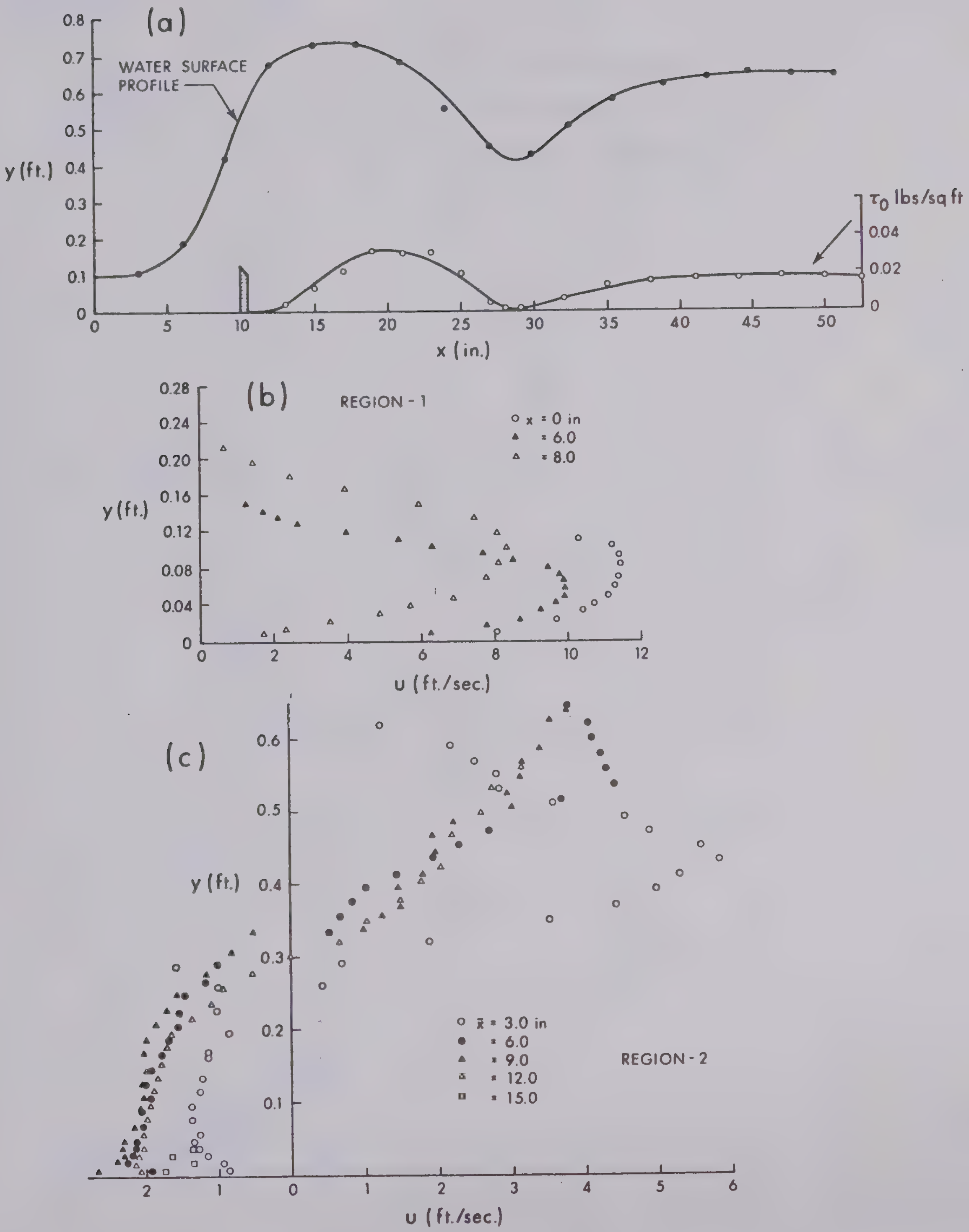

FIG·V-12. FLOW PATTERNS FOR K = 0 AND SUBCRITICAL TAILWATER.

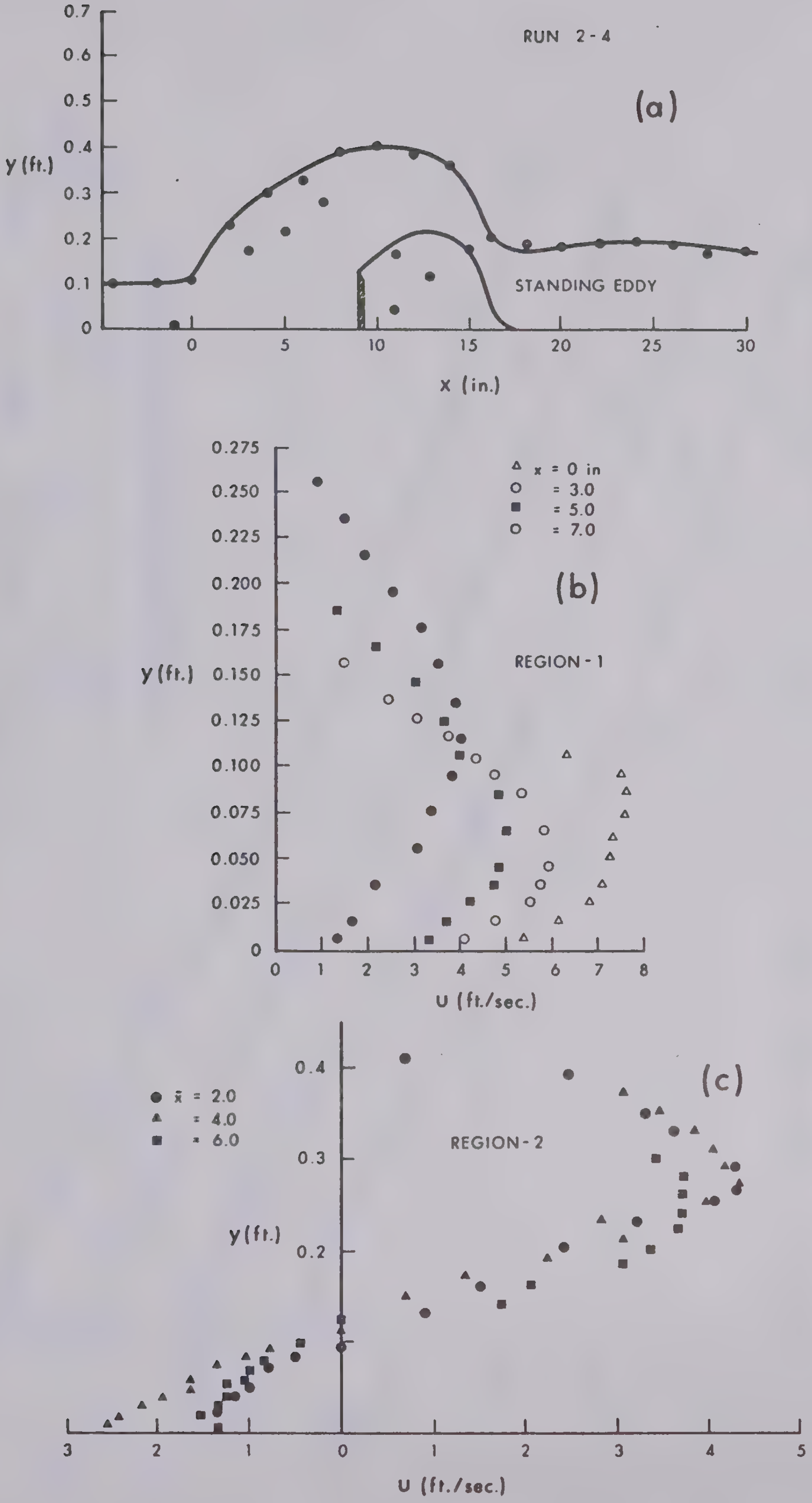

FIG.V-13. FLOW PATTERNS FOR K = 0 AND SUPERCRITICAL TAILWATER.

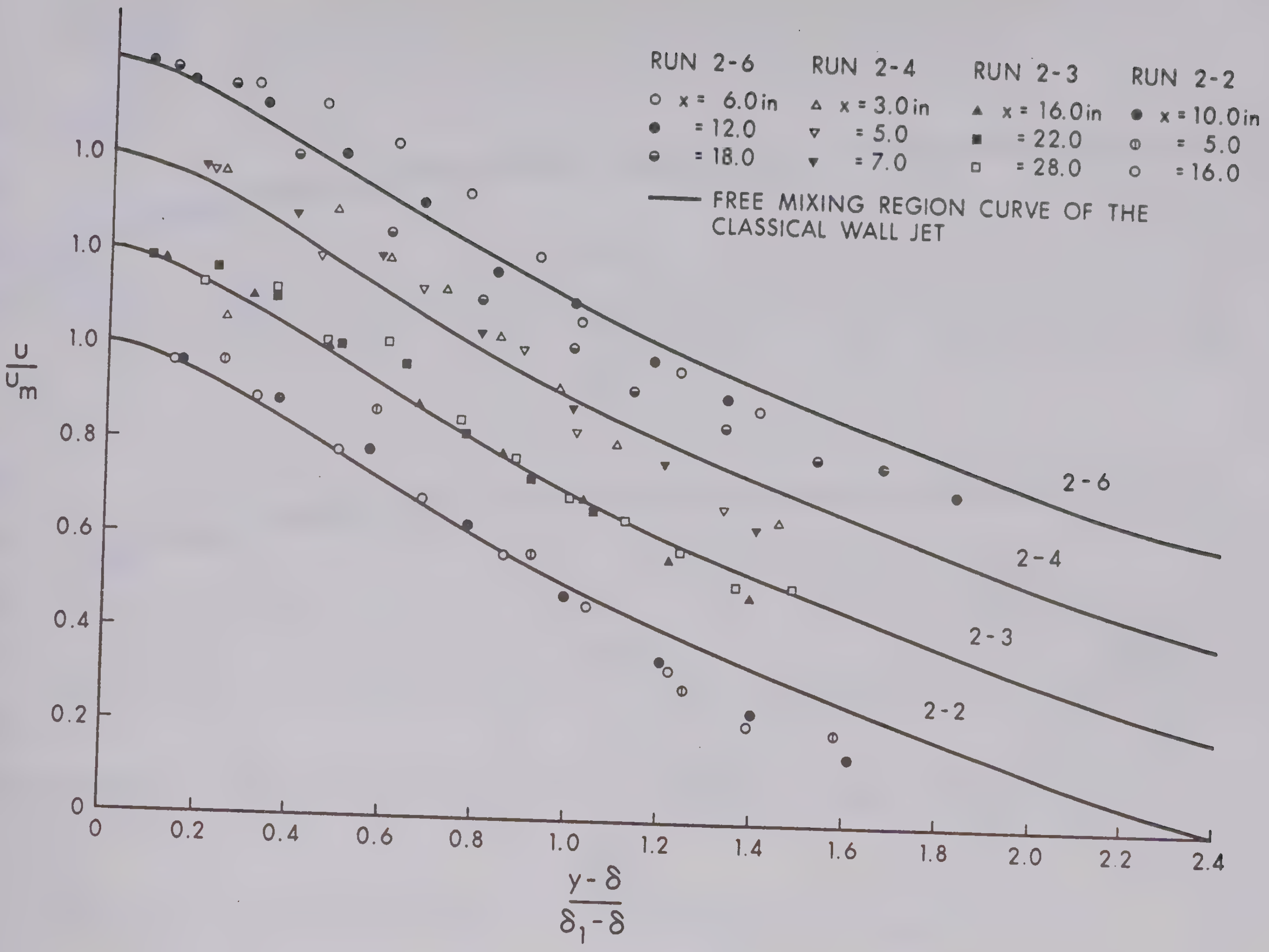

FIG.V-14. VELOCITY DISTRIBUTION IN THE FREE MIXING ZONE.

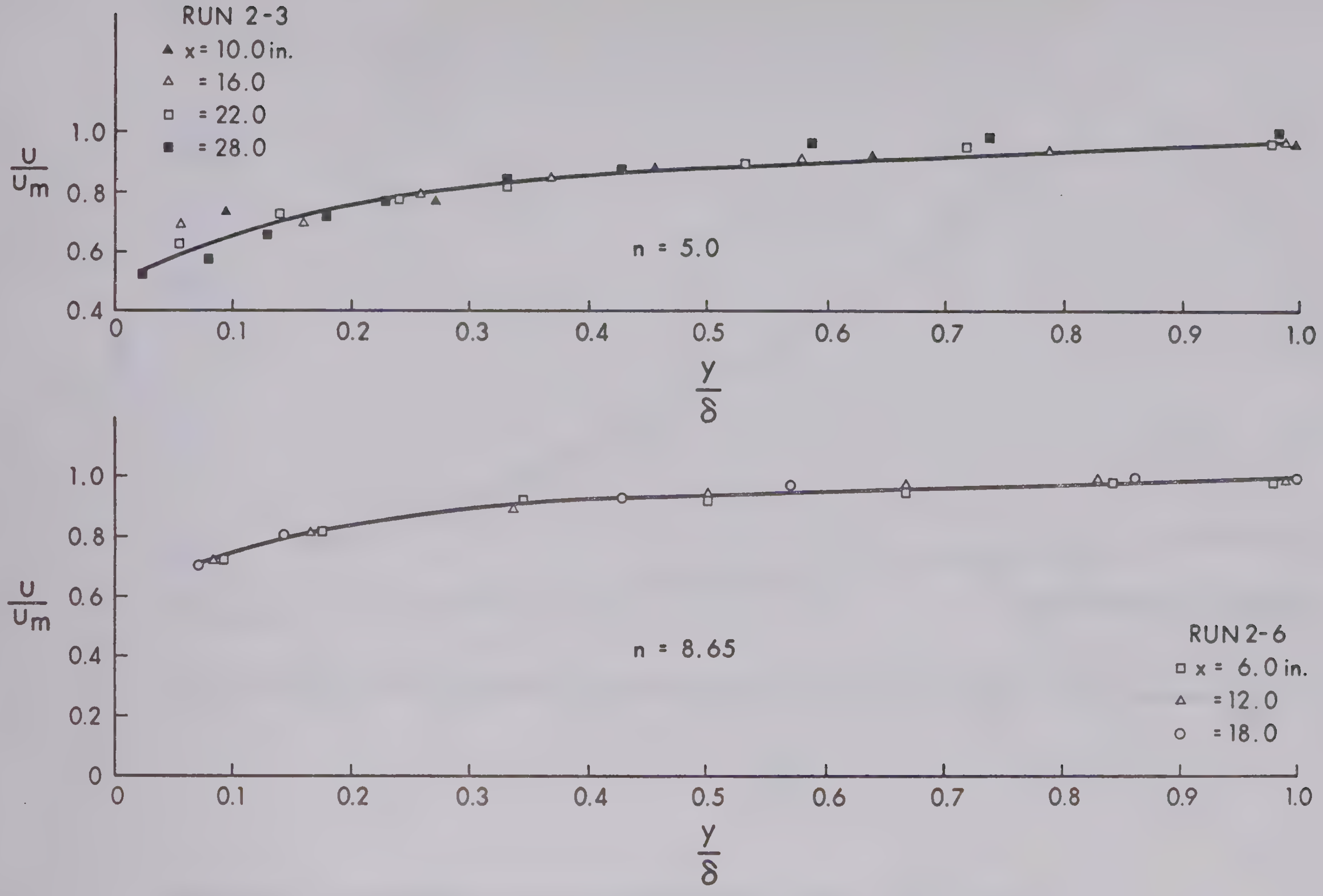

FIG. V-15. VELOCITY DISTRIBUTION IN THE BOUNDARY LAYER.

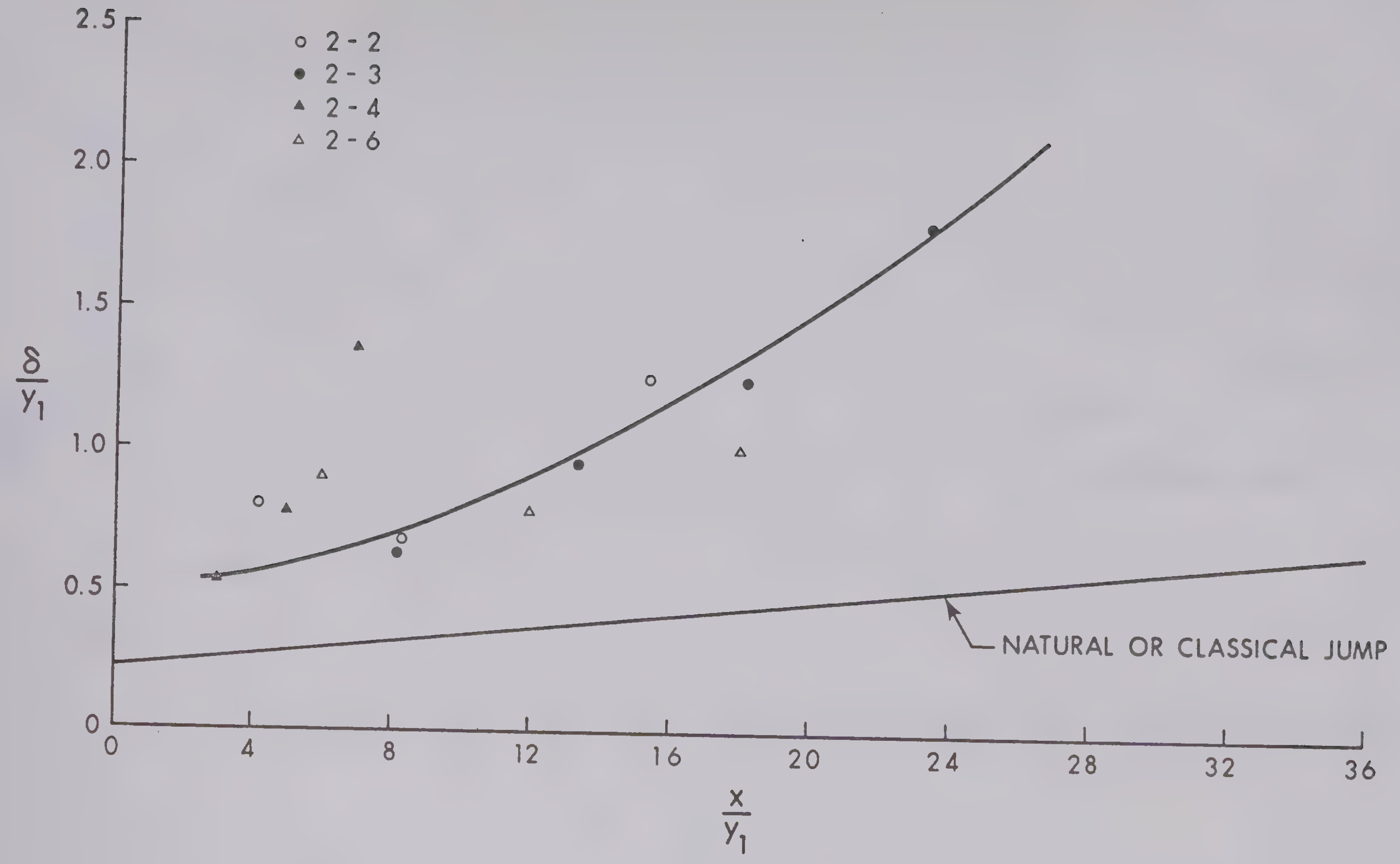

FIG.V-16. GROWTH OF THE BOUNDARY LAYER THICKNESS.

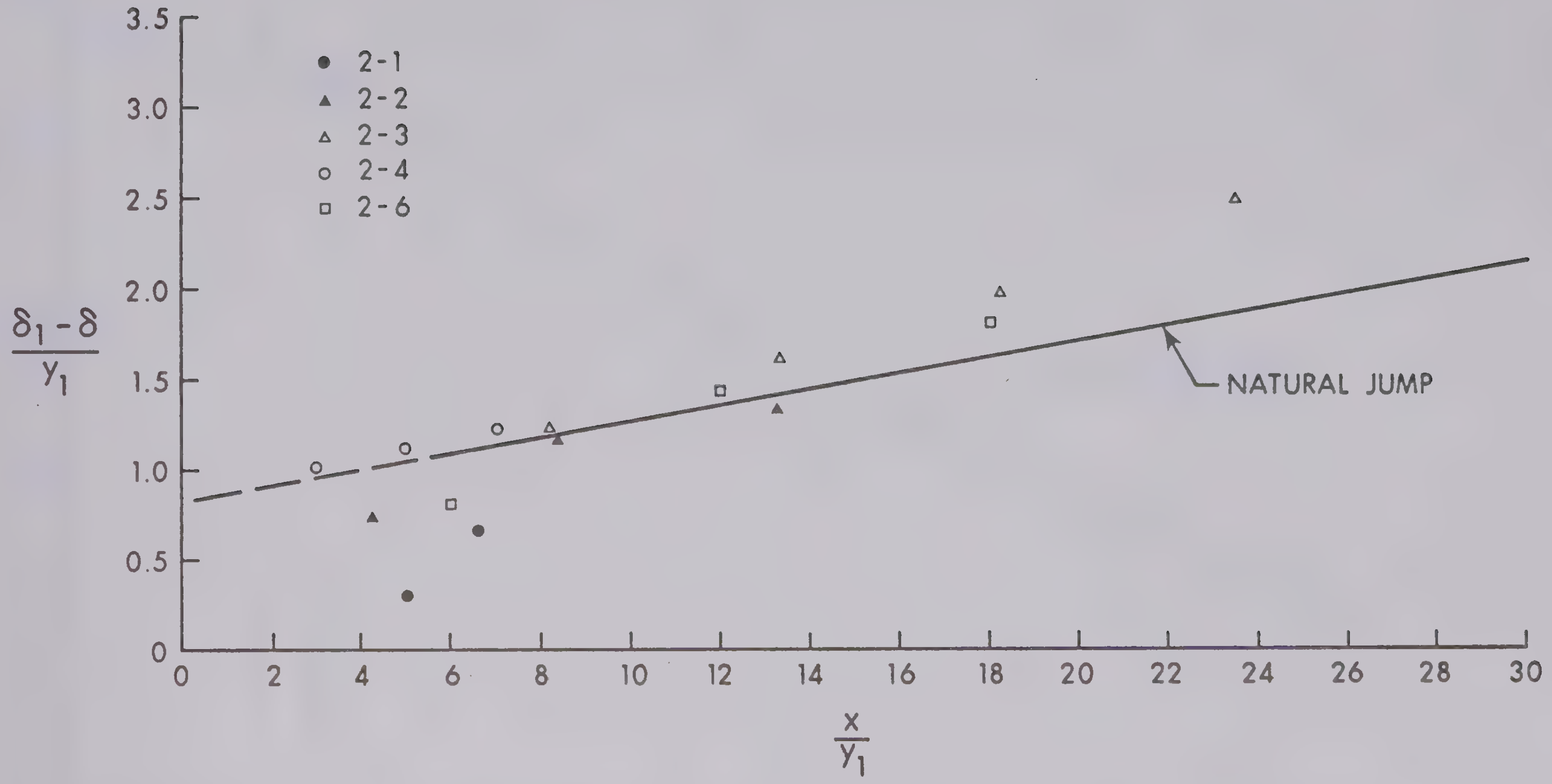

FIG.V-17. GROWTH OF THE LENGTH SCALE $\frac{\delta_1 - \delta}{y_1}$ WITH x/y_1 .

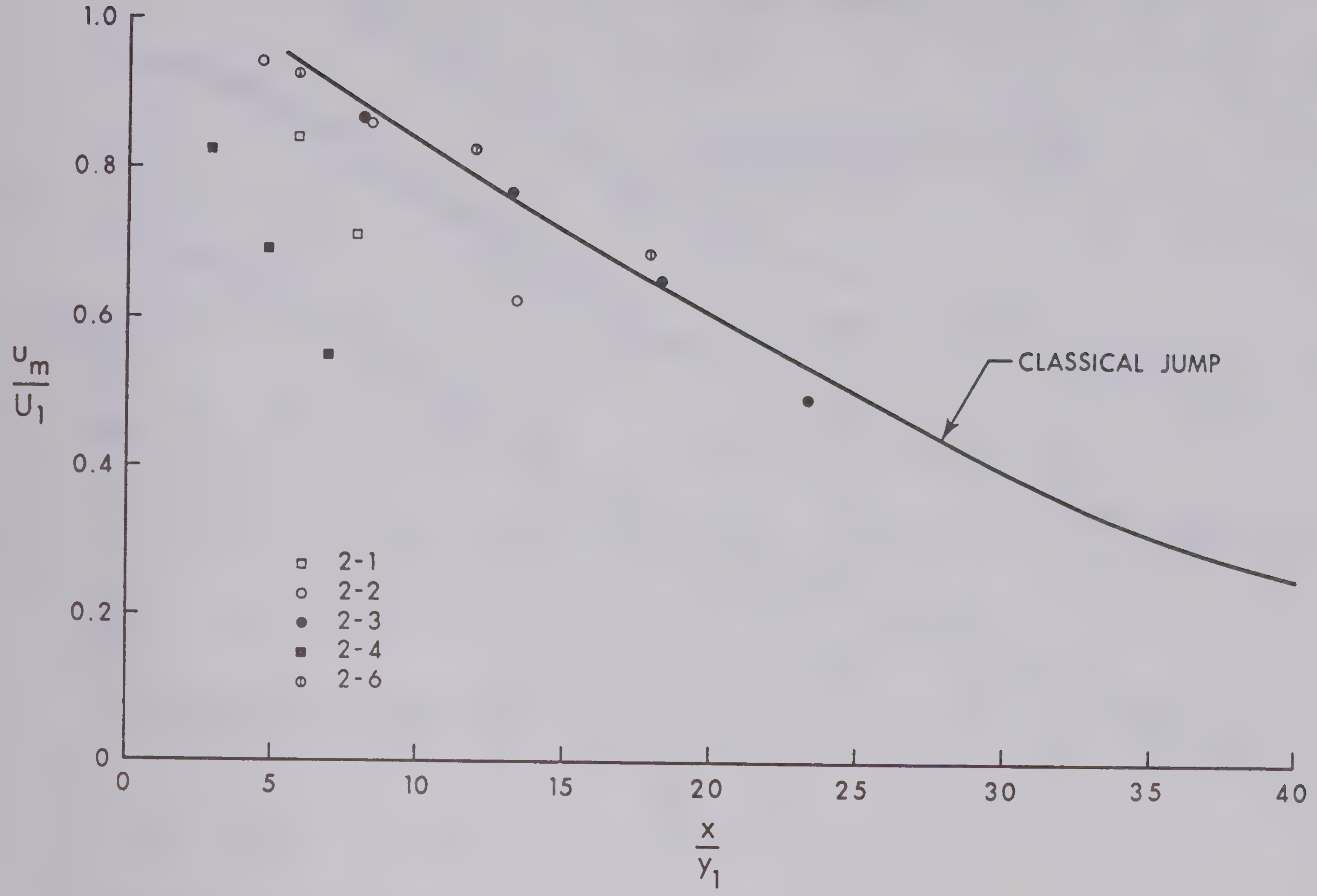

FIG.V-18. VARIATION OF THE VELOCITY SCALE.

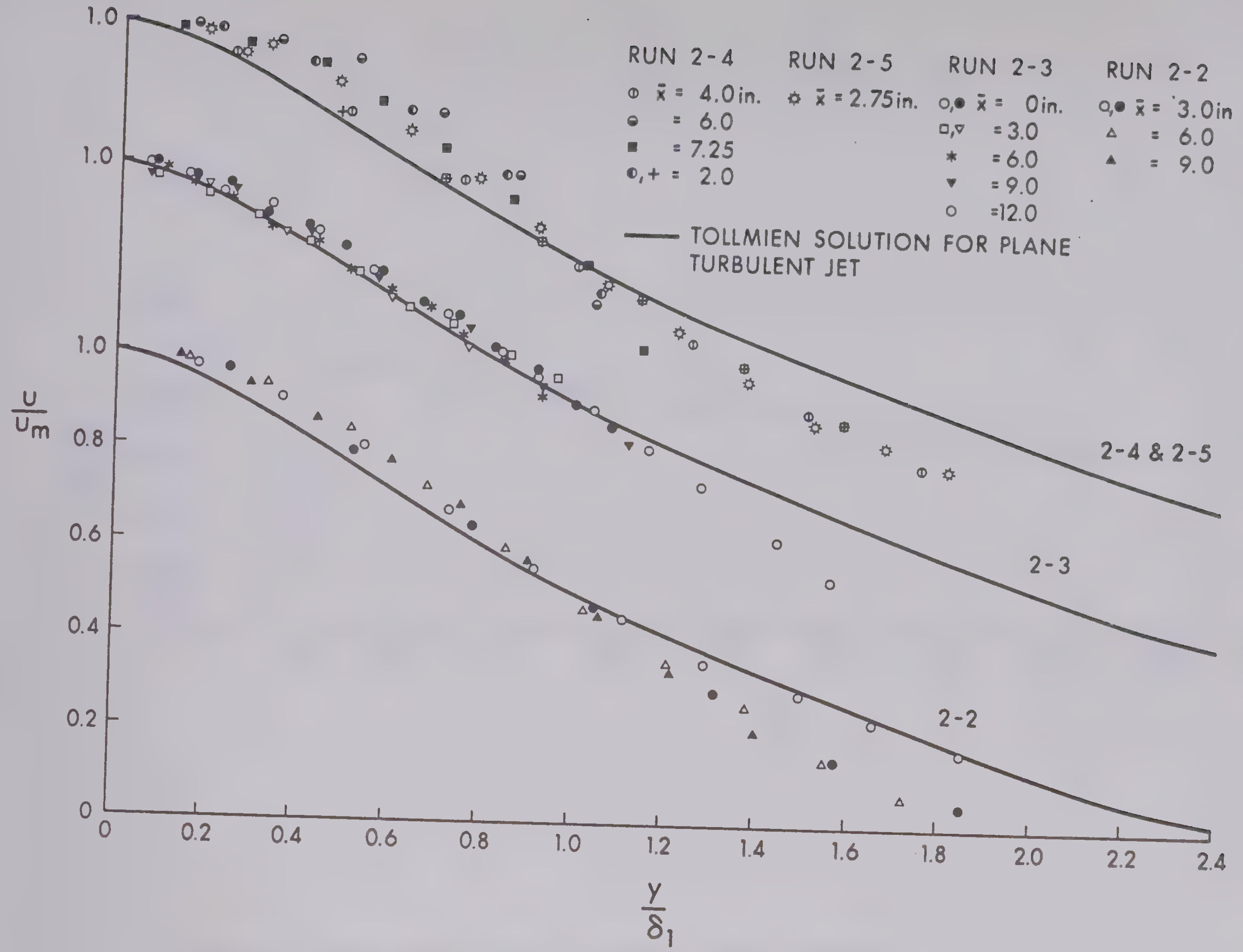

FIG·V-19. VELOCITY DISTRIBUTION IN THE CURVED FREE JET.

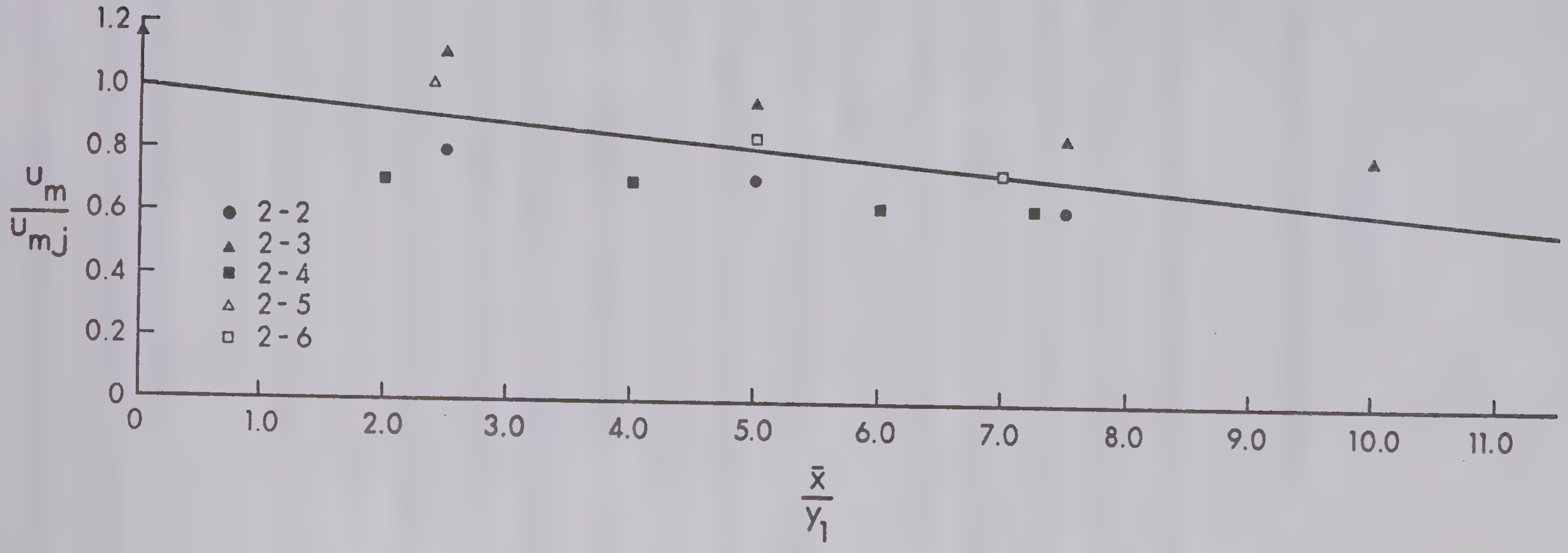

FIG.V-20. VELOCITY SCALE DECAY FOR REGION – 2.

CHAPTER VI

CONCLUSIONS AND RECOMMENDATIONS

6.1 Conclusions

Three practical hydraulic engineering problems have been studied analytically and experimentally with the help of free jet and wall jet models as an initial step towards understanding the mechanics of the phenomena. These are, the plane turbulent wall jets with finite submergence, the mechanics of sloping channel jumps and the mechanics of forced hydraulic jumps.

These studies have been discussed in Chapters III through V and the conclusions of the various studies have been given in respective chapters. The significant conclusions are reproduced in this chapter for convenience and recommendations are made for further study.

6.1.1 Plane Turbulent Wall Jets with Finite Submergence

The plane turbulent wall jets with finite submergence and with or without pressure gradient has been analysed theoretically. The correlation of theoretical predictions with the experimental observations was found to be reasonably good. The attempt to analyse the reverse flow has not been successful.

6.1.2 Mechanics of Sloping Channel Jumps

The turbulent wall jet model is found to be quite useful in predicting some of the mean flow characteristics. Simple power-law

type expressions have been developed for the velocity and length scales. Prediction of c_f was successful only for the steeper slopes.

The boundary layer flow analysis has indicated the fact that in the case of free jumps formed on steeper bed slopes the effect of adverse pressure gradient decreases and in the case of submerged jumps the assumption of flow similarity is reasonably valid.

6.1.3 Mechanics of Forced Hydraulic Jumps

The drag on the baffle wall has been analysed and a design chart for a preliminary design of stilling basins has been presented. The mean flow characteristics of four types of forced hydraulic jumps have been analysed using the models of plane turbulent wall jet and plane turbulent curved free jet in the proper regions. Some observations in the eddying region behind the baffle wall have also been presented.

6.2 Recommendations for Further Study

The following topics are recommended for further study:

1. The backward flow region in the plane turbulent wall jet with finite submergence and turbulence characteristics in the entire region.
2. Study of free and submerged hydraulic jumps on bed slopes steeper than 25% including the turbulence characteristics.
3. Study of jumps on adverse bed slopes.
4. Study of various types of forced hydraulic jumps formed with the help of baffle piers.
5. The theoretical analysis of curved jet region and the eddying regions of forced hydraulic jumps.

LIST OF REFERENCES

1. Abramovich, G.N., "The Theory of Turbulent Jets," M.I.T. Press, Cambridge, Mass., 1963 (English Translation).

2. Albertson, M.L., Dai, Y.G., Jensen, R.A., and Rouse, H., "Diffusion of Submerged Jets," Trans. ASCE, vol. 115, 1950.

3. Argyropolous, P.A., "General solutions of the Hydraulic Jump in Sloping Channels," Jrl. ASCE., Hyd. Div. Vol. 88, July 1962.

4. Bradshaw, P. and Gee, M.T., "Turbulent Wall Jets with and without an External Stream," Aero. Soc. Council, London, R. and M. No. 3252, 1962.

5. Bradbury, L.J.S., "The Structure of a Self-Preserving Jet," J. of Fluid Mech., Vol. 23, 1965.

6. Bradley, J.N. and Peterka, A.J., "Hydraulic Design of Stilling Basins : Stilling Basin with sloping apron (Basin V)", J. of Hyd. Div., Proc. ASCE., Oct. 1957.

7. Bradley, J.N., and Peterka, A.J., "Hydraulic Design of Stilling Basins : Basin III," Proc. paper 1403, ASCE, J. Hyd. Div., Oct. 1957.

8. Bradley, J.N. and Peterka, A.J., "Hydraulic Design of Stilling Basins : Basin I," Proc. paper 1401, ASCE, J. Hyd. Div., Oct. 1957.

9. Eskinazi, S. and Kruka, V., "Mixing of a Turbulent Wall Jet into a Free Stream," Proc. ASCE., J. of Engg. Mech. Div. Proc. paper, 3106, April 1962.

10. Eskinazi, S. and Kruka, V., "The Wall Jet in a Moving Stream," J. of Fluid Mech., Vol. 20, 1964.

11. De Mello Flores, J.O. : "Le Ressault" La Houille Blanche, PP. 811-822, No. 6, December 1954.

12. Forthmann, E., "Turbulent Jet Expansion," NACA., TM789, March, 1936 (English Translation).

13. Forster, J.W. and Skrinde, R.A., "Control of the Hydraúlic Jump by Sills," Trans. ASCE., 1950.

14. Glauert, M.B., "The Wall Jet," J. of Fluid Mech., Vol. 1, 1956.

15. Göertler, H., Z. Angew. Math. Mech. 22 (1942), 244.

16. Govinda Rao, N.S., and Rajaratnam, N., "The Submerged Hydraulic Jump," Proc. ASCE., J. Hyd. Div. Jan. 1963.

17. Harleman, D.R.F., "Effect of Baffle Piers on Stilling Basin Performance," J. Boston Soc. of Civil Engineers, April 1955.

18. Hickox, G.H., "Graphical Solution for Hydraulic Jump," Civil Engg., Vol. 4, 1934.

19. Keffer, J.F. and Baines, W.D., "The Round Turbulent Jet in a Cross-Wind," J. of Fluid Mech. England, Vol. 15, 1963.

20. Kindsvater, C.E., "The Hydraulic Jump in Sloping Channels," Trans. ASCE, 1944.

21. Lau, L., "Flow Characteristics of Wall Jets on Smooth, Rough and Porous Walls," M.A.Sc. Thesis, Dept. of Mech. Engg. University of Toronto, Toronto, 1963.

22. Liu, H.K., "Diffusion of flow from a submerged sluice gate," M.Sc. Thesis, State Univ. of Iowa, Iowa, Feb. 1949.

23. Myers, G.E., Schauer, J.J., and Eustis, R.H., "The Plane Turbulent Wall Jet, Part - I - Jet Development and Friction Factor," Tech. Rept. 1, Mech. Engineering Dept. Stanford University, Stanford, California, June 1961.

24. McCorquodale, J.A., and Regts, E.H., "A Theory of the Forced Hydraulic Jump," Trans. Engg. Inst. of Canada, Vol. 11, No. C-1, Aug. 1968.

25. Newman, B.G., "The deflection of Plane Jets by adjacent boundaries... Coanda Effect," Chap. "Boundary Layer and Flow Control," Vol. I, Ed. by Lachman, G.V., Pergamon Press, N.Y., 1961.

26. Patel, V.C., "Calibration of the Preston Tube and limitations on its use in Pressure Gradients," J. of Fluid Mech., Vol. 23, 1965.

27. Patrick, M.A., "Experimental investigation of the mixing and penetration of a round turbulent jet in-jected perpendicularly into a transverse stream," Trans. Inst. of Chem. Engrs., England, Vol. 45, 1967.

28. Pratte, B.D., and Baines, W.D., "Profiles of the round turbulent jet in a cross-flow," Proc. ASCE., J. Hyd. Div., Nov. 1967.

29. Preston, J.H., "The determination of turbulent skin-friction by means of Preston-Tubes," J. of Royal Aero. Soc. London, Vol. 58, 1954.

30. Rajaratnam, N., "Submerged hydraulic jump," Proc. ASCE., J. Hyd. Div., July, 1965.

31. Rajaratnam, N., "The Hydraulic Jump as a Wall Jet," Proc. ASCE, J. Hyd. Div., Sept. 1965.

32. Rajaratnam, N., "Submerged Sluice Gate Flow as a Wall Jet Problem," Proc. 2nd Australian Conf. on Hydraulics and Fluid Mech., Aukland, New Zealand, 1965.

33. Rajaratnam, N., and Subramanya, K., "Annotated Bibliography on Wall Jets," Techn. Rept., Dept. of Civil Engg., Univ. of Alta., Edmonton, 1967.

34. Rajaratnam, N., and Subramanya, K., "Diffusion of Rectangular Wall Jets in Wider Channels," J. of Hydraulic Research, I.A.H.R., Delft., Vol. 5, No. 4, 1967.

35. Rajaratnam, N., and Subramanya, K., "Plane Turbulent Reattached Wall Jets," Proc. ASCE., J. Hyd. Div., March 1968.

36. Rajaratnam, N., and Subramanya, K., "Profile of the Hydraulic Jump," Proc. ASCE., J. of the Hyd. Div., May 1968.

37. Rajaratnam, N., "On the Preston Tube with a Hemi-spherical Nose," Civil Engg. and Public Works Review, England, Nov. 1965.

38. Rajaratnam, N., "The Hydraulic Jump in Sloping Channels," Jrl. Central Board of Irrigation and Power, India, Vol. 23, No. 2, April 1966.

39. Rajaratnam, N., and Subramanya, K., "An Annotated Bibliography on Wall Jets," Tech. Rept. Dept. Civil Engg., Univ. of Alta., Edmonton, July, 1967.

40. Rajaratnam, N., and Muralidhar, D., "The Prandtle Tube as a Preston Tube," Civil Engg. and Public Works Review, England, May 1968.

41. Rajaratnam, N., "The forced hydraulic jump," Water Power, London, England, Pt. - 1, Jan. 1964 and Pt. -2, Feb. 1964.

42. Rajaratnam, N., "Plane Turbulent Wall Jets on Rough Boundaries," Water Power, London, April, May and June 1967.

43. Rand, W., "Flow over a vertical sill in an open channel," Proc. ASCE, J. Hyd. Div.,July 1965.

44. Schwarz, W.H., and Cosa t, W.P., "The two dimensional turbulent Wall Jet," J. of Fluid Mech., Vol. 10, Pt. 4, 1961.

45. Schlichting, H., "Boundary Layer Theory," Sixth English Edition, Published by McGraw-Hill Book Co., 1968.

46. Sigalla, A., "Measurements of Skin Friction in a Plane Turbulent Wall Jet," J. Royal Aero. Soc., England, Vol. 62, 1958.

47. Tollmien, W., Z. Angew., Math., Mech., 6(1926), 468.

48. Zijnen,"**Measurements** in a plane jet," Appl. Sci. Res. Vol., 7., 1957.

B30009